

UNIVERSITA' DEGLI STUDI DI NAPOLI FEDERICO II
SCUOLA DI DOTTORATO DI RICERCA IN INGEGNERIA INDUSTRIALE
FACOLTA' DI INGEGNERIA



DOTTORATO DI RICERCA IN INGEGNERIA
DEI MATERIALI E DELLE STRUTTURE – XXI CICLO

**Kinetic Analysis and Characterization
of Epoxy Resins Conventionally and Microwave Cured**

Guido Saccone

Tutor: Chiarissimo Prof. Domenico Acierno

Co – Tutor: Egregio Dr. Eugenio Amendola

Anni Accademici 2005-2008

Acknowledgments

I thank my supervisor Prof. Ing. Domenico Acierno, who always supported me with interesting scientific discussions and for giving me the possibility to attend various conferences on microwave engineering.

I gratefully thank my supervisor Prof. Dr. Eugenio Amendola for his precious teachings and above all for his strong support in every moment of my research activity during these three years. It has been always challenging, but also very pleasant working together. I hope that this is only the starting point of future collaborations in dielectric heating of thermosetting resins.

I thank Ing. Aniello Cammarano for his very useful help during this work.

I thank Mr. Giovanni Napolitano for his contribution to analysis and elaboration of calorimetric and kinetic data.

I thank Mr. Luigi Lisbo, Mr. Mario De Angioletti, Mr. Massimo Lombardo and Mrs. Mariarosaria Marcedula for their technical very precious support.

I thank Ing. Claudio Mazzon for his useful assistance about microwave plant.

I thank Dr. Marida Fasano and Mr. Antonio Capone for their useful support for bibliographic research.

I thank all the lecturers of PhD Industrial Engineering School for their competent and qualified contributions to our postgraduate education.

I thank my colleagues Valeria Caggiano, Gabriella Callegaro and Anna Maria Scamardella. During these three years, we really supported one another in every moment.

I gratefully thank my girlfriend Dora for her very precious moral support.

I thank my mother for the patience, who has showed me during this work.

Preface

Advanced fiber-reinforced polymer-matrix composites are nowadays extensively used as metal replacement in the production of aerospace, automotive and marine parts. The most widely used matrix materials for advanced composites are thermoset epoxy resins, which are processed by cure, consisting in conversion of liquid monomers into three-dimensional thermoset network via chemical reactions and formation of crosslinks between the main chains. Thermoset polymer are also used in microelectronics industry in which the curing of such systems have become the bottleneck of the whole production process. Epoxy resins have graduated from a laboratory curiosity to a multitude of applications, becoming an integral part of the adhesive industry, printed board circuitry, beyond aircraft and spacecraft design.

During processing, heat is supplied to the sample by conduction, convection and radiation from thermal energy sources. The use of conventional thermal energy sources in the manufacturing of composites results in long processing times and large temperature gradients, especially in thicker samples. In the search for an alternative energy source for the thermoset cure, considerable interest has been entrusted in the application of electromagnetic waves in the microwave frequency range.

Microwaves are electromagnetic radiations in the frequency range from 300 MHz to 300 GHz. These radiations are typically used in telecommunication and dielectric heating of materials. Some examples of industrial applications are in the field of plastics processing (welding and forming), wood processing (seasoning and gluing), textiles, paper and board (drying), food (post-baking and drying) and ceramics (drying).

Industrial microwave ovens generally operate at a frequency of 2,45 GHz, corresponding to a wavelength of 12,2 cm.

In contrast to thermal heating, which involves heat conduction and the resulting thermal lag, microwaves can generate heat directly within the sample and thus offer possible advantages of higher efficiency, fast production rate, lower capital cost, more uniform cure and improved physical-mechanical properties.

The main objective of this work is to investigate the possible advantages of the microwave curing process of epoxy systems in term of reaction kinetic and properties of the final product. The “specific microwave effect” has also been studied.

Contents

1	Introduction	18
1.1	Thermosetting Resins	18
1.2	Epoxy Resins	21
1.2.1	Properties	22
1.2.2	Applications	24
1.2.3	Crosslinking Mechanism	26
1.3	Electromagnetic Radiations	29
1.3.1	Basic Principles	30
1.3.2	Brief History of Electromagnetism	30
1.3.3	Electromagnetic Field	31
1.3.4	Maxwell's Equations	32
1.3.5	Lorentz Force Law	35
1.3.6	Electromagnetic Waves	35
1.4	Microwaves	37
1.4.1	Microwave Applications	38
1.5	Conventional Heating	39
1.6	Electrical Volumetric Heating	41
1.7	Volumetric and Conventional Heating: a Comparison	41
1.8	Microwave/Materials Interaction	42

1.8.1	Dielectric Properties	43
1.8.2	Dielectric Relaxation	44
1.8.3	Energy Conversion	49
2	Experimental	53
2.1	Materials	53
2.1.1	Characteristics of Fresh Mixture	53
2.1.2	Characteristics of Epoxy System Conventionally Cured	54
2.1.3	Sample Preparation	54
2.2	Microwave Plant	56
2.2.1	Microwave Radiation System Mechanism	57
2.2.2	VPMS	63
2.2.3	Insulator	64
2.2.4	Control Panel	65
2.2.5	Automatic Cycle and Parameters Selection	66
2.3	Microwave Oven Characterization in Dynamic Operative Conditions	68
2.3.1	Sample Position	69
2.3.2	Energy Density Distribution	70
2.3.3	Influence of the Tray Velocity	74
2.3.4	Location of the IR Sensor Reading Cone	76
2.3.5	IR Sensor Calibration	77
2.4	Microwave Oven Characterization in Static Operative Conditions	81
2.5	Datalogger	83
2.6	Optimization of the Process Conditions	85
2.6.1	Vessel Material	86
2.6.2	Influence of the Air Temperature	88
2.6.3	Influence of the Mixture Thickness	91
2.6.4	Influence of other parameters	91

3 Results and Discussion	93
3.1 Calorimetric Analysis	94
3.1.1 Thermo-gravimetric Characterization	94
3.1.2 DSC Characterization	96
3.2 DSC Kinetic Analysis	100
3.2.1 DSC Isothermal Scan	100
3.2.2 Data Elaboration	102
3.2.3 Reaction Rate-Degree of Cure Plot	103
3.2.4 Kinetic models	104
3.2.5 Non-linear Regression	107
3.2.6 Arrhenius Plot	111
3.3 Comparison MW versus DSC	113
3.3.1 Specific Microwave Effect	113
3.3.2 Static Operative Conditions	114
3.3.3 Dynamic Operative Conditions	131
3.4 Kinetic analysis in Microwave Field with Avrami Method	141
3.5 Dynamical-Mechanical Analysis	144
3.5.1 Storage Modulus	147
3.5.2 Glass Transition Temperature	147
3.6 Comparison of Flexural Elastic Modulus	149
3.6.1 Stress-Strain Plot	151
3.7 Spectroscopic Characterization	153
3.7.1 FT-IR Spectra	153
3.7.2 FT-NIR Spectra	155
3.8 Sensitizers	156
3.8.1 Organic oligomers	156
3.8.2 Metallic Nanopowders	159

CONTENTS **9**

4	Conclusions and Outlook	162
4.1	Outlook	163
	Appendix	165
A	A Brief History of Microwave Oven	165
	Bibliography	169

List of Tables

1.1	Epoxy resins average properties.	25
1.2	Meaning of the symbols appearing in the Maxwell's equations. . .	34
2.1	Characteristic of epoxy system before curing.	54
2.2	Characteristics of epoxy system cured, according to the supplier protocol.	55
2.3	Microwave oven parameters, selected for the determination of the energy density distribution in dynamic operative conditions.	72
2.4	Parameters selected for IR calibration with wood.	79
2.5	Parameters selected for IR calibration with EC 57 epoxy prepolymer.	80
2.6	Parameters selected for energy density comparison between posi- tions of coordinates (0,0,2) and (0,-5,2) [cm].	82
2.7	Properties of some materials used as vessel for microwave experiments.	87
2.8	Shape and size of the PP vessel used for microwave experiments. . .	87
2.9	Shape and size of the polytetrafluoroethylene mould used for dynamical- mechanical characterization.	88
2.10	Parameters selected for investigating the influence of the air tem- perature.	88
3.1	Results of DSC dynamic scans at different heating rates.	97

3.2	Average values of ΔH_{TOT} and T_g	98
3.3	Microwave oven parameters for the complete conversion of an epoxy sample.	99
3.4	Temperatures of isothermal DSC.	100
3.5	Operative conditions of isothermal DSC.	101
3.6	Kinetic constants and reaction orders obtained at every isothermal temperature.	109
3.7	Average reaction orders values.	109
3.8	Kinetic parameters for conventional curing reaction.	112
3.9	Time required for the complete conversion of the epoxy system during MW cure processes at different radiation powers.	116
3.10	Residual enthalpy against time during MW cure process at 1000 W.	117
3.11	Residual enthalpy against time during MW cure process at 1500 W.	118
3.12	Residual enthalpy against time during MW cure process at 2000 W.	118
3.13	Time, temperature max and degree of conversion for MW cure at 1500 W.	123
3.14	Numerical values used for the evaluation of $\alpha_{0,5+\tau}$ for MW cure at 1500 W.	126
3.15	Time, temperature max and degree of conversion for MW cure at 2000 W.	126
3.16	Time, temperature max and degree of conversion for DSC cure at 44°C/min.	129
3.17	Microwave parameters for the complete conversion of epoxy system in dynamic operative conditions.	132
3.18	Time, temperature max and degree of conversion for MW cure. . .	136
3.19	Time, temperature max and degree of conversion for DSC cure. . .	138

3.20 Ratio between the conversion in MW at different powers and DSC with comparable thermal profile.	140
3.21 Avrami kinetic parameters at different powers.	142
3.22 MW kinetic parameters at different powers.	143
3.23 Parameters of the MW cycle.	146
3.24 Quantity of epoxy components used during the MW cycle.	146
3.25 DMA parameters.	147
3.26 Comparison of dynamical-mechanical properties between samples conventionally and microwave cured.	149
3.27 Size of specimens used for flexural tests.	150
3.28 Flexural elastic modulus for specimens conventionally and microwave cured.	153
3.29 Quantity of the components of the epoxy mixture used for experi- ments with the organic sensitizer.	157
3.30 Microwave oven parameters used for the experiments with the sen- sitzers.	157
3.31 Quantity of the components of the epoxy mixture used for experi- ments with nickel nanopowders.	160

List of Figures

1.1	Diglycidyl ether of bisphenol A.	21
1.2	Typical epoxy prepolymer components.	22
1.3	Building application of epoxy resins.	26
1.4	Chemical structure of a typical epoxy prepolymer.	26
1.5	General structure of a diamine hardener agent.	27
1.6	Diamino stilbene (DAS).	27
1.7	Diaminoazobenzene (DAAB).	27
1.8	Scheme of crosslinking reaction.	28
1.9	Molecular structure of an epoxy resin.	29
1.10	Schematic representation of an electromagnetic wave.	36
1.11	Electromagnetic spectrum.	37
1.12	Resistor and capacitor in series.	44
1.13	Phazor diagram for current and voltage.	45
1.14	Resistor and capacitor in parallel.	46
1.15	Model of a dipole used in the Debye description of an ideal liquid.	47
1.16	The (a) Maxwell and (b) Voigt models for viscoelasticity.	48
1.17	Relationship between the dielectric loss factor and ability to absorb microwave power for some common materials.	51
2.1	Schematic microwave oven structure.	58

2.2	Wave propagation in a rectangular waveguide.	58
2.3	Multimodal applicator.	59
2.4	Front oven view.	60
2.5	Right side oven view.	61
2.6	Left side oven view.	62
2.7	Back oven view.	62
2.8	Front view and microwave distribution inside the cavity.	63
2.9	Side oven view and magnetron position.	63
2.10	Scheme of power supplying in a microwave oven without (A) and with (B) VPMS.	64
2.11	Surface of the oven tray with grid and three-dimensional Cartesian coordinates system.	69
2.12	Repetitive unit of polypropylene.	71
2.13	Beaker distribution on the tray surface.	71
2.14	Plot of energy density distribution along x-y plane, in dynamic op- erative conditions.	72
2.15	Influence of the height and the radial position on dielectric heating of beaker of water, in dynamic operative conditions.	73
2.16	ΔT^* measured at 1, 2 and 3 cm of height above the tray surface. . .	74
2.17	Influence of the tray velocity on the temperature increase.	75
2.18	Plot of ΔT^* obtained with a wood surface.	79
2.19	Plot of ΔT^* obtained with 50 ml of EC 57 epoxy prepolymer. . . .	81
2.20	Datalogger electronic circuits.	83
2.21	Datalogger outer view.	84
2.22	Samples cured with 2000 W for 10 min and with air temperature of 60°C (A), 50°C (B), 40°C (C), 30°C (D).	89

2.23	Onset temperature of a fresh epoxy mixture, measured with a DSC dynamic scan at 10°C/min.	90
3.1	Thermogravimetric signal of K 21 at 10°C/min.	94
3.2	Thermogravimetric signal of EC 57 at 10°C/min.	95
3.3	Thermogravimetric signal of EC 57-K 21 mixture at 10°C/min. . .	96
3.4	Cure enthalpy of EC 57-K 21 mixture with dynamic scan at 10°C/min.	97
3.5	T _g of a sample cured with dynamic scan at 10°C/min.	98
3.6	T _g of a sample microwave cured with 1500 W for 300 s.	99
3.7	Overlay of isothermal DSC at the seven selected temperatures. . .	102
3.8	Plot of experimental reaction rate versus degree of cure for isothermal DSC at 100°C.	104
3.9	Fitting of experimental DSC data of isothermal at 100°C with autocatalytic equation.	108
3.10	Comparison of experimental and theoretical α' versus α plot for isothermal DSC at 100°C.	110
3.11	Comparison of experimental and theoretical specific heat flow for isothermal DSC at 100°C.	111
3.12	Arrhenius plot.	112
3.13	DSC dynamic scan of sample microwave cured for 175 s at 1500 W.	116
3.14	Residual energy after MW cure process at 1500 W for 125 s.	119
3.15	Thermal profile during MW cure process at 1000 W.	120
3.16	Comparison of thermal profiles between MW cure process at 1500 W and a DSC dynamic scan at 44°C/min.	120
3.17	Comparison of thermal profile between MW cure process at 2000 W and a DSC dynamic scan at 70°C/min.	121
3.18	DSC dynamic scan at 70°C/min on an indium sample.	121
3.19	Standard DSC dynamic scan at 10°C/min on an indium sample. .	122

3.20 Degree of conversion against reaction time for MW cure process at 1500 W.	123
3.21 Comparison of experimental and fitting data of degree of conversion against reaction time for a MW cure process at 1500 W.	124
3.22 Degree of conversion against reaction time for MW cure process at 2000 W.	126
3.23 Total cure energy with DSC dynamic scan at 44°C/min.	128
3.24 Partial energy measured at 124°C with DSC dynamic scan at 44°C/min.	128
3.25 Degree of conversion versus reaction time in DSC cure process at 44°C/min.	129
3.26 Comparison of degree of cure between MW at 1500 W and DSC at 44°C/min.	130
3.27 Comparison of degree of cure between MW at 2000 W and DSC at 70°C/min.	131
3.28 DSC dynamic scan of sample microwave cured with the operative conditions reported in Table 3.17.	132
3.29 Comparison of the thermal profiles between MW cure process and DSC dynamic scan.	134
3.30 Total cure energy with DSC dynamic scan at 20°C/min.	135
3.31 Residual energy after 240 s of MW cure.	136
3.32 Degree of conversion versus reaction time in MW field.	137
3.33 Partial energy measured at 103, 33°C with DSC at 20°C/min.	138
3.34 Degree of conversion versus reaction time in DSC.	139
3.35 Comparison of degree of cure between MW and DSC.	139
3.36 Avrami plot with the data obtained through MW experiments at 1500 W.	142
3.37 DSC Dynamic scan of epoxy resin microwave cured for DMA.	146

3.38 Comparison of storage modulus of epoxy samples conventionally and microwave cured.	148
3.39 Comparison of glass transition temperature of the epoxy system thermally and microwave cured.	148
3.40 Comparison of stress-strain curves of samples conventionally and microwave cured.	152
3.41 EC 57 FT-IR spectrum.	154
3.42 Zoom of FT-IR spectrum of an epoxy sample microwave cured. . .	154
3.43 K 21 FT-NIR spectrum between 4000 and 6000 cm^{-1}	155
3.44 Comparison of FT-NIR spectra in the region between 4000 and 6000 cm^{-1}	156
3.45 Comparison of the thermal profiles between the epoxy system incorporating 2 p.h.r. of an organic sensitizer with the same resin free from additives.	158
3.46 Comparison of the thermal profiles between the epoxy system containing 20 p.h.r. of nickel nanopowders with the same resin free from additives.	160
A.1 One of the first domestic microwave oven.	167

Chapter 1

Introduction

In this chapter a brief description of epoxy resins and electromagnetic waves will be presented. The first section is dedicated to a short introduction of thermosetting resins, their properties and applications. The second section is focused on epoxy resins as particular class of thermosetting polymers. The third section illustrates the basic principles and the main properties of electromagnetic radiations with particular emphasis on microwaves and their interactions with materials.

1.1 Thermosetting Resins

Thermosetting resins are an important class of polymers.

They become permanently and irreversibly hard when heat is applied and do not soften upon subsequent heating [1]. During the initial heat treatment, covalent crosslinks are formed between the adjacent molecular chains. These bonds anchor the chains together¹ to resist the vibrational and rotational chain motions at high temperatures. Only heating to excessive temperatures will cause break of these crosslink bonds and polymer degradation. Therefore a thermoset material

¹At chemically active sites, as for example unsaturated or epoxy groups.

cannot be melted and re-shaped after it is cured. This implies that thermosets cannot be recycled, except as filler material. Thermosetting polymers are generally harder and stronger than thermoplastics and have better dimensional stability² and are also better suited to high-temperature applications up to the decomposition temperature of the material. They are usually liquid or malleable prior to curing and designed to be molded into their final form, or used as adhesives.

Thermosetting resins are generally composed by two components. The first is the prepolymer and the second is the hardener or curing agent³. This is used for starting chemical reactions with the prepolymer forming a three-dimensional network with a larger molecular weight, resulting in a material with high melting point. In this final structure the main chain of the prepolymer are joined together through crosslinks realized by the hardener agent. Curing process may be done through heat⁴, chemical reactions or irradiation. It can happen only if there is a chemical affinity between the functional groups of prepolymer and hardener agent.

For example in epoxy resins the prepolymer possesses an oxirane or epoxy ring, that is a strong functional group and the typical hardener agent is an aliphatic or aromatic diamine.

Some examples of thermosets polymerization mechanisms are:

- Step-growth polymerization, through elimination reaction, between phenol and formaldehyde forming phenolic resins;
- Reaction between isocyanate groups and diols forming polyurethanes;
- Transesterification of dimethyl terephthalate and ethylene glycol forming polyester resins.

²Due to their 3-D network.

³In some systems catalysts, fillers, pigments, plasticizers and other additives can be present.

⁴Generally above 200°C.

Worldwide the current consumption of thermoset resins across the whole industrial spectrum amounts to 21,6 million tonnes. Industry growth rates are forecast to be in excess of 2,5% per annum. The worldwide industry is thriving and producing lightweight, high performance, high quality products for an ever-expanding range of markets.

The applications of thermosets are many and varied. One of the primary uses is as the matrix in composite materials. Composites are now accepted as high performance engineering materials in many fields such as automotive, aerospace and marine. They are made using a range of techniques from autoclave moulding to resin transfer moulding.

Adhesives are another major application area for thermosets and progress has been rapid. For example, a few years ago adhesives were restricted to relatively low performance applications, while today the range of formulations makes it possible to assemble aircraft and automotive components. Construction is a major market.

A large volume of thermosets is used in the coatings industry. This has undergone rapid change in recent years as manufacturers strive to reduce VOC emissions, by reducing the use of solvents and bringing in ultraviolet curing formulations.

Recycling is another environmental issue that is being tackled by manufacturers. Thermoset materials are designed for a long lifetime and can therefore be difficult to break down. However, methods of re-use and recycling are available. Innovations in materials include the use of natural fiber reinforcement in composites and the application of biopolymers as the matrix materials.

Thermosets include a wide range of materials:

- acrylics;
- alkyds;
- amino resins;

- bismaleimides;
- *epoxy*;
- furane;
- phenolics;
- polyimides;
- unsaturated polyesters;
- polyurethanes;
- vinyl esters.

New materials are being developed such as cyanate esters and arylzene resins, together with hybrid resins.

1.2 Epoxy Resins

Epoxy resins are substantially polyethers, but they maintain this name depending on the material used for producing them and because, before polymerization, they contain the epoxy or ethoxyline group inside the prepolymer.

In Figure 1.1 the molecular structure of a typical epoxy prepolymer is illustrated.

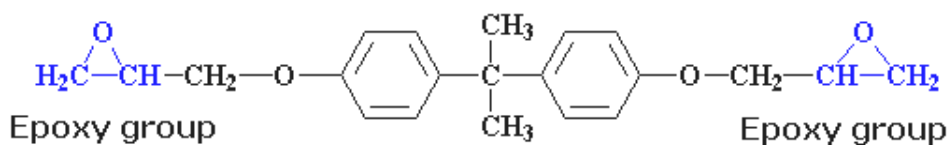


Figure 1.1: Diglycidyl ether of bisphenol A.

The diglycidyl ether of bisphenol A is the most used epoxy prepolymer. It is produced through a step-growth polymerization reaction between bisphenol A and epichlorohydrin using sodium hydroxide as catalyst. These molecules are illustrated in Figure 1.2.

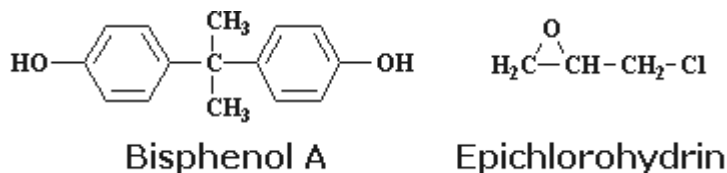


Figure 1.2: Typical epoxy prepolymer components.

Generally an excess of epichlorohydrin is used for assuring the presence of epoxy groups at both side of the polymer. It has a low molecular weight⁵. Depending on it this prepolymer is a viscous liquid or fragile solid with high melting point. Other molecules containing hydroxyl groups as hydroquinone, glycol and glycerol can be used in place of bisphenol A.

The epoxy resins belongs to the major industrial plastics [2]. They were first synthesized by Pierre Castan in Switzerland and S. O. Greenlee in the United States late in the 1930s. In common with phenolic and polyester resins, the epoxies are thermosetting materials. When converted by a curing agent, the thermosetting resins become hard, infusible systems. The system may be visualized as a network crosslinked in all three dimensions in which it will be seen that movement of a molecule in any direction is opposed by the crosslinking arrangement.

1.2.1 Properties

The thermosetting epoxy resins possesses a number of unusually valuable properties immediately amenable to use in the formulation of adhesives, sealing liquids,

⁵About 900-3000 u.

cold solders, castings, laminates and coatings. The more important of these properties are:

Versatility. Numerous curing agents for the epoxies are available and the epoxies are compatible with a wide variety of modifiers. Hence the properties of the cured epoxy-resin system can be engineered to widely diverse specifications.

Good handling characterization. Many epoxy systems can be worked at room temperature and those which cannot, require only moderate heat during mixing. Before the curing agent is incorporated, the resins have indefinite shelf life, provided they are properly made and do not contain any caustic. The ratio of curing agent to resin is not as critical as with some thermosetting materials. It should be held fairly close to the empirically determined optimum amount if best results are to be obtained, and weighing should be done with care. If too much or too little curing agent is present, the solvent resistance and heat-distortion temperature will be reduced. In general, however, a few per cent error in either direction may be tolerated in most applications, and some curing agents permit even wider margins. Cure can be accomplished in almost any specified time period by regulation of cure cycles and proper selection of curing agent. In many cases, pot life, viscosity and cure schedules can be accommodated to the production situation without seriously influencing the properties of the cured system.

Toughness. Cured epoxy resins are approximately seven times tougher than cured phenolic resins. The relative toughness has been attributed to the distance between crosslinking points and the presence of integral aliphatic chains.

High adhesive properties. Epoxy resins have high adhesive strengths arising from the polarity of aliphatic hydroxyl and ether groups present in the initial resin chain and in the cured system. The polarity of these groups serves to create electromagnetic bonding forces between the epoxy molecules and the adjacent surface. The epoxy groups, likewise, will react to provide chemical bonds with

surfaces, such as metals, where active hydrogens may be found. Since the resin passes relatively undisturbed (i.e. with slight shrinkage) from the liquid to the solid state, the bonds initially established are preserved.

Low shrinkage. The epoxy resins differ from many thermosetting compounds in that they give off no by-products during cure, and in the liquid state, are highly associated. Cure is by direct addition and shrinkage is on the order of 2% for an unmodified system, indicating that little internal rearrangement of the molecules is necessary. The condensation and crosslinking of the phenolic and polyester resins, on the other hand, yield significantly higher shrinkage values.

Inertness. Cured epoxy resins are very inert chemically. The ether groups, the benzene rings and, when present, the aliphatic hydroxyls in the cured epoxy system are virtually invulnerable to caustic attack and extremely resistant to acids. The chemical inertness of the cured epoxy system is enhanced by the dense, closely packed structure of the resinous mass, which is extremely resistant to solvents. Moreover epoxy resins can exhibit:

- excellent dielectric properties;
- enhanced resistance to low temperature (until -50°C);
- elevated waterproof;
- low inflammability;
- very good tolerance to various environmental conditions.

The average properties of epoxy resins are summarized in Table 1.1

1.2.2 Applications

The main application of epoxy resins is in the field of covering, because this material has unique properties of flexibility, adhesion and chemical resistance.

Average Properties of Epoxy Resins	
Density	1,25 Kg/m ³
Tensile Strength	60 MPa
E	2,5 GPa
Elongation at Break	2 %
Flexural Strength	60 MPa
Operating Temperature	< 100°C

Table 1.1: Epoxy resins average properties.

Therefore they are used for paints and adhesives, foams, industrial floors, covering of metallic materials and presswork of parts with sealing of electronic circuits.

Epoxy resins can be formed and laminate and it is possible to create materials reinforced with glass fibers, that have mechanical, electrical and chemical properties better than that obtained with other polymers, as unsaturated polyester resins.

They are used also as advanced fiber-reinforced polymer-matrix for production of aerospace, automotive and marine parts.

However the elevated price of this polymer prevents its more extensive diffusion.

In Figure 1.3 a typical application of epoxy resin is illustrated.



Figure 1.3: Building application of epoxy resins.

1.2.3 Crosslinking Mechanism

Epoxy resins can be polymerized by the anionic-chain-addition mechanism [3]. The polymerization is catalyzed by strong bases, such as alkoxide ions, and results in polyethers. Each step generates a new alkoxide center, which can react with another monomer molecule by nucleophilic ring-opening.

Epoxy resins undergo curing processes with many substances like polyamine, polyamides, phenol-formaldehyde, urea-formaldehyde, acids and acid anhydrides. Coupling and condensation reactions can happen during this process.

Another important hardener agents are diamines. The epoxy and amino groups are shown in Figures 1.4 and 1.5.

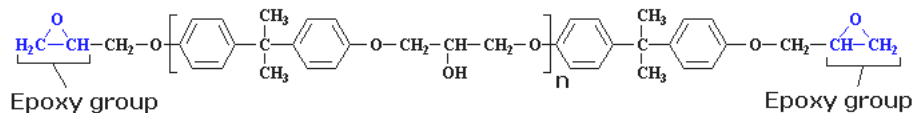


Figure 1.4: Chemical structure of a typical epoxy prepolymer.

In Figure 1.4 n can be of order of 25.



Figure 1.5: General structure of a diamine hardener agent.

In Figure 1.5 R is a generic organic group, typically an aromatic molecule, as illustrated in Figures 1.6 and 1.7.

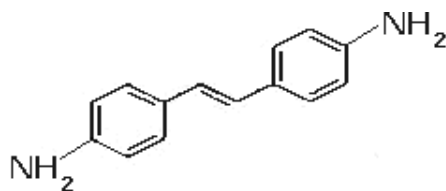


Figure 1.6: Diamino stilbene (DAS).

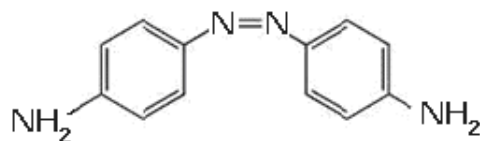


Figure 1.7: Diaminoazobenzene (DAAB).

In the case of reactions with amines there is the opening of epoxy ring forming a beta-hydroxyaminic bond.

Acids and acid anhydrides react through esterification of secondary hydroxyl groups located on epoxy resins backbone.

Epoxy resins can also undergo curing processes with cationic polymerization, using as catalysts Lewis acids such as BF_3 and forming polyethers.

An epoxy prepolymer, as that illustrated in Figure 1.4, if chemically activated by an appropriate energy source, is able to link other macromolecules of the same type generating a very long chain. Moreover hardener agents can create chemical crosslinks between these macromolecular chains forming a three-dimensional network, with unique characteristics.

The reaction between the epoxy prepolymer and the amino groups forms reticulation crosslinks as shown in Figure 1.8

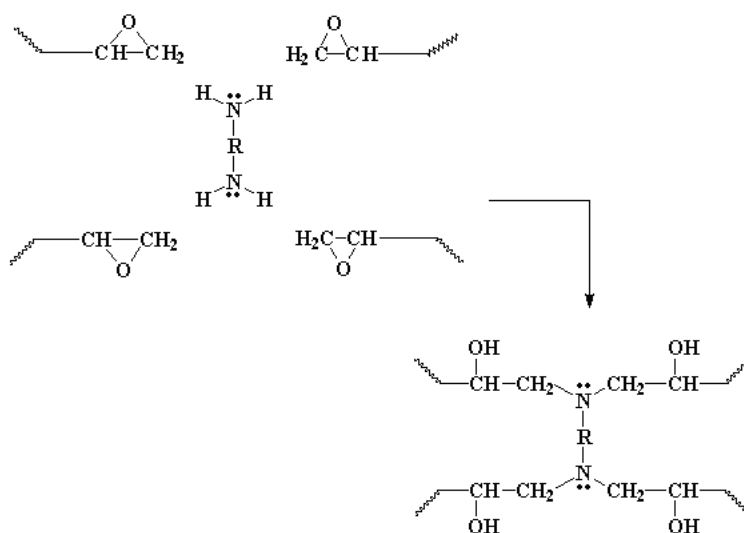


Figure 1.8: Scheme of crosslinking reaction.

Figure 1.8 represents the formation of four crosslinks between epoxy and amino groups, through the opening of the epoxy rings and formation of hydroxyl groups. This polymerization reaction is not accompanied by the formation of subpro-

ducts and it generates the three-dimensional network of the thermosetting resin, as illustrated in Figure 1.9.

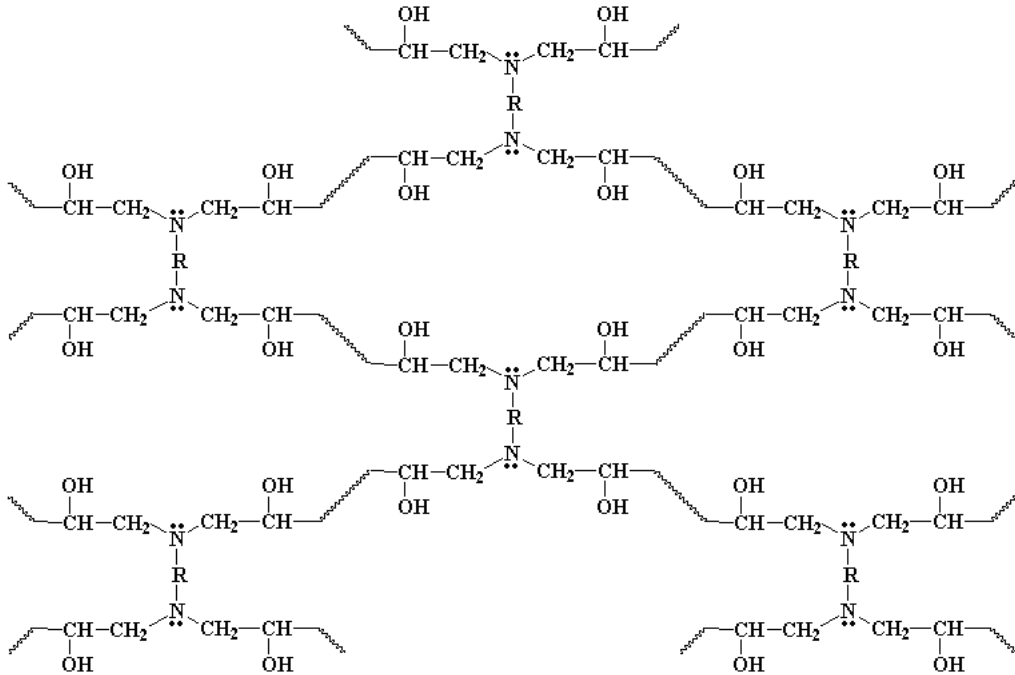


Figure 1.9: Molecular structure of an epoxy resin.

1.3 Electromagnetic Radiations

In this section a synthetic exposition of principles of microwaves and dielectric heating will be presented. It will begin from the fundamental laws of electromagnetism up to a description of a microwave circuit and applications of this technology.

1.3.1 Basic Principles

Electromagnetism describes the relationship between electricity and magnetism. An electromagnetic field exerts a force on particles with electric charge, and is in turn affected by the presence and motion of these particles.

A changing magnetic field produces an electric field. This is the phenomenon of electromagnetic induction, the basis of operation of electrical generators, induction motors, and transformers. Similarly, a changing electric field generates a magnetic field. Because of this interdependence of the electric and magnetic fields, it makes sense to consider them as a single coherent entity, i.e. the *electromagnetic field*.

The magnetic field is produced by the motion of electric charges, i.e., electric current. The magnetic field causes the magnetic force associated with magnets.

1.3.2 Brief History of Electromagnetism

About the year 1819 Oersted discovered that a magnetic field is produced if the terminals of a voltaic cell are joined by a wire [4]. For this, and other reasons, it is possible to say that an electric current is flowing through the wire and through the cell. This was the first discovery that magnetic fields could be produced by electric current.

At the time of discovery Oersted did not suggest any satisfactory explanation of the phenomenon, nor did he try to represent the phenomenon in a mathematical framework [5]. However, three months later he began more intensive investigations. Soon thereafter he published his findings, proving that an electric current produces a magnetic field as it flows through a wire. The CGS unit of magnetic induction (oersted) is named in honor of his contributions to the field of electromagnetism.

His findings resulted in intensive research throughout the scientific community in electrodynamics. They influenced French physicist André-Marie Ampère's developments of a single mathematical form to represent the magnetic forces be-

tween current-carrying conductors. Oersted's discovery also represented a major step toward a unified concept of energy.

Oersted was not the first person to examine the relation between electricity and magnetism. In 1802 Gian Domenico Romagnosi, an Italian legal scholar, deflected a magnetic needle by electrostatic charges. He interpreted his observations as *The Relation* between electricity and magnetism. Actually, no galvanic current existed in the setup and hence no electromagnetism was present. An account of the discovery was published in 1802 in an Italian newspaper, but it was largely overlooked by the contemporary scientific community.

This unification, which was observed by Michael Faraday, extended by James Clerk Maxwell, and partially reformulated by Oliver Heaviside and Heinrich Hertz, is one of the accomplishments of 19th century mathematical physics. It had far-reaching consequences, one of which was the understanding of the nature of light. As it turns out, what is thought of as "light" is actually a propagating oscillatory disturbance in the electromagnetic field, i.e., an electromagnetic wave. Different frequencies of oscillation give rise to the different forms of electromagnetic radiations, from radio waves at the lowest frequencies, to visible light at intermediate frequencies, up to gamma rays at the highest frequencies.

1.3.3 Electromagnetic Field

The electromagnetic field is a physical field produced by electrically charged objects. It affects the behaviour of charged objects in the vicinity of the field.

The electromagnetic field extends indefinitely throughout space and describes the electromagnetic interactions. It is one of the four fundamental forces of nature⁶.

⁶The others are gravitation, the weak interaction and the strong interaction. Actually Sheldon L. Glashow, Abdus Salam and Steven Weinberg have demonstrated that the electromagnetic and weak interaction can be unified.

The field can be viewed as the combination of an electric and a magnetic field.

The electric field E [V/m] is a field intensity, or stress, at a point in space due to the presence of a charged body. So it is produced by stationary charges. The magnetic field B [A/m] is defined as the field intensity at the centre of a circular loop of conductor of radius r [m] carrying a current I [A] where:

$$B = \frac{I}{2\pi r} \quad (1.1)$$

A circular loop is chosen because this is the simplest practical geometry which takes account of the magnetic field of the return path of the current, and conforms with an easily realized experiment. So it is produced by moving charges⁷.

Stationary and moving charges are often described as the sources of the electromagnetic field. The way in which charges and currents interact with the electromagnetic field is described by:

- Maxwell's equations;
- The Lorentz force law.

From a classical perspective, the electromagnetic field can be regarded as a smooth, continuous field, propagated in a wavelike manner.

Whereas, from a quantum mechanical point of view, the field is seen as quantised, being composed of individual photons.

1.3.4 Maxwell's Equations

In 1873 the British physicist J.C. Maxwell published his famous "Treatise on electricity and magnetism", including the Maxwell equations, which embody and describe mathematically all phenomena of electromagnetism. In classical electromagnetism, Maxwell's equations are a set of four partial differential equations

⁷Currents.

that describe the properties of the electric and magnetic fields and relate them to their sources, charge and current density. According to these equations light is an electromagnetic wave.

The equations are given in SI units, as matter of fact Maxwell's equations are not unchanged in other unit systems.

The following set of equations expresses the differential form of Maxwell's laws in terms of free charge and current:

$$\begin{aligned}
 \nabla \cdot \vec{D} &= \rho_f && \text{Gauss'law} \\
 \nabla \cdot \vec{B} &= 0 && \text{Gauss'law for magnetism} \\
 \nabla \times \vec{E} &= -\frac{\partial \vec{B}}{\partial t} && \text{Faraday's law of induction} \\
 \nabla \times \vec{H} &= \vec{J}_f + \frac{\partial \vec{D}}{\partial t} && \text{Ampère's circuital law}
 \end{aligned} \tag{1.2}$$

While the integral form is expressed by the following set of equations:

$$\begin{aligned}
 \oint_S \vec{D} \cdot d\vec{A} &= Q_{f,S} && \text{Gauss'law} \\
 \oint_S \vec{B} \cdot d\vec{A} &= 0 && \text{Gauss'law for magnetism} \\
 \oint_{\partial S} \vec{E} \cdot d\vec{l} &= -\frac{\partial \Phi_{B,S}}{\partial t} && \text{Faraday's law of induction} \\
 \oint_{\partial S} \vec{H} \cdot d\vec{l} &= I_{f,S} + \frac{\partial \Phi_{D,S}}{\partial t} && \text{Ampère's circuital law}
 \end{aligned} \tag{1.3}$$

where the symbols used in the equations 1.2 and 1.3 are explained in the Table 1.2

Maxwell's equations are generally applied to macroscopic averages of the fields, which vary wildly on a microscopic scale in the vicinity of individual atoms⁸. It is only in this averaged sense that one can define quantities such as the *permittivity* and *permeability* of a material. At the microscopic level, Maxwell's equations, ignoring quantum effects, describe fields, charges and currents in free space, but at this level of detail one must include all charges, even those at an atomic level, generally it is an intractable problem.

⁸Where they undergo quantum mechanical effects as well.

Symbol	Meaning
$\nabla \cdot$	Divergence operator
$\nabla \times$	Curl operator
$\frac{\partial}{\partial t}$	Partial derivative with respect of time
S	Gaussian surface
\vec{E}	Electric field
\vec{B}	Magnetic field
\vec{D}	Electric displacement field
\vec{H}	Magnetizing field
ρ_f	Free charge density
\vec{J}_f	Free current density
$\oint_S \vec{D} \cdot d\vec{A}$	The flux of \vec{D} over any closed S
$\oint_S \vec{B} \cdot d\vec{A}$	The flux of \vec{B} over any closed S
$\oint_{\partial S} \vec{E} \cdot d\vec{l}$	Line integral of \vec{E} along the boundary ∂S
$\oint_{\partial S} \vec{H} \cdot d\vec{l}$	Line integral of \vec{H} along the boundary ∂S
$Q_{f,S}$	Net unbalanced free electric charge enclosed by S
$\Phi_{B,S}$	Magnetic flux over any surface S
$\Phi_{D,S}$	Electric displacement flux over any surface S
$I_{f,S}$	Net free electrical current passing through the surface S

Table 1.2: Meaning of the symbols appearing in the Maxwell's equations.

1.3.5 Lorentz Force Law

The Lorentz force is the force on a point charge due to electromagnetic fields. It is given by the following equation in terms of the electric and magnetic fields:

$$\vec{F} = q \left(\vec{E} + \vec{v} \times \vec{B} \right) \quad (1.4)$$

In this equation \vec{F} is the Lorentz force [N], q is the electric charge of the particle [C], \vec{E} is the electric field [$\frac{V}{m}$], \vec{v} is the instantaneous velocity of the particle [$\frac{m}{s}$], \times is the vector cross product and \vec{B} is the magnetic field [T].

A positively charged particle will be accelerated in the same orientation as the \vec{E} field, but will curve perpendicularly to both the instantaneous velocity vector \vec{v} and the \vec{B} field according to the right-hand rule.

1.3.6 Electromagnetic Waves

Electromagnetic (EM) radiation is a self-propagating wave in space or through matter. EM radiation has an electric and magnetic field component which oscillate in phase perpendicular to each other and to the direction of energy propagation.

A schematic representation of an electromagnetic wave is illustrated in Figure 1.10.

Electromagnetic radiation is classified into types according to the frequency of the wave, these types include:

- Radio waves;
- *Microwaves*;
- Infrared;
- Visible light;
- Ultraviolet;

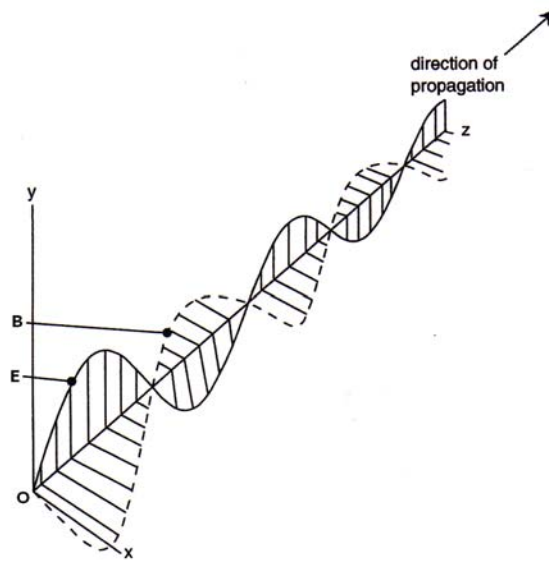


Figure 1.10: Schematic representation of an electromagnetic wave.

- X-rays;
- Gamma rays.

Of these, Radio waves have the longest wavelengths and Gamma rays have the shortest.

The electromagnetic spectrum is shown in Figure 1.11.

EM radiation carries energy and momentum, which may be imparted when it interacts with matter.

Electromagnetic waves were first postulated by James Clerk Maxwell and subsequently confirmed by Heinrich Hertz. Maxwell derived a wave form of the electric and magnetic equations, revealing the wave-like nature of electric and magnetic fields, and their symmetry. Because the speed of EM waves predicted by the wave equation coincided with the measured speed of light, Maxwell concluded that light itself is an EM wave.

According to Maxwell's equations 1.2 and 1.3 a time-varying electric field gene-

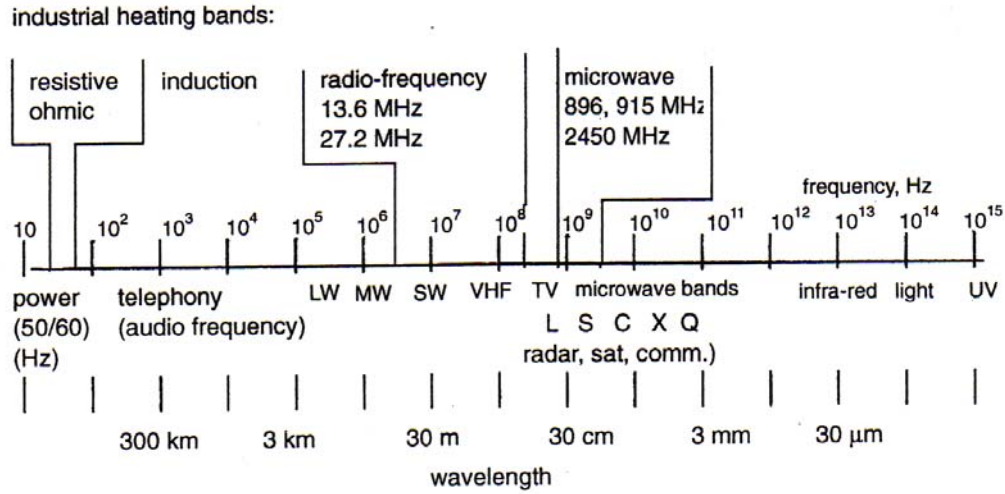


Figure 1.11: Electromagnetic spectrum.

rates a magnetic field and vice versa.

Therefore, as an oscillating electric field generates an oscillating magnetic field, the magnetic field in turn generates an oscillating electric field, and so on. These oscillating fields together form an electromagnetic wave.

A quantum theory of the interactions between electromagnetic radiations and matter such as electrons is described by the theory of quantum electrodynamics.

At every frequency the propagation speed of an EM radiation is equal to the speed of light c that in the free space is exactly:

$$c = 299.792.458 \frac{\text{m}}{\text{s}} \quad (1.5)$$

1.4 Microwaves

Microwaves (MW) are electromagnetic radiations with wavelength ranging from 1 mm to 1 m, or frequencies between 0.3 and 300 GHz. Therefore they are included between radio waves and infrared.

The spectrum of microwaves is subdivided into:

- ultra-high frequency (UHF) 0,3 - 3 GHz;
- super-high frequency (SHF) 3 - 30 GHz;
- extremely high frequency (EHF) 30 - 300 GHz.

Above 300 GHz, the absorption of electromagnetic radiations by terrestrial atmosphere is so great that it is effectively opaque, until the atmosphere becomes transparent again in the so-called infrared and optical window frequency ranges.

In the electromagnetic wave spectrum the microwaves are situated in a position much higher of the frequency used for the electric energy distribution (50 Hz corresponding a wavelength of ≈ 6000 Km), but much lower of visible light (million of GHz and wavelength of few micron).

The region of the spectrum included between 1 and 25 cm is usually used in civil and military radar. For this reason the domestic and industrial microwave ovens operate at specified frequencies of 2,45 GHz and 900 MHz (corresponding to wavelength of 12,2 and 33,3 cm).

1.4.1 Microwave Applications

Microwave are extensively used in many fields from decades. For example they are used in satellite broadcasting and communications, because, instead of radio waves, they cross the terrestrial atmosphere without interferences. Moreover the available band is wider with microwaves than with radio waves. Therefore, using microwaves, is possible to send an higher quantity of informations.

Radar systems use microwaves to identify the presence and position of moving and fixed objects in the distance. Some communications protocols, as bluetooth, are based on microwaves.

Even microwaves can transfer energy in the distance as was discovered during the second war world. In the 70s and 80s years the U.S.A. National Aeronautics and Space Administration Agency (NASA) studied the possibility to use a satellite systems with photovoltaic panels for producing electric energy and transfer it on the earth through a microwave beam.

Another very important application of microwave technology is the dielectric heating. Modern industrial-microwave-heating systems are used for a diversity of processes in the food industry, tempering and thawing, continuous baking, vacuum drying, pasteurisation and sterilization, and in the ceramics, rubber and plastics industries, as well as many specialized processes in the chemical industry where there is great interest in vacuum processing. In the last ten years microwave technology has been successfully applied in various industrial fields:

- *Chemical-pharmaceutical*: powder dehydration, polymerization and fusion of resins;
- *Wood and cork*: drying, dehydration, sterilization and bacteria inactivation;
- *Farming and food*: dehydration, cooking, thawing, pasteurisation and sterilization;
- *Rubber and plastic*: preheating, dehydration and fusion of materials;
- *Textile and clothes*: drying, colour fixing and moisture correction;
- *Ceramic and brick*: dehydration.

1.5 Conventional Heating

Of all the process used in manufacturing industry there can be little doubt that heating is the most commonplace, widely used in the food, chemical textile

and engineering industries for drying, promoting chemical or physical change, and many other purposes [6]. Yet it remains one of the most difficult techniques to control, being slow and imprecise when practiced in the usual way of heating the surface of the workpiece by radiation, convection or conduction or, commonly, a poorly controlled mixture of all three, and even if perfection were achieved in surface heating, the process time is limited by the rate of heat flow into the body of the workpiece from the surface, which is determined entirely by the physical properties of the workpiece: its *specific heat*, *thermal conductivity* and *density*. These last three are combined into one parameter, the *thermal diffusivity*, which uniquely determines the temperature rise within a material as a function of time and depth from the surface, subject to a given set of conditions at the surface. Nothing can be done in the application of surface heating to accelerate heating once the surface has reached a specified maximum temperature. Internal temperature distribution is then limited by the thermal diffusivity of the material.

Because, in conventional heating, all the heat energy required in the workpiece must pass through its surface, and the rate of heat flow to within is limited by temperature and the thermal diffusivity, the larger the workpiece, the longer the heating takes.

Everyone's experience is that surface heating is especially slow in a thick material. It is not only slow but nonuniform, with the surfaces, and in particular edges and corners, being much hotter than the inside. Consequently, the quality of the treated workload is variable and frequently inferior to what is desired.

Imperfect heating resulting from these difficulties is a frequent cause of product reject and energy waste. Above all the extended process time results in large production areas devoted to ovens. Large ovens are slow to respond to impressed temperature changes, take a long time to warm up and have high heat capacities. Their sluggish performance results in a failure to respond to sudden changes in

production requirements: management control becomes difficult, subjective and expensive.

1.6 Electrical Volumetric Heating

By electrical means, *volumetric heating* is possible wherein all the infinitesimal elements constituting the volume of a workload are each heated individually, ideally at substantially the same rate. The heat energy injected into the material is transferred through the surface electromagnetically, and does not flow as a heat flux, as in conventional heating. The rate of heating is no longer limited by thermal diffusivity and surface temperature, and the uniformity of heat distribution is greatly improved. Heating times can often be reduced to less than 1% of that required using conventional techniques, with effective energy variation within the workload less than 10%.

Any material can be heated directly by electrical volumetric heating provided that it is neither a perfect electrical conductor nor a perfect insulator, implying that the range extends from metals to dielectric materials which could be considered quite good insulators.

1.7 Volumetric and Conventional Heating: a Comparison

That a fixed continuous power dissipation into a dry, passive workload causes its average temperature to rise linearly with time is of fundamental importance, distinguishing it from conventional heating, in which the average temperature of the workload asymptotically reaches the oven temperature, and cannot rise above it.

In principle, with volumetric heating the average temperature of the workload continues to rise as long as power is applied, irrespective of the temperature of the oven walls or of the air inside the oven. The question sometimes asked, “what is the temperature of the microwave oven?”, has no fundamental relevance. The temperature and humidity inside the oven do, however, have an important secondary effect on the system performance because of surface heat transfer, causing surface heating or cooling depending on conduction.

Unlike conventional heating ovens, microwave ovens are very efficient in converting energy into heat in the workload. In a large industrial oven, the microwave efficiency, defined as the percentage of the applied microwave energy which is dissipated as heat in the workload, can be in the region of 95%, and the conversion of electrical power into microwave power can have an efficiency of 85%. Moreover, a conventional oven has to be heated to a temperature substantially in excess of the required temperature in the workload; a microwave oven, if heated at all, is normally heated to a temperature no greater than the required surface temperature of the workload. The radiation and convection heat losses from the microwave oven are therefore significantly less because of its lower temperature.

Further energy saving arises because a microwave oven has instantaneous control of power, which means that equilibrium conditions are rapidly reestablished after a change, and start-up can be rapid. Very fast feedback control loops can be used to control process parameters accurately, leading to improved product quality.

1.8 Microwave/Materials Interaction

Energy is transferred to materials by interaction of the electromagnetic fields at the molecular level, and the dielectric properties ultimately determine the ef-

fect of the electromagnetic field on the material. Thus, the physics of the microwave/materials interaction is of primary importance in microwave processing. The interaction of microwaves with molecular dipoles results in rotation of the dipoles, and energy is dissipated as heat from internal resistance to the rotation. In the following section, the principles behind microwave/materials interactions, power absorption, and measurement of dielectric properties are presented. Whenever possible, simplified models and analogies for microwave/materials interactions are presented to assist in understanding the physics behind the material response.

1.8.1 Dielectric Properties

For heat to be generated within the material, the microwaves must be able to enter the material and transmit energy. The dielectric constant ϵ^I and the dielectric loss factor ϵ^{II} quantify the capacitive and conductive components of the dielectric response. These components are often expressed in terms of the complex dielectric constant ϵ^* :

$$\epsilon^* = \epsilon^I - j\epsilon^{II} \quad (1.6)$$

Another commonly used term for expressing the dielectric response is the loss tangent:

$$\tan\delta = \frac{\epsilon^{II}}{\epsilon^I} \quad (1.7)$$

There exist a number of properties that contribute to the dielectric response of materials. These properties include electronic polarization, atomic polarization, ionic conduction, dipole (orientation) polarization, and Maxwell–Wagner polarization mechanisms. At microwave frequencies, dipole polarization is thought to be the most important mechanism for energy transfer at the molecular level [7, 8]. In addition, in composite materials, Maxwell–Wagner polarization, which results from the accumulation of charge at the material interface, is also an important heating mechanism [7].

In dielectric materials, the local charge moves in response to an applied electric field. Within materials, there exists bound charge and free charge, and motion of the bound charge results in polarization. Polarization of electric charge where the translational motion is restricted or polarization of molecules where the rotational motion is restricted results in a lag between the electric field and the polarization. This time lag, known as the relaxation time, is due to dissipation of energy as heat within the material. Microwave heating is a result of this dielectric relaxation.

1.8.2 Dielectric Relaxation

Relaxation phenomena are often encountered in a variety of chemical, mechanical or electrical systems. Relaxation times are generally defined by differential equations of the following form where h and k are variables:

$$\tau \frac{\partial k}{\partial t} + k = h \quad (1.8)$$

The relaxation phenomenon in dielectric materials is analogous to relaxation in electrical circuits. Models that describe the relaxation of dielectric materials are often based on electrical circuits that are composed of resistors and capacitors in series or parallel.

The simplest circuit that exhibits a relaxation time is a resistor and capacitor in series, as shown in Figure 1.12.

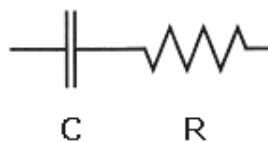


Figure 1.12: Resistor and capacitor in series.

By summing up the voltage, V , across both the resistor and the capacitor, the

following differential equation for charge, Q , in the circuit can be obtained:

$$R \frac{\partial Q}{\partial t} + \frac{Q}{C} = V \quad (1.9)$$

where R and C stand for resistance and capacitance, respectively, and t is the time. Equation 1.9 can be rearranged in the form of equation 1.8:

$$\tau \frac{\partial Q}{\partial t} + Q = CV \quad (1.10)$$

where $\tau = RC$ is the relaxation time. The solution to this differential equation, where the applied voltage is sinusoidal and assumed to be $V_0 e^{j\omega t}$ in complex, polar coordinates is:

$$Q^*(\omega, t) = \frac{V_0}{\omega Z(\omega)} e^{j(\omega t - \delta)} \quad (1.11)$$

where δ is the angle between the charge vector, Q^* , and the voltage vector, V^* , in a phazor representation in the complex plane, as illustrated in Figure 1.13.

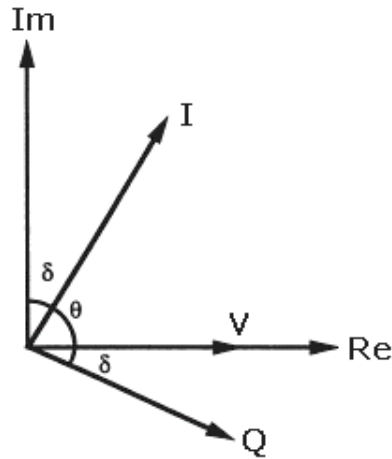


Figure 1.13: Phazor diagram for current and voltage.

The lag between the charge and the voltage is directly proportional to δ when the power dissipation is small. Also, in equation 1.11 ω is the angular frequency and $Z(\omega)$ is the impedance.

An important circuit used as a model for dielectric materials is a series resistor and capacitor in parallel with a capacitor, as shown in Figure 1.14.

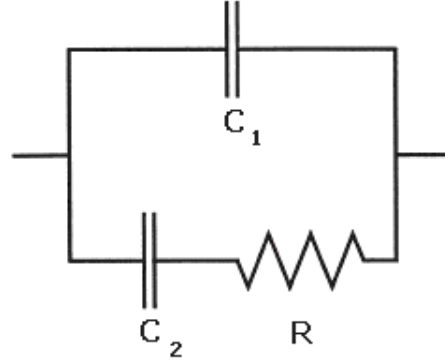


Figure 1.14: Resistor and capacitor in parallel.

From elementary circuit analysis, the impedance of this circuit can be determined:

$$Z = \left(\frac{j\omega C_1}{Rj\omega C_1 + 1} + j\omega C_2 \right)^{-1} \quad (1.12)$$

where C_1 and C_2 are the capacitances defined in Figure 1.14 . The relationship between the charge and the voltage is defined as the following [9]:

$$Q^*(\omega, t) = C^*(\omega)V^*(\omega, t) \quad (1.13)$$

where C^* is the complex capacitance. Therefore, the relation between impedance and capacitance can be determined for a sinusoidal varying current as:

$$Z(\omega) = \frac{1}{1 + j\omega C^*(\omega)} \quad (1.14)$$

From equations 1.12 and 1.14 the complex capacitance can be determined:

$$C^* = C_1 + \frac{C_2}{1 + \omega^2 C_2^2 R^2} - \frac{j\omega R C_2^2}{1 + \omega^2 C_2^2 R^2} \quad (1.15)$$

This form of the complex capacitance is identical to the form of the classical Debye solution for an ideal dielectric liquid. There are several ways to derive the

Debye equations based on the microscopic interaction of the dipoles with applied electromagnetic fields [9, 10]. The classical Debye description of an ideal dielectric liquid is useful to understand the physics behind the interaction of microwaves with materials at the molecular level. In the Debye description, a single molecule with a small electric dipole is assumed to be at the center of a spherical volume. When there is no electromagnetic field present, the dipoles are randomly oriented throughout the material. When the electromagnetic field is applied, the dipoles tend to orient in the direction of the electric field, as illustrated in Figure 1.15.

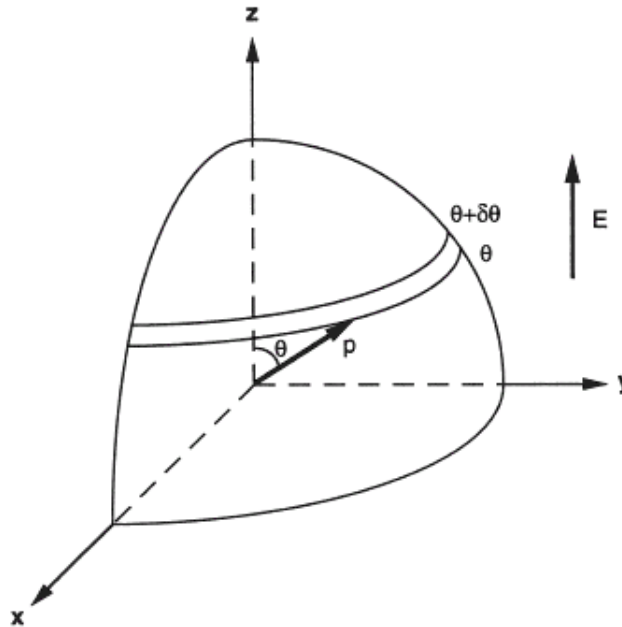


Figure 1.15: Model of a dipole used in the Debye description of an ideal liquid.

A force balance on the dipole yields the following equation:

$$I \frac{\partial^2 \theta}{\partial t^2} + C \frac{\partial \theta}{\partial t} - p E \sin \theta = 0 \quad (1.16)$$

where E is the magnitude of the electric field, θ , the angle between the dipole

and the microwave field, I , the dipole moment of inertia, C , the internal viscous damping within the material, and p , the dipole moment.

From the foregoing equation of motion, a statistical analysis of the dipole orientations could be considered, and the following relation for the complex dielectric constant can be obtained [10]:

$$\epsilon^* = \epsilon_\infty + \frac{\epsilon_0 - \epsilon_\infty}{1 + (\omega \tau)^2} - \frac{j(\epsilon_0 - \epsilon_\infty)\omega \tau}{1 + (\omega \tau)^2} \quad (1.17)$$

where ϵ_0 is the dielectric constant where the frequency is zero and ϵ_∞ is the dielectric constant where the frequency is infinite. This is identical to the form of equation 1.15 where the capacitance has been replaced by the dielectric constants.

The Debye solution for an ideal liquid is quite simplified and is often not applicable to many materials. The Debye model results in only one relaxation time, and often materials exhibit more than one relaxation time. As a result, more complicated models have been developed to describe the dielectric behavior of different types of materials [8]. The Debye model for dielectric properties is analogous to the Voigt and Maxwell models consisting of springs and dashpots that are used in polymer viscoelasticity, as shown in Figure 1.16.

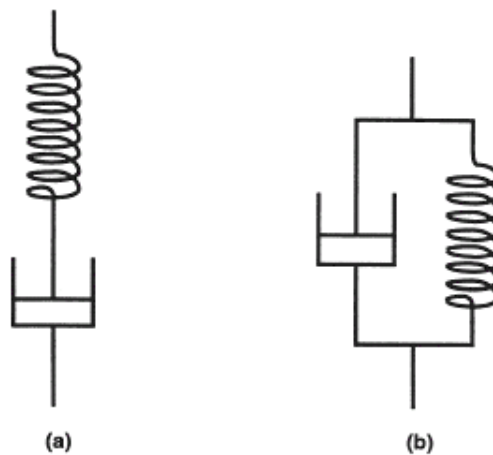


Figure 1.16: The (a) Maxwell and (b) Voigt models for viscoelasticity.

Although these models are often not applicable to many materials, they form the foundation from which more complicated models are formed. The phenomenon of relaxation in dielectric materials is analogous to viscoelasticity because the governing equations are of the same form [11]. Although the Debye model is simplified, it shows that the relaxation time is affected by the structure of the material. The ability of materials to heat is related to the ability of the dipoles to orient in the electromagnetic field, and this ability to orient defines the dielectric properties.

1.8.3 Energy Conversion

The dielectric properties of materials in combination with the applied electromagnetic fields result in the conversion of electromagnetic energy to heat. The power that is transmitted to an object can be determined by the use of the Poynting Vector Theorem [12], which can be derived from the Maxwell equations 1.2 and 1.3. The power that is transmitted across the surface, S , of a volume, V , is given by the real portion of the following equation:

$$\frac{1}{2} \oint_S \vec{E} \times \vec{H}^* dS \quad (1.18)$$

where $\vec{E} \times \vec{H}^*$ is the Poynting vector and $*$, in this case, denotes complex conjugate. Using the divergence theorem, the Maxwell equations 1.2 and 1.3, and by assuming materials properties for the volume the following equation can be obtained for the real portion of the Poynting power theorem:

$$\frac{1}{2} \int_V \left(\omega \mu^{\text{II}} \vec{H} \cdot \vec{H}^* + \omega \epsilon^{\text{II}} \vec{E} \cdot \vec{E}^* + \sigma \vec{E} \cdot \vec{E}^* \right) dV \quad (1.19)$$

where μ^{II} represents the imaginary component of the magnetic permeability and σ is the conductance. In dielectric materials, the magnetic permeability is usually small and the first term can be neglected. In addition, $\omega \epsilon^{\text{II}}$ can be considered

as an equivalent conductance [12]. If the electric field is assumed to be uniform throughout the volume, the following simplified equation for power, P , absorbed per unit volume can be obtained from equation 1.19:

$$P = 2\pi f \epsilon'' E^2 \quad (1.20)$$

As energy is absorbed within the material, the electric field decreases as a function of the distance from the surface of the material. Therefore, equation 1.20 is valid for only very thin materials. The penetration depth is defined as the distance from the sample surface where the absorbed power is $1/e$ of the absorbed power at the surface. Beyond this depth, volumetric heating due to microwave energy is negligible. Assuming the dielectric constant of free space is ϵ_0 , the penetration depth is given by the following equation [7]:

$$d = \frac{c \epsilon_0}{2\pi f \epsilon''} \quad (1.21)$$

The penetration depth and knowledge of how the electric field decreases from the surface are particularly important in processing thick materials. If the penetration depth of the microwave is much less than the thickness of the material only the surface is heated. The rest of the sample is heated through conduction. Equation 1.21 shows the dependence of the penetration depth on the frequency of operation.

Equations 1.20 and 1.21 give an insight as to which dielectric materials are suitable for microwave processing. Materials with a high conductance and low capacitance (such as metals) have high dielectric loss factors. As the dielectric loss factor gets very large, the penetration depth approaches zero. Materials with this dielectric behavior are considered reflectors. Materials with low dielectric loss factors have a very large penetration depth. As a result, very little of the energy is absorbed in the material, and the material is transparent to microwave energy. Because of this behavior, microwaves transfer energy most effectively to

materials that have dielectric loss factors in the middle of the conductivity range, as illustrated in Figure 1.17.

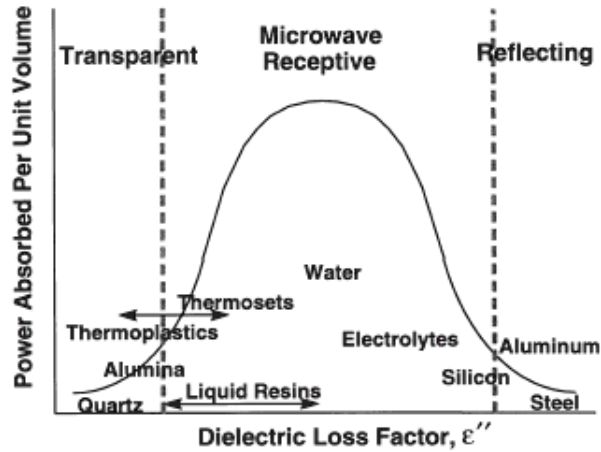


Figure 1.17: Relationship between the dielectric loss factor and ability to absorb microwave power for some common materials.

In contrast, conventional heating transfers heat most efficiently to materials with high conductivity.

Although equations 1.20 and 1.21 are useful for assessing the effect of electrical properties on microwave power absorption, material processing is much more complex. The dielectric properties are dependent on the mobility of the dipoles within the structure, and therefore the dielectric properties are functions of temperature, frequency, and, for reacting systems, degree of reaction. Therefore, the ability of the material to absorb energy changes during processing. For example, at room temperature silicon carbide (SiC) has a loss factor of 1,71 at 2,45 GHz. The loss factor at 695°C for the same frequency is 27,99 [13].

The phase shift of current in electrical circuits is analogous to how energy is dissipated in dielectric materials. As mentioned before, dipole polarization lags behind the electric field due to internal forces in the material. The phase shift,

δ , between the dipole displacement and the electric field result in dielectric losses. The in-phase component of the dipole displacement with the electric field is power absorbed by the dielectric material as heat. In alternating current electrical circuits, the current is out of phase with the voltage. The complex power is the product of the complex current and voltage [14]:

$$S = \vec{V}^* \vec{I}^* \quad (1.22)$$

where S is the complex power. If the preceding equation is rewritten in terms of the complex capacitance, as defined earlier, the following equation results:

$$S = j\omega C^* \vec{V} \vec{V}^* \quad (1.23)$$

where the real portion is the power dissipated in the electrical circuit. This is analogous to the Poynting power theorem in dielectrics.

Chapter 2

Experimental

In this chapter a description of materials, equipments and operative procedures will be presented.

2.1 Materials

The epoxy system investigated is composed by *EC 57*, a DGEBA¹ prepolymer based on bisphenol A and epichlorhydrin, and *K 21*, an aliphatic diammine² used as hardener agent, both supplied by *Elantas Camattini S.p.A.* This fluid, not charged, bicomponent epoxy-amine system is developed for the resin transfer moulding process.

2.1.1 Characteristics of Fresh Mixture

The characteristics of the epoxy system, before curing process, as illustrated in the technical datasheet are reported in Table 2.1.

¹See the section 1.2 on page 22.

²3,6,9,12-tetraazatetradecano 1,14 diamine.

Characteristic	Notes	Values
Colour of EC 57	–	Pale yellow
Colour of K 21	–	Pale yellow
Density at 25°C of EC 57	ASTM D 1475	1,14 – 1,16 g/ml
Density at 25°C of K 21	ASTM D 1475	0,99 – 1,01 g/ml
Weight ratio of K 21	For 100 g of resin	15 – 20 g
Viscosity at 25°C	–	500 – 800 cPs

Table 2.1: Characteristic of epoxy system before curing.

2.1.2 Characteristics of Epoxy System Conventionally Cured

According to technical datasheet the characteristics of the epoxy system, conventionally cured for 24 h at room temperature and following 15 h at 60°C are reported in Table 2.2.

2.1.3 Sample Preparation

In the work reported here formulation with 20 p.h.r. of K 21 into EC 57³ has been prepared.

For ensuring a good reproducibility of the test the same procedure has been repeated in every experiment.

Primarily the components of the mixture have been *weighted* on a technical scales. The reagents have been collected from their butts, with glass pipette, previously calibrated and poured in a polypropylene (PP) vessel. The first component introduced into the vessel has been K 21, because it is the limiting reagent.

³Corresponding to stoichiometric ratio.

Characteristic	Notes	Values
Colour	–	Amber
Density	ASTM D 792	1,09 – 1,12 g/ml
Hardness Shore	ASTM D 2240	87 – 88 D/15
Greatest T_g after 3 h at 100°C	ASTM D 3418	108 – 112°C
Linear shrinkage	–	1,70 – 2,20%
Water absorption	ASTM D570	0,80 – 1,00 %
Greatest exercise temperature	–	100°C
Flexural strength	ASTM D 790	85 – 95 $\frac{MN}{m^2}$
Greatest deformation	ASTM D 790	5,4 – 6,1 %
Flexural elasticity modulus	ASTM D 790	2600 – 2800 $\frac{MN}{m^2}$
Tensile strength	ASTM D 638	50 – 60 $\frac{MN}{m^2}$
Elongation at break	ASTM D 638	4 – 5 %
Compression strength	ASTM D 695	90 – 100 $\frac{MN}{m^2}$

Table 2.2: Characteristics of epoxy system cured, according to the supplier protocol.

Then the components have been mechanically and carefully *mixed* and *stirred*, with a steel spatula, until clear mixture has been obtained. During this phase, generally air bubbles are formed inside the mixture. For this reason the system has been submitted to a *degassing* treatment, under vacuum at room temperature for 20 min. In this way the bubbles rise to the surface of the mixture and then it is possible to remove them with a technical spoon, or directly during the microwave radiation.

During the mixture preparation the conversion is completely negligible.

2.2 Microwave Plant

The samples, microwave cured, have been polymerized using a microwave multimodal cavity produced by *Microglass s.r.l.* placed in the *Department of Materials and Production Engineering (DIMP) of University of Naples "Federico II"*.

This is a laboratory scale microwave oven, equipped with three heating mechanisms:

1. Hot air;
2. Infrared radiations;
3. Microwaves radiations.

These can be used singularly or in combined way. The exposure time, under infrared and microwave radiations, can be chosen by the user, selecting the sample-holder tray velocity and the total number of passages to perform or the time with immovable tray. Moreover the plant can be used with *moving* or *immovable* tray. In this second case the sample is fixed under the waveguide for a preset time in order to use the oven as a static cavity.

If the oven is used in static operative conditions the automatic cycle can be subdivided in three steps:

1. *Entrance*: in this phase the tray enters inside the radiations cavity with the velocity, selected by the user, passing under the infrared region. If the IR heating is active, during this phase the infrared lamp is turned on;
2. *Permanence under waveguide*: after entrance of sample-holder tray, the safety door is closed and the microwave generator is turned on. During this phase, the hot air heating is also active and is based on the temperature set by the user;
3. *Exit*: when the second phase is ended, the microwave radiations is turned off, and the tray goes out, with the velocity set by the user, crossing the IR region. The automatic cycle is finished.

If the oven is used in dynamic operative conditions the second phase foresees the *alternating forward and backward movement* of the tray under the waveguide for the number of passages and the velocity selected by the user.

2.2.1 Microwave Radiation System Mechanism

The principle of operation of a microwave oven can be schematically presented through three blocks: radiations generator, waveguide and applicator as illustrated in Figure 2.1. The *radiations generator* is a magnetron, an electronic tube, suitable for generate high powers in microwave field. The magnetron of the microwave oven used in this work can supply powers from 0,5 to 2 KW. It is provided of an electronic kit, that delivers energy only if inside the oven the appropriate safety conditions are satisfied. In case of out of order conditions the control panel provides to interrupt the microwave radiations, displaying an error message on the control panel and opening the safety door.



Figure 2.1: Schematic microwave oven structure.

The *waveguide* has the function of transferring the energy from the point in which it is generated to the point in which it is used, avoiding considerable losses. It is produced in metallic material so the radiations travel through subsequent reflections. The waveguide has the length proportional to the frequency of the waves propagating within. A schematic representation of a waveguide is illustrated in Figure 2.2.

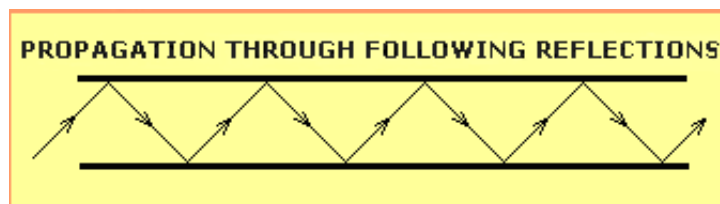


Figure 2.2: Wave propagation in a rectangular waveguide.

The *applicator* is the device used for the energy distribution on the workpiece. This is a structure expressly designed for the dielectric heating under microwave radiations. A good applicator carries out this task in an efficient, safe, reliable, repeatable and economic way. Generally the applicators can be subdivided in two categories

1. *monomodal*;
2. *multimodal*.

In monomodal applicators, at least one of their dimensions is of the order of the wave length, propagating within. For this reason the field conformation is well determined and relatively little influenced by the presence of the workpiece to heat.

While multimodal applicators are “box” with metallic walls much larger than the wave length used for the radiations. A schematic representation of a multimodal applicator is shown in Figure 2.3.

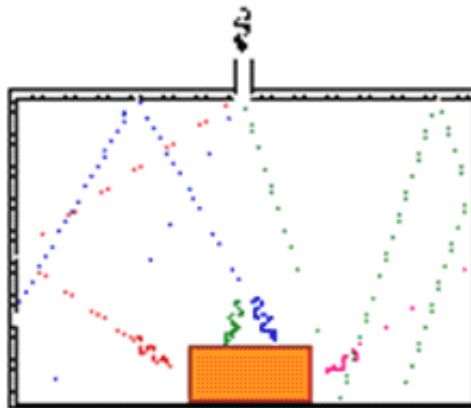


Figure 2.3: Multimodal applicator.

This structure is a *resonant* cavity, in which there are a lot of propagation modes and therefore the overlap of numerous waves, moving in different directions. This phenomenon is due to multiple reflections from the metallic walls. The introduction of a *mode stirrer*, formed by moving metallic surfaces, and the movement of the workpiece, improves the dielectric heating uniformity.

In the microwave plant used in this work there is a mode stirrer and the sample can be submitted to an alternating forward and backward movement. The microwave oven is provided of a system, that links together the waveguide with a monomodal applicator, both inserted in a multimodal cavity. This particular combination has been carried out for satisfying the features, required by the

equipments, used for example for dielectric heating, drying and polymerization.

The *cooling system* of the microwave oven is based on recirculation of air. This is inhaled from a fan, placed at the bottom of the oven, and then blown on electric resistances, and therefore put in the cavity, through a pipe, positioned at the begin of microwave region on the top of the cavity. In this way the temperature can be maintained at the value selected by the user.

The *temperature control* is devolved to a main PLC (Programmable Logic Controller). The PLC manages the electric resistances according to the signal received from temperature probes inserted in the inhaling system, and the value set by the user.

In Figure 2.4, 2.5, 2.6 and 2.7 are presented some pictures of the microwave oven used for performing the microwave experiments.

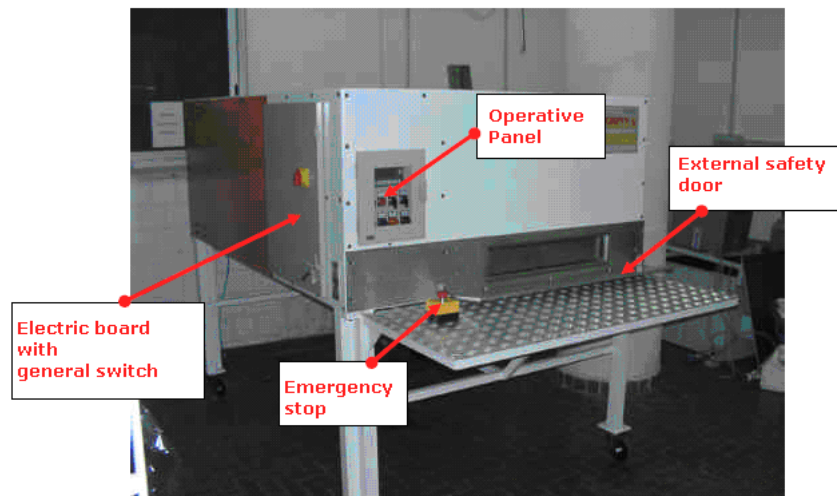


Figure 2.4: Front oven view.

Two schemes are reported in Figures 2.8 and 2.9, the first showing the microwave distribution inside the cavity and the second illustrating the position of the magnetron.

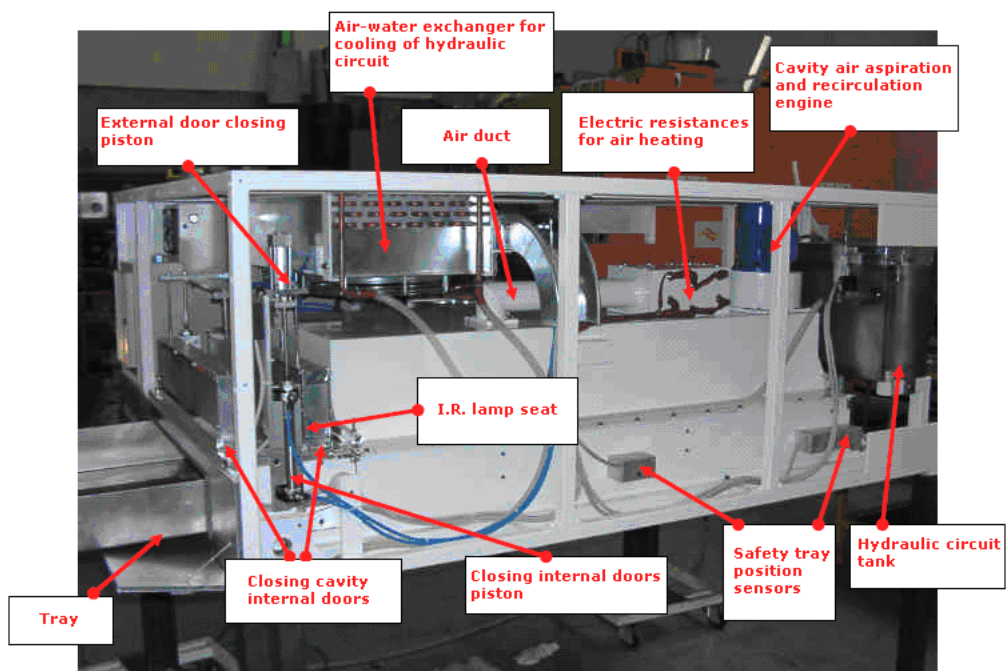


Figure 2.5: Right side oven view.

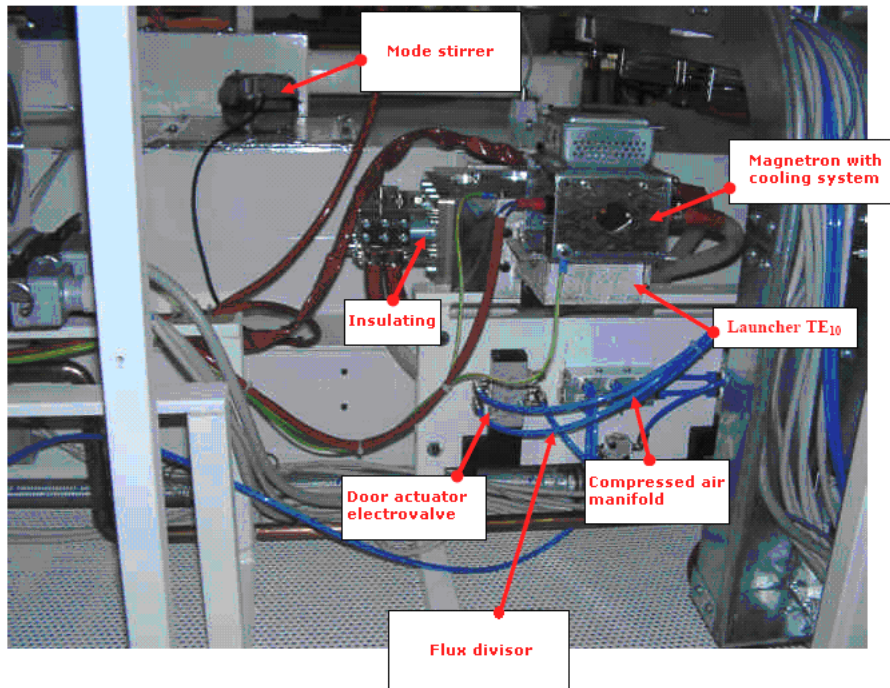


Figure 2.6: Left side oven view.

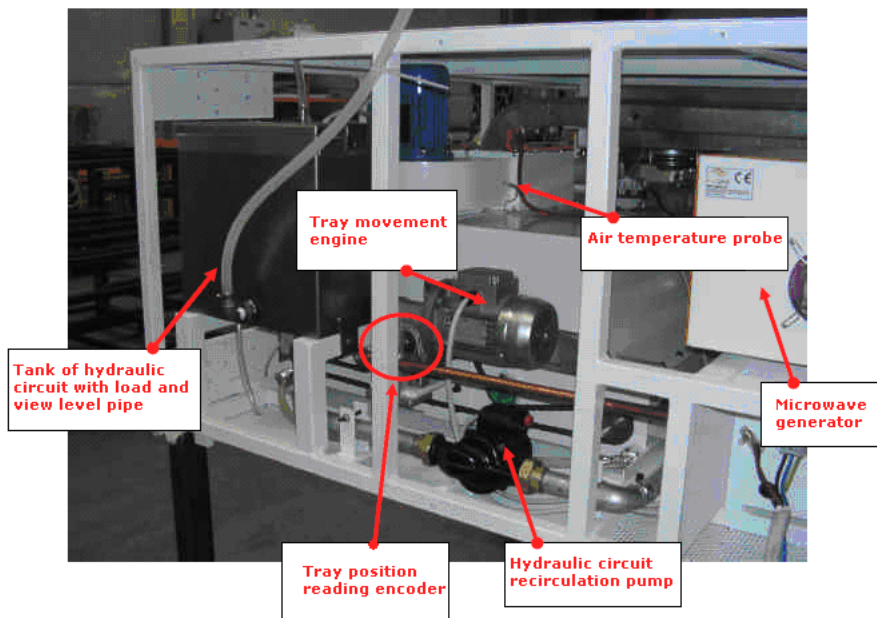


Figure 2.7: Back oven view.

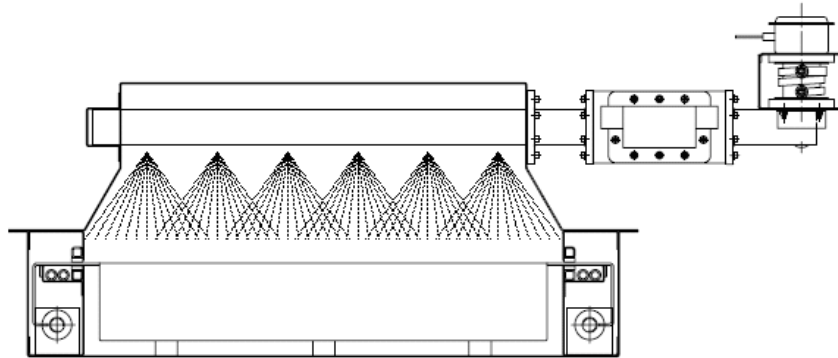


Figure 2.8: Front view and microwave distribution inside the cavity.

The microwave plant has a mode stirrer, ensuring at a distance from the metallic surfaces, an isotropic statistical distribution of electromagnetic field.

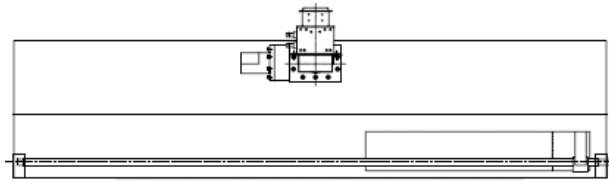


Figure 2.9: Side oven view and magnetron position.

2.2.2 VPMS

The microwave oven, produced by Microglass s.r.l. uses a *Variable Power Microwave System* (VPMS). While domestic microwave ovens use a *time-slicing* control system of the applied power. This last method enables the application always of the greatest power, but for time intervals proportional to the power selected by the user. For example, if a oven has a maximum power of 1000 W, and if an operator chooses to use the oven with the 25% of the maximum power, the time-slicing device applies a power of 1000 W for the 25% of the selected time. A

schematic comparison between the microwave working without and with VPMS is illustrated in Figure 2.10.

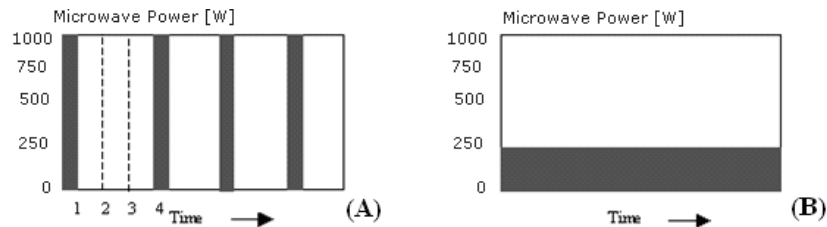


Figure 2.10: Scheme of power supplying in a microwave oven without (A) and with (B) VPMS.

While using a VPMS system, the power is applied *continuously* and it corresponds to the values set by the user. Considering again the above example, if an operator chooses a power of 25% of the maximum value, the VPMS system supplies 250 W for the whole cycle time, as illustrated in Figure 2.10 (B).

This system offers the main advantage of a more uniform sample curing, without the overheating, due to the application of the maximum power. Fu et al. [15] have investigated the power absorbed and reflected by epoxy samples, polymerized with the both power control systems, and they have demonstrated that a continuously power supplying ensures higher reaction rate.

2.2.3 Insulator

In the microwave plant produced by Microglass s.r.l. there is an electric insulator between the magnetron and the waveguide. Its operation is based on ferrites, placed in its centre, and dipped in a magnetic field, generated by two permanent magnets, collocated in the centre on the outside of the insulator.

The insulator performs two important functions:

1. Enables the operation of the magnetron in the best matching conditions,

regardless of the absorbing load, placed inside the applicator cavity. In this way the load impedance remains constant for the magnetron, that can supply always the same power;

2. Screens the magnetron from the electromagnetic waves, reflected by the load. This energy is switched on the dummy load⁴, positioned on the third door of the insulator.

2.2.4 Control Panel

The microwave plant is provided with a control panel with the following buttons:

- *Start cycle*: for beginning the automatic cycle;
- *Stop cycle*: for finishing the automatic cycle;
- *Selector manual/automatic*: switch from the manual to the automatic movement of the tray;
- *Tray in/out*: switch, that moves the tray forward or backward inside the cavity, when the manual selector is switched on.

On the control panel there are also the following informing lights:

- *Current*: white light, informing the turning on of prototype;
- *Radiation*: violet light, informing the turning on of microwave radiation inside the cavity;
- *Cycle error*: orange light, informing the presence of anomalies of the automatic cycle;

⁴Water load.

- *Emergency*: red light, informing an out of order working of the prototype.

On the control panel, there is a display, on which the main parameters of the microwave oven, useful for the automatic cycle are visualized. There are a couple of buttons, the first for opening the pages of the display and the second for changing the current value of the operative parameters.

Before programming the cycle is necessary to *initialize* the oven. The initialization occurs when the start cycle button is pushed and enables the determination of the movement limits. The tray goes inside the cavity, until it reaches the maximum limit, then the tray goes out assuming the position for the sample load.

The prototype is provided of an *emergency stop button* for safety reason, according to EN 60947-5-1 standard.

2.2.5 Automatic Cycle and Parameters Selection

A window, that resumes all the parameters of the automatic cycle, appears on the display after initialization process. All the parameters can be selected using the buttons $<$ and $>$ ⁵. These buttons enable the switching from one page to another. The parameters can be modified pushing the $+$ and $-$ buttons, on the corresponding page.

The parameters are:

- *Tray movement*: in this page, the operation of the oven with moving or immovable tray, and therefore in dynamic or static conditions, can be chosen;
- *Number of seconds with immovable tray*: the time of microwave radiation with immovable tray can be set in this page. The sample is placed under the waveguide for a time between 1 up to 9999 s;

⁵Placed on the sides of the display.

- *The number of tray passages in MW region:* if the oven operates with moving tray, the number of passages under MW region can be selected in this page. This value is shown on the display of the main window. On the left side the current passage is visualized, while on the right side there is the total number of passages. The number of passages must be included between 1 and 50;
- *Tray velocity in MW region:* in this page the tray speed through the MW region can be set. This velocity must be a percentage of the maximum speed, that is equal to 560 cm/min;
- *Tray velocity in IR region:* the tray speed under IR lamp can be selected in the same way of the MW tray velocity;
- *Microwave radiation:* in the main window the power [W], selected by the user, is shown. The power can be switched from 500 W up to 2000 W with a discrete step of 500 W. This is possible opening the power window;
- *Infrared heating:* in the main window the activation on or off of IR radiation is displayed, it is also possible to change this value opening the IR page. On the main window the velocity of the tray through IR region is also indicated;
- *Air temperature:* on the left side of the main window the effective air temperature [°C] circulating in the cavity is shown, while on the right side there is the value selected by the user. Opening the page corresponding to the air temperature, it is possible to modify this value in a range from 20 up to 80°C, using the + and – buttons.

Selected all the parameters the automatic cycle can be started, pushing the corresponding button. A green light appears in this button during the whole

automatic cycle. The cycle can be interrupted in any moment pushing the *stop cycle* button.

During the cycle the sample temperature can be monitored, through an IR sensor, placed in the centre above the microwave cavity. On the control panel there is a window for the visualization of the sample temperature during the microwave heating. In this page three values are shown:

1. The maximum temperature during the cycle max_C ;
2. The greatest temperature during every passage max_P ;
3. The sample temperature in the moment in which the workpiece passes under the IR sensor T_{old} .

2.3 Microwave Oven Characterization in Dynamic Operative Conditions

Before using the plant for curing the epoxy resin, some preliminary experiments have been performed for characterization, and therefore optimization of MW oven, working both with moving and immovable tray. In particular the identification of position on the tray, corresponding to the greatest electromagnetic energy density has been very important. This purpose has been performed, studying the electromagnetic energy distribution inside the applicator. Figure 2.11 shows a three-dimensional system of coordinates with origin in the centre of tray, introduced for the correct detection of the position in the volume, described by the tray.

The basis of the tray illustrated in Figure 2.11 is a square surface of 60 cm of side. On this surface a grid of 6 rows and 6 columns has been drawn. In this way 36 squares of 10 x 10 cm have been cut out.

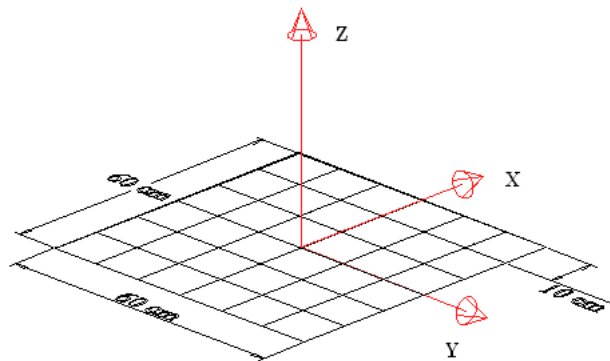


Figure 2.11: Surface of the oven tray with grid and three-dimensional Cartesian coordinates system.

The use of the grid and the experiments illustrated below have been performed for determining:

- The position in which placing the sample;
- Influence of tray velocity on the dielectric heating;
- Calibration of the IR sensor.

2.3.1 Sample Position

The position on the x-y surface in which placing the sample has been determined, taking into account two important aspects, both for the microwave oven characterization, and for carrying out the experiments with the epoxy system:

1. The maximum energy density;
2. The reading cone, individuated by the IR sensor.

In fact for exploiting the full potentiality of the oven it is necessary to place the sample in the position of maximum energy distribution. Moreover since the microwave plant is provided of an IR sensor for the temperature measurement, it

is also important to position the sample along the reading cone of this sensor, especially when the oven is used with moving tray and there are not other reliable temperature monitoring systems⁶. In fact recording the temperature profile, during the curing process, is useful for the kinetic study and for a comparison between microwave and DSC crosslinking reaction⁷.

2.3.2 Energy Density Distribution

The MW oven is provided of a system of vertical electromagnetic energy distribution inside the cavity, as illustrated in Figure 2.8. A mapping of applicator has been carried out for detecting the effective distribution of energy inside the cavity. Therefore some experiments have been performed for determining the dependence of energy density distribution along x-y and z axes. These experiments are based on the reasonable hypothesis that the energy density in any given position is proportional to the temperature raising of a fixed amount of a sample microwave sensitive, like tap water, when heated inside the oven, operating in the same conditions, and placed in this position.

For the first case a cylindrical beaker of polypropylene of a total volume of 250 ml has been used. Vessels of PP have been selected, because they are transparent to microwaves, have a good thermal resistance⁸, are enough cheap and not very fragile. The repetitive unit of PP is illustrated in Figure 2.12. Polypropylene is a growth-step propylene polymer. It has an isotactic structure⁹, with elevated crystallinity. The isotactic omopolymer is very crystalline, and therefore it has a little transparency. While adding the 1,7% of ethylene a long copolymer, with random groups distribution, is obtained. This copolymer is very used as vessel

⁶See the section 2.5 on page 83.

⁷See the section 3.3 on page 113.

⁸ $T_f = 180^\circ\text{C}$.

⁹Every group is on the same side of the backbone.

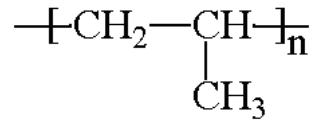


Figure 2.12: Repetitive unit of polypropylene.

in domestic microwave ovens for food heating. In fact the crystallinity variation makes the material very transparent.

The beaker has been filled with tap water for a total volume of 250 ml. The initial water temperature has been measured with a digital thermocouple. Therefore the beaker has been placed, first in the centre of the vessel, and then in position always more peripheral. The Figure 2.13 shows a schematic representation of the beaker distribution on the tray surface.

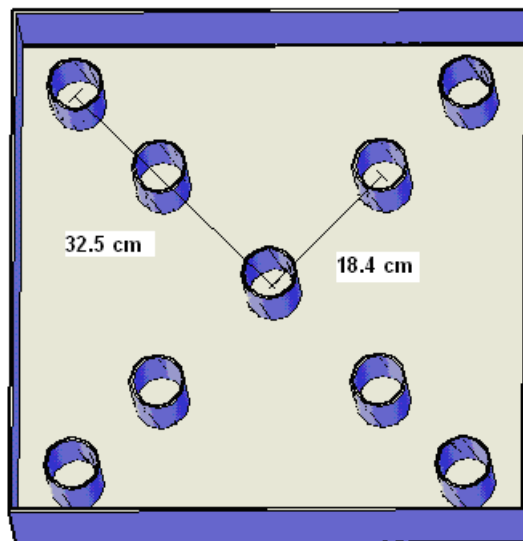


Figure 2.13: Beaker distribution on the tray surface.

Beaker has been cooled and the water substituted, after each cycle. A cycle with the parameters reported in Table 2.3 has been set. The water temperature has

been measured after each cycle. The results are illustrated in the Figure 2.14.

Parameters	Value
MW radiation time	120 s
Irradiated power	2000 W
Tray velocity in MW region	224 cm/min
IR heating	OFF
Air temperature	25°C

Table 2.3: Microwave oven parameters, selected for the determination of the energy density distribution in dynamic operative conditions.

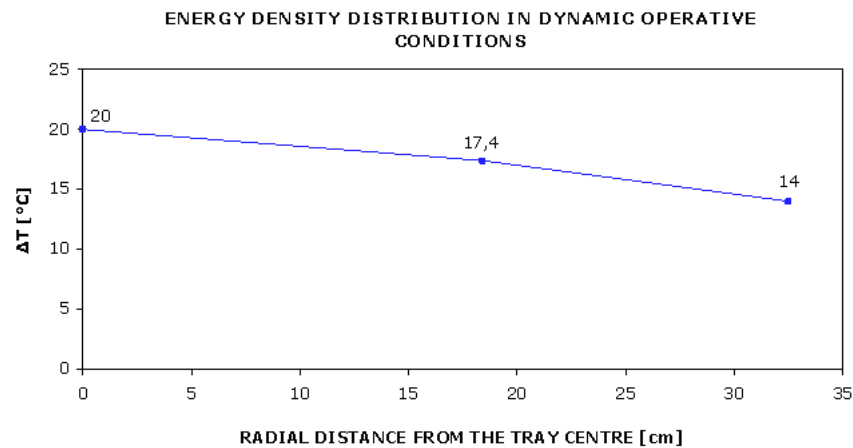


Figure 2.14: Plot of energy density distribution along x-y plane, in dynamic operative conditions.

In the centre the average temperature increase is higher and equal to $\approx 20^{\circ}C$, while in the corners, at a radial distance from the centre of about $32,5\text{ cm}$ the ΔT is $\approx 14^{\circ}C$. In a semiperipheral region at a distance from the centre of $18,4\text{ cm}$ the temperature raising is intermediary between the other two and equal to $\approx 17,4^{\circ}C$.

From the Figure 2.14 an almost linear decreasing profile of the energy density in function of the distance from the centre is observed.

For the study of dependence of energy density distribution in function of z coordinate a beaker of PP of a volume of 50 ml filled with 50 ml of tap water has been used. The beaker full of water has been placed in the first phase directly on the basis of the tray in the centre and subsequently in position always more peripheral and finally in the corners. In the second phase the beaker has been placed over a cylindrical glass pedestal of 1, 2 and 3 cm of height, but in the same x-y positions. The thermal gradient of the water has been measured with a digital thermocouple after an automatic cycle, with the parameters listed in Table 2.3. Three measurements have been performed for every thermal gradient for a more reliability of data. The same x-y-z Cartesian coordinates systems, showed in Figure 2.11, has been used for detecting the beaker position into the applicator cavity. The results are illustrated in Figure 2.15.

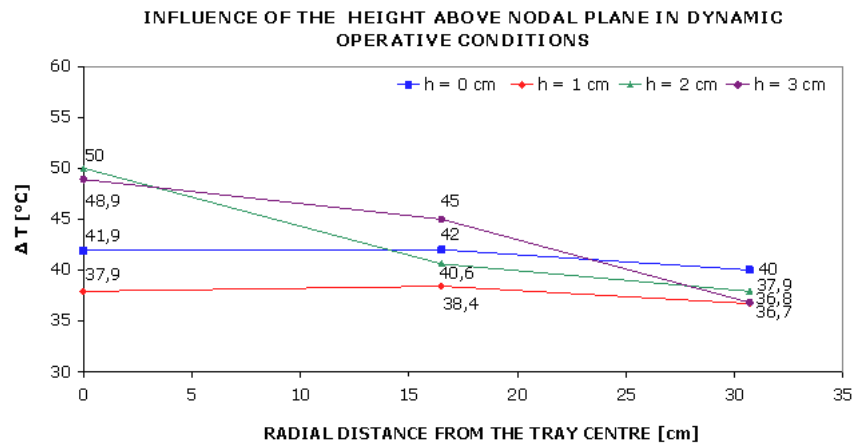


Figure 2.15: Influence of the height and the radial position on dielectric heating of beaker of water, in dynamic operative conditions.

The thermal gradients $\Delta T_{\text{average}}$ in function of radial distance from the centre have been reported. The $\Delta T_{\text{average}}$ are the temperature rise $T_f - T_i$ for every height,

in the centre and for the radial distances of $16,5$ and $30,7$ cm, evaluated as an average of measured values.

While the ΔT^* are the difference of $\Delta T_{\text{average}}$, when the beaker is placed at 1 , 2 and 3 cm of height and the $\Delta T_{\text{average}}$, when the beaker is positioned on the tray at $z = 0$.

The profile of ΔT^* is shown in Figure 2.16.

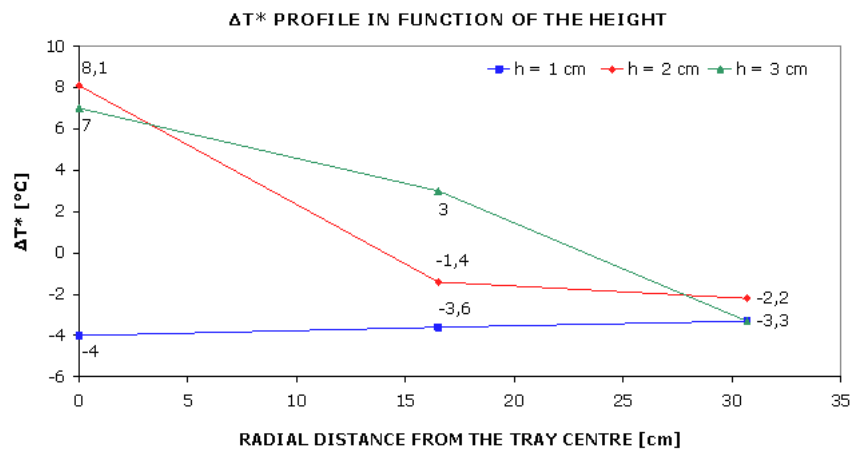


Figure 2.16: ΔT^* measured at 1, 2 and 3 cm of height above the tray surface.

Therefore, reassuming the results illustrated in Figures 2.14, 2.15 and 2.16, the position of maximum energy density is in the *centre of the tray surface at 2 cm of height*. For this reason in all the experiments with the microwave oven operating in dynamic conditions the sample has been collocated in this position.

2.3.3 Influence of the Tray Velocity

The tray velocity in the MW region is another parameter that must be selected before starting the cycle. The influence of this parameter on the dielectric heating has been studied. The experiments have been carried out using a beaker of a volume of 250 ml with the same quantity of tap water. The beaker has been placed

in the centre of the tray. The initial and final temperature has been measured, using a digital thermocouple after a cycle under MW radiations with the operative conditions reported in Table 2.3. The velocity of the tray has been modified in every cycle, starting from the safety value of 224 cm/min, equivalent to the 40% of maximum velocity up to 560 cm/min, that is the greatest tray velocity. The number of tray passages has been modified in a way to maintain constant the time of exposure under MW radiation. Velocities less than 224 cm/min have been discarded, because there is the hazard that the hermetic door of the applicator¹⁰ could hit the tray not completely entered in the cavity. Figure 2.17 illustrates the obtained results.

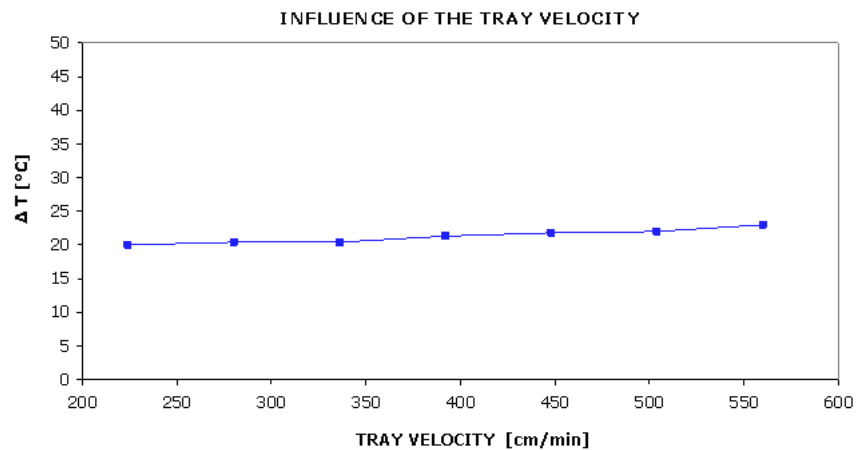


Figure 2.17: Influence of the tray velocity on the temperature increase.

The tray velocity does not exert any meaningful effect on the dielectric heating. While the *time of MW radiation* is the key parameter for the temperature raising.

¹⁰That is automatically closed.

2.3.4 Location of the IR Sensor Reading Cone

In dynamic operative conditions the sample temperature measurement, under MW radiation is devolved upon an IR sensor.

In fact, in this conditions, the use of the datalogger is not possible as explained in the section 2.5 on page 83.

While at the begin¹¹ and the end¹² of the cycle the temperature has been measured with a digital thermocouple, during the microwave heating process the temperature can be read by the IR sensor, placed in the centre of the oven on the top of the applicator cavity.

For this reason the width of the reading cone and the trustworthiness of the measured data have been determined.

The system is not monitored continuously, but only when the workpiece is under the IR beam, due to the movement of the tray, that goes forward and backward along y-direction, during the automatic cycle. Therefore the IR sensor provides temperature measurements, whose maximum values correspond to the passage of the sample under the sensor.

Before everything the reading corridor, described by the beam, emitted by the IR sensor has been located for determining the best position for temperature monitoring. This purpose has been accomplished using a PP beaker of 50 ml of tap water. The beaker has been submitted to microwave radiation with the operative conditions listed in Table 2.3.

In every experiment the water has been substituted, carrying back the temperature at room value.

The Cartesian grid has been used for a more reliable detection of the best position and the relative distance from the boundary of the tray. The sensor does

¹¹Before loading the workpiece.

¹²When the sample goes out from the internal cavity.

not read the water temperature, when the beaker has been placed at increasing distance from the centre, along x-direction¹³. While the sensor is able to read the water temperature, if the beaker is put in the tray centre or shifted along y-direction. This investigation has allowed the identification of a reading corridor of about 2 cm along the centre of the tray in the y-direction.

The diameter of the vessel used for the curing processes is of about 5 cm. Therefore if the workpiece is placed in the position (0,0,z) the temperature, shown on the display of the control panel¹⁴ is the actual sample temperature and not an average, between the tray and the sample.

2.3.5 IR Sensor Calibration

In dynamic operative conditions the IR sensor has been used for monitoring the sample temperature, because is unthinkable to interrupt the cycle¹⁵ at regular time for measuring the temperature with a digital thermocouple, and it is not possible to use the datalogger, as explained in the section 2.5, on page 83. Moreover during the MW exposure the temperature can not be measured using a thermocouple, without an electromagnetic screen, because the microwaves can induce strong currents along the thermocouple metallic wires, causing its breakdown. Analogous consideration for mercury thermometers. While the alcohol thermometers are not sufficiently reliable, because this liquid can interact with the applied electromagnetic field, absorbing part of the supplied energy. The IR temperature monitoring system can be considered suitable. *However this measurement depends on the material reflexivity coefficient.*

After location of IR sensor reading corridor, the reliability of the data provided

¹³That is perpendicular to that of the tray movement.

¹⁴That is the value measured by the IR sensor.

¹⁵And so on the curing process.

by the sensor has been verified. In fact during the experiments for microwave oven characterization, a discrepancy between the *water* temperature measured with digital thermocouple and with the IR sensor has been noticed. Particularly for elevated temperatures¹⁶, the sensor marks a value lower of $\approx 20^{\circ}\text{C}$ than that measured by digital thermocouple at the end of the cycle. Therefore temperature measurements for the IR sensor calibration have been performed on a wood surface and on the liquid epoxy prepolymer EC 57. These materials have been chosen, because they are microwave sensitive and are representative of the two states of the sample, liquid and solid, before and after the curing process.

The first sample is a *wood* table of 200,3 g of weight and 30 x 20 x 0,8 cm of size.

The second sample is the epoxy prepolymer EC 57 of a volume of 50 ml, poured in a PP vessel of 180 ml of capacity.

In both the cases the difference between the temperature values measured by a digital thermocouple and the maximum temperature reading, provided by the IR sensor, has been estimated. This difference has been indicated as ΔT^* .

For the wood six tests have been performed with constant values of tray velocity and air temperature, without IR heating, but with different powers and radiation times, as reported in Table 2.4.

In this Table there are some apparent contradictory results, for example with a power of 1000 W the wood temperature raising is lower than that with 500 W¹⁷. This can be explained, because the initial wood temperatures are not the same. The same results are shown in the Figure 2.18.

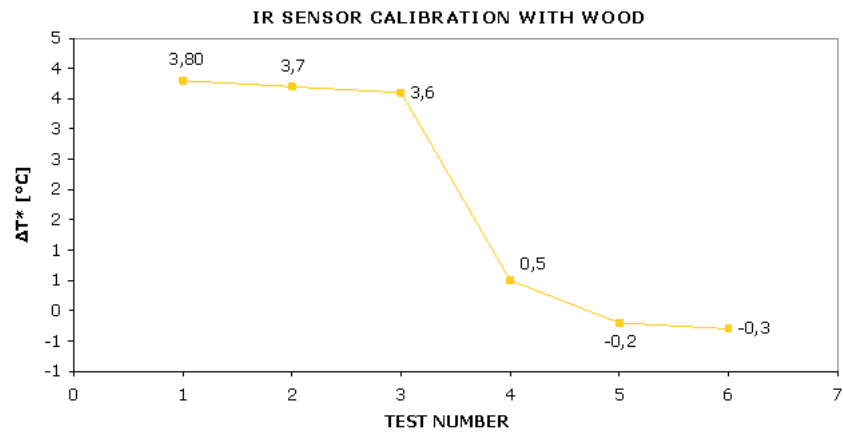
For the epoxy prepolymer EC 57 five tests have been carried out with the parameters listed in Table 2.5.

¹⁶Greater than 70°C .

¹⁷With the same operative conditions.

Test number	1	2	3	4	5	6
MW radiation time [s]	300	300	300	300	450	600
Irradiated power [W]	500	1000	1500	2000	2000	2000
Tray velocity [$\frac{\text{cm}}{\text{min}}$]	224	224	224	224	224	224
IR heating	OFF	OFF	OFF	OFF	OFF	OFF
Air temperature [°C]	25	25	25	25	25	25
Thermocouple temperature [°C]	38,8	38,7	43,6	45,5	51,8	52,7
IR sensor temperature [°C]	35	35	40	45	52	53
ΔT^* [°C]	3,8	3,7	3,6	0,5	-0,3	-0,3

Table 2.4: Parameters selected for IR calibration with wood.

Figure 2.18: Plot of ΔT^* obtained with a wood surface.

Test number	1	2	3	4	5
MW radiation time [s]	30	60	90	120	150
Irradiated power [W]	500	500	500	500	500
Tray velocity [$\frac{\text{cm}}{\text{min}}$]	224	224	224	224	224
IR heating	OFF	OFF	OFF	OFF	OFF
Air temperature [$^{\circ}\text{C}$]	25	25	25	25	25
Thermocouple temperature [$^{\circ}\text{C}$]	29,9	36,7	45,6	49,6	51
IR sensor temperature [$^{\circ}\text{C}$]	28	38	47	51	52
ΔT^* [$^{\circ}\text{C}$]	1,9	-1,3	-1,4	-1,4	-1

Table 2.5: Parameters selected for IR calibration with EC 57 epoxy prepolymer.

The liquid resin temperature has been measured, placing the thermocouple probe on the bottom of the beaker in order to use always the same spatial reference. The obtained results are illustrated in Figure 2.19.

Both for wood surface and for epoxy prepolymer the ΔT^* decreases, and so on a best agreement is achieved, enhancing the material temperature.

For higher temperature¹⁸ other measurements have not been necessary, because in this case a good agreement between IR sensor and digital thermocouple reading has been noticed.

The only limitation of the IR sensor is its unreliable temperature monitoring at low temperature¹⁹ for liquid material, like water. For this reason the temperature measured with digital thermocouple²⁰, before starting the automatic cycle, has been used for the sample thermal profile determination.

¹⁸Greater than 100 $^{\circ}\text{C}$.

¹⁹Lower than 30 $^{\circ}\text{C}$.

²⁰Generally 25 $^{\circ}\text{C}$.

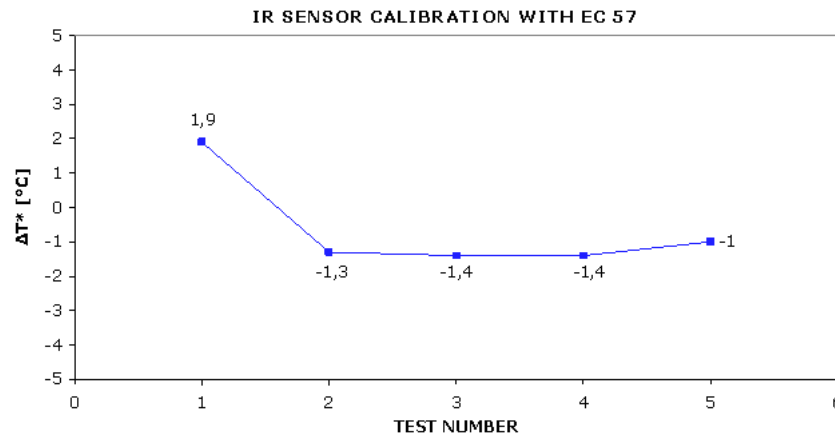


Figure 2.19: Plot of ΔT^* obtained with 50 ml of EC 57 epoxy prepolymer.

2.4 Microwave Oven Characterization in Static Operative Conditions

The investigation of the energy density distribution on the sample-holder tray, when the oven operates as a static cavity, has been performed with the same procedure, illustrated in the previous section.

Also in this case the position of greatest energy density is the centre of the tray at 2 cm of height.

Since the IR sensor is placed 5 cm behind the waveguide²¹, for monitoring the sample temperature during the microwave cure process with the IR sensor it is necessary to collocate the workpiece in the position (0,-5,2) [cm]. In fact, although in static operative conditions the temperature is recorded in more carefully by the datalogger, described in the section 2.5 on page 83, also the reading provided by the IR sensor is important.

The energy density in the position of (0,0,2) [cm], in which the sample is placed

²¹Positioned in the centre of the applicator cavity.

during the experiments performed with movable tray has been compared with that read in the point of coordinates (0,-5,2) [cm], that is the position used when the microwave oven operates as a static cavity.

Experiments have been carried out using beaker filled with tap water and the microwave oven parameters listed in Table 2.6.

V_{water}	25 ml
MW radiation time	60 s
Irradiated power	1500 W
IR heating	OFF
Air temperature	25°C

Table 2.6: Parameters selected for energy density comparison between positions of coordinates (0,0,2) and (0,-5,2) [cm].

In the first case microwave automatic cycles have been performed with a velocity of 224 cm/min and the beaker placed in the position of (0,0,2) [cm]. The average temperature increase $\Delta T_{\text{average}}$ of 29,6°C has been measured.

While the $\Delta T_{\text{average}}$, arising from experiments, carried out, using the same parameters, but with immovable tray and putting the sample in the point of coordinates (0,-5,2) is equal to 24,1°C.

Therefore the energy density in the point of coordinates (0,0,2) when the oven works in dynamic operative conditions is greater of the 22,82% than that in the position of (0,-5,2) when the oven is used as a static cavity.

This consideration is useful for a suitable comparison of the microwave cure processes carried out in the two different conditions.

2.5 Datalogger

This is a device for in situ real-time monitoring of the sample temperature and electromagnetic field intensity during the microwave cure process.

It consists of an hermetic aluminum box, containing electronic circuits, conveniently screened against electromagnetic interferences, with a radio absorbing trimming.

The datalogger operation is based on a PIC18 Microchip, on which the software for managing the acquisition, storage and transfer of the information to the PC is installed. In the Figures 2.20 and 2.21 the inner and outer view of the datalogger are presented.



Figure 2.20: Datalogger electronic circuits.

The probe for the temperature measurement is a thermocouple stem of a diameter of 1 mm, with a mineral insulation and an AISI 310 stainless steel outer shell, stretching out from the box. The probe can measure a greatest temperature

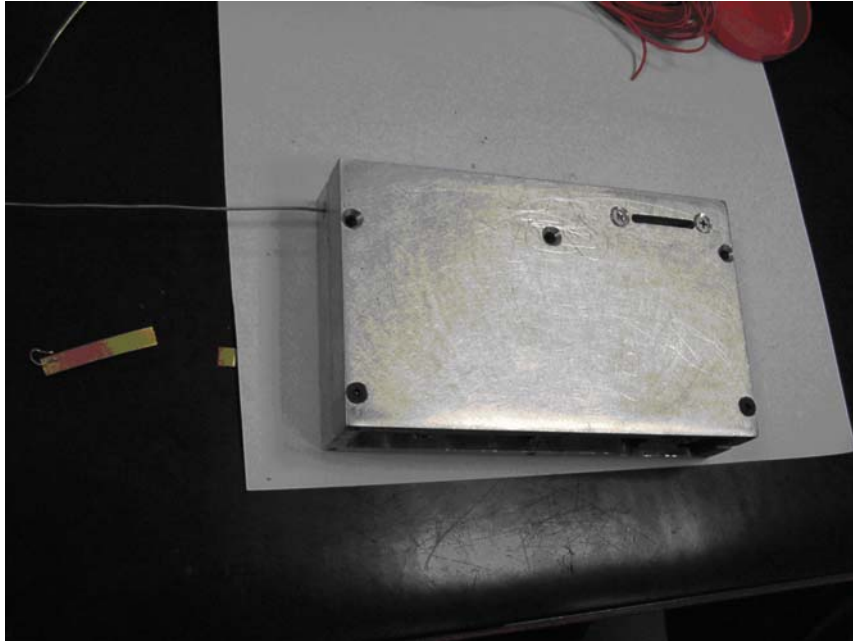


Figure 2.21: Datalogger outer view.

of 1100°C. While the electromagnetic field intensity is measured using a small MACOM MA4E2054 antenna, placed under a red strip. The antenna is followed by a suitable conditioning circuit. It enables the conversion of the received signal ranging between 0 and 5 V.

The datalogger records the sample temperature and the EM field intensity every 0,5 seconds. These data can be saved on a PC both in text and Microsoft Office Excel format.

After preliminary testing the most suitable operative conditions for using the datalogger have been determined.

For decreasing the electromagnetic field intensity on the receiving antenna the red strip has been covered with several layers of aluminum adhesive tape and the logger has been placed on a wet sponge with the red strip turned down. For the

same reason a wood²² table of the same logger size has been put on it.

For improving the reliability of temperature measurement the tip of the stem has been spread with thermoconductive oil. The tip has been placed under the bottom of the vessel for avoiding mechanical and electrical interferences with the epoxy mixture. The sample has been positioned on a disc of teflon at about 2 cm of height.

The aluminum box has been hermetically closed for preventing the damage of the electronic circuits.

The datalogger has been used only during the experiments performed in static operative conditions, because with movable tray two unwanted phenomena occur:

1. Mechanical vibrations impeding an accurate temperature measurement;
2. Onset of parasitic electric currents along the stem generating remarkable temperature overshoots.

2.6 Optimization of the Process Conditions

For exploiting the full potentiality of the microwave oven²³ for the polymerization of the epoxy system it is necessary to place the sample in the centre of the applicator cavity at 2 cm of height, when the plant operates with moving tray, or in the position of coordinates (0,-5,2) [cm], when the it works as a static cavity. In dynamic operative conditions the tray velocity of 224 cm/min has been also selected for safety reason.

A preliminary qualitative optimization of the operative conditions has been carried out for the best performance of the microwave curing processes.

²²Material microwave sensitive.

²³As verified through its characterization.

2.6.1 Vessel Material

The first parameter under investigation has been the *material of the vessel* containing the reacting mixture.

The main requirement that the material must satisfy is the transparency to microwave. In fact these materials do not get warm directly, when radiated, and instead allow the absorption by the sample of the maximum quantity of the available energy.

Materials reflecting the radiations, as metals, must be absolutely avoided.

Moreover the vessel material must be inert to polymerization reactions and sufficiently resistant to high temperatures.

The first qualitative tests have been performed using transparent commercial glasses of polystyrene (PS), a thermoplastic polymer with a $T_g \approx 100^\circ\text{C}$ and a $T_m \approx 270^\circ\text{C}$. However in some cases during the curing process temperatures higher than 160°C have been reached. Therefore the PS vessel has undergone the glass transition, with consequent mechanical stability loss and following softening.

For this reason vessels of PP have been chosen, because polypropylene is a thermoplastic polymer, microwave transparent, with a good thermal resistance²⁴, and it preserves its mechanical properties up to the melting point at a temperature of about 180°C . However the best material for carrying out microwave experiments is polytetrafluoroethylene, because it microwave transparent, very non reactive, it has an elevated mechanical stability and excellent antiadhesive properties, but it is very expensive. In Table 2.7 a summary of the properties of some materials, when used as vessels for microwave experiments, is reported.

Therefore the experiments for the kinetic analysis have been performed with PP cylindrical vessels of the size reported in Table 2.8. The vessels, placed on a glass pedestal of 2 cm of height, has been cut at about 4-5 cm of height for enabling

²⁴ $T_g \approx -17^\circ\text{C}$.

Material	Behaviour	Notes
Metals	Absorbing/Reflecting	Hazard of electric discharges
Glass	Transparent	Not reusable
Cellulose	Transparent/Absorbing	Energy dissipation
Polyethylene	Transparent	Low thermal resistance
Polypropylene	Transparent	Suitable
Polystyrene	Transparent	Low thermal resistance

Table 2.7: Properties of some materials used as vessel for microwave experiments.

the entrance inside the applicator cavity²⁵.

PP beaker Geometry	
Shape	Cylindrical
Volume	180 ml
Height	8 cm
Diameter	5 cm

Table 2.8: Shape and size of the PP vessel used for microwave experiments.

While experiments for the dynamical-mechanical characterization have been carried out with a polytetrafluoroethylene mould of geometry described in Table 2.9.

²⁵That is 10 cm height.

Polytetrafluoroethylene Mould Geometry	
Shape	Parallelepiped
Length	150 mm
Width	150 mm
Thickness	4 mm

Table 2.9: Shape and size of the polytetrafluoroethylene mould used for dynamical-mechanical characterization.

2.6.2 Influence of the Air Temperature

The *air temperature* inside the microwave oven cavity exerts a meaningful effect on the cure process of the epoxy system. This parameter can be selected at the beginning of the automatic cycle in a range from 20 up to 80°C, but for safety reason it is not advisable to overcome for a long time the temperature of 60°C. Some qualitative experiments have been carried out with sample of thickness of 1 cm, submitted to the same power and radiation time, and changing only the air temperature. In Table 2.10 the parameters of the performed tests are reported.

Test	T _{air} [°C]	Power [W]	Tray Velocity [$\frac{\text{cm}}{\text{min}}$]	IR	Time [s]
1	60	2000	224	OFF	600
2	50	2000	224	OFF	600
3	40	2000	224	OFF	600
4	30	2000	224	OFF	600

Table 2.10: Parameters selected for investigating the influence of the air temperature.

In every test the sample has been completely cured, assuming different colours

in function of the air temperature, as illustrated in Figure 2.22.

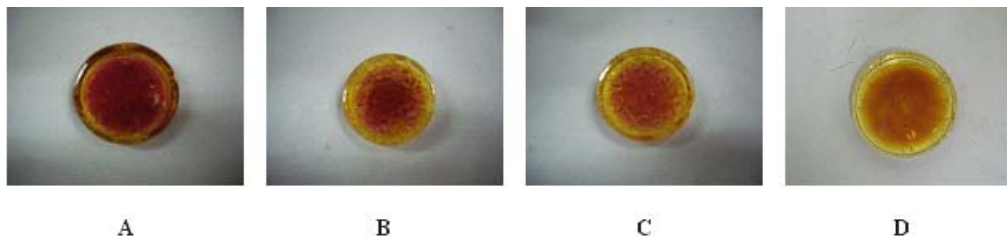


Figure 2.22: Samples cured with 2000 W for 10 min and with air temperature of 60°C (A), 50°C (B), 40°C (C), 30°C (D).

The crosslinking reaction begins more quickly at higher temperatures, with a consequent thermal degradation of the cured system. Decreasing the air temperature the colour of polymerized sample is lighter, as illustrated in Figure 2.22. The centre of each sample is of dark red, because this is the region that dissipates, in the worse way, the heat generated during the reaction.

A sample of 1 cm of thickness, with air temperature of 60°C, and without MW radiation, submitted to a cycle of 16 passages (4 min) appears very hard at the end of the cycle. As reported on the technical datasheet of Elantas Camattini S.p.A. 60°C is also the temperature, at which a conventional cure of 15 h can be performed. Moreover analyzing the curve of the specific heat flow versus temperature, obtained with a differential scanning calorimeter (DSC) test heating rate of 10°C/min, illustrated in Figure 2.23, about 60°C is also the onset temperature²⁶.

Finally a temperature of 25°C has been selected for performing the experiments in order to avoid the hazard of thermal degradation of the sample.

²⁶The temperature at which the steepest portion of the curve begins.

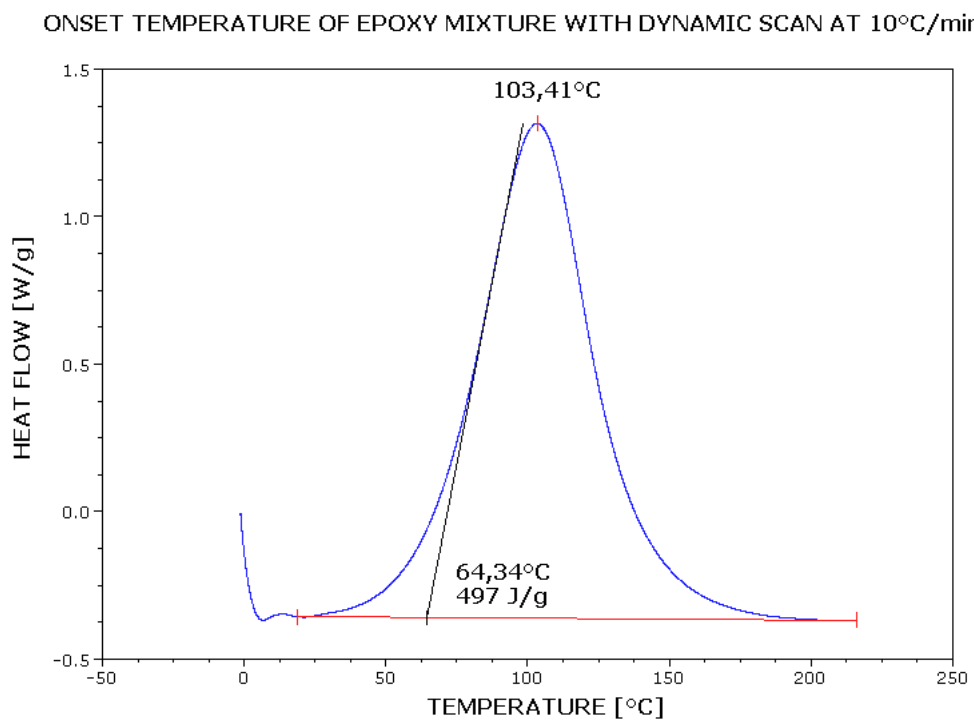


Figure 2.23: Onset temperature of a fresh epoxy mixture, measured with a DSC dynamic scan at 10°C/min.

2.6.3 Influence of the Mixture Thickness

The *thickness of the sample* is another parameter investigated. This is a factor of great importance for the heat exchange and therefore for the curing process.

The crosslinking reaction does not start for samples of thickness less than 1 mm, and also increasing the time of MW radiation the material appears sticky²⁷. The reason seems to be, that quantity so small of epoxy resin absorbs very badly the MW radiation. While there is the hazard of thermal degradation of samples of thickness higher than 1 cm.

Epoxy resin has a low thermal conductivity and therefore the energy dissipation is not efficient with mixture of high thickness.

Finally a thickness of about *1-2 mm* and a power of *1500 W*, have been recognized as the best combination for ensuring a good energy transfer between the microwave radiation and the epoxy samples.

2.6.4 Influence of other parameters

There are moreover other parameters, that can influence dielectric heating of a sample, some of these are reported below:

- *The geometry*: samples of regular shape can be heated more quickly;
- *The moistness*: the dielectric loss and so on the heating rate are higher when there is a great amount of water;
- *The ionic concentration*: the presence of high ionic concentration increases the heating rate;
- *Phase transitions*: phenomena like transition from ice to liquid water, crystallization, viscosity changes can modify significantly the capacity of a ma-

²⁷That is an indication of not complete conversion.

terial of absorbing electric energy and then the transformation of energy to heat;

- *Specific heat coefficient*: this parameter can determine apparently dysfunctional behaviour of samples undergoing dielectric heating;
- *Frequency*: the frequency of MW radiations are fixed at values of 915 MHz or 2,45 GHz. The first one is more indicated for solid samples of big dimensions, while the second is more suitable for samples in a liquid state or of small dimensions;
- *Power*: the power generated in industrial microwave plants ranges from 2 to 100 KW. As expected the heating rate increases with the power. However an excessive heating rate can cause the formation of non uniform products and of various imperfections;
- *Mode stirrer*: these are devices for generating perturbation of electromagnetic field inside the applicator cavity for improving its uniform distribution.

Chapter 3

Results and Discussion

The objective of the work reported here is to study an alternative curing process of epoxy systems based on microwave dielectric heating. The possible advantages of this crosslinking mechanism, in comparison with thermally activated process, have been investigated through the following techniques:

- Kinetic analysis;
- Final properties characterization.

The kinetic analysis of the epoxy resin is important both for a better understanding of structure-property relationships and for optimizing the processing conditions. In fact the physical and mechanical properties of the system largely depend upon the extent of cure, while their processability is dependent on the rate of polymerization.

While the characterization of the final properties enables a direct comparison of the efficiency of the microwave versus conventional curing process.

In this chapter the experimental results and analysis and elaboration of the data will be presented. The first section is dedicated to calorimetric characterization of the epoxy system conventionally and microwave cured. The second section

is focused on a comparison of the cure kinetic of epoxy system thermally and microwave crosslinked. The following section shows the dynamical, mechanical and spectroscopic characterization of the epoxy system under investigation. Finally a brief discussion about organic and metallic sensitizers will be reported.

3.1 Calorimetric Analysis

The calorimetric analysis has been the first step for the characterization of the epoxy resin, used in this work. For this purpose thermo-gravimetric (TGA) and differential scanning calorimeter (DSC) measurements have been performed.

3.1.1 Thermo-gravimetric Characterization

TGA measurements have been carried out on the single components of epoxy mixture for estimating the possible unwanted presence of moisture inside the prepolymer or inside the hardener agent.

In the Figure 3.1 the scan of the hardener agent K 21 between room temperature up to 350°C with heating rate of 10°C/min is shown.

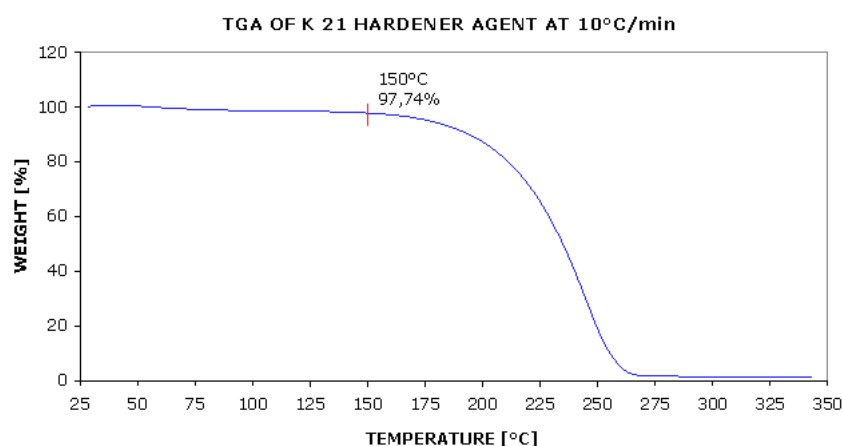


Figure 3.1: Thermogravimetric signal of K 21 at 10°C/min.

There is a weight loss of about 2,3% around 150°C, that is attributed to moisture contained inside it. In fact this compound is lightly hygroscopic.

Figure 3.2 shows the TGA of EC 57 epoxy prepolymer between room temperature up to 700°C with heating rate of 10°C/min. EC 57 is practically moisture free, in fact the weight loss at 150°C is of only 0,88%.

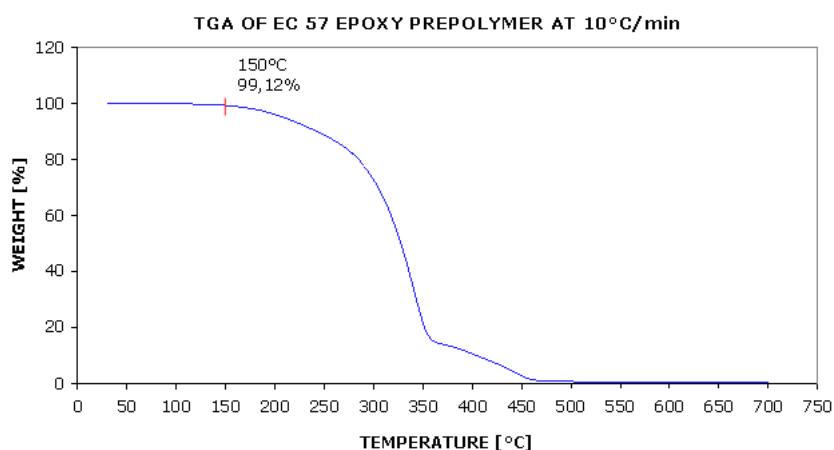


Figure 3.2: Thermogravimetric signal of EC 57 at 10°C/min.

The thermo-gravimetric analysis on epoxy mixture has instead allowed the determination of the temperature range in which carrying out the DSC calorimetric experiments and the possible presence of volatiles substances.

A typical scan of fresh epoxy mixture¹ between room temperature up to 800°C with heating rate of 10°C/min is illustrated in Figure 3.3.

The epoxy mixture contains a low percentage of volatiles components (about 5%). The thermal degradation of the epoxy system begins at a temperature of about 300°C. For this reason the DSC dynamic scans have been performed up to a maximum value of 220 – 250°C.

¹Obtained stirring together EC 57 and K 21 in a weight ratio of about 5:1.

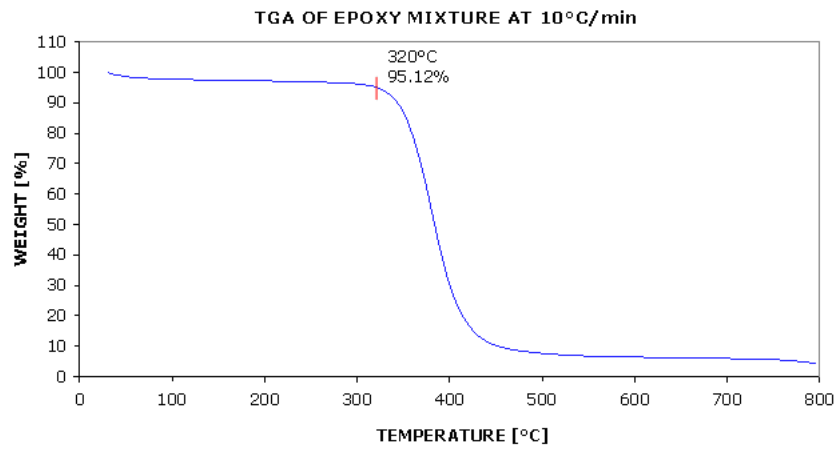


Figure 3.3: Thermogravimetric signal of EC 57-K 21 mixture at 10°C/min.

3.1.2 DSC Characterization

A detailed differential scanning calorimeter analysis of epoxy system has been performed. The total enthalpy of the curing process has been measured through DSC dynamic scans at different heating rates.

The signal obtained with a dynamic DSC at 10°C/min from 0°C up to 220°C is illustrated in Figure 3.4.

The total cure energy can be calculated through linear integration of the signal of the specific heat flow versus temperature according to equation 3.1.

$$\Delta H_{\text{TOT}} = \int_{T_0}^{T_f} \phi \, dT \quad (3.1)$$

where ϕ is the specific heat flow in W/g. In fact the area under the peak is a measure of the heat generated² during the polymerization process.

In the DSC, illustrated in Figure 3.4, the measured cure energy is equal to:

$$\Delta H_{\text{TOT}} = 497 \text{ J/g} \quad (3.2)$$

A following dynamic scan at heating rate of 10°C/min from room temperature

²The up direction in the plot corresponds to exothermic heat flow.

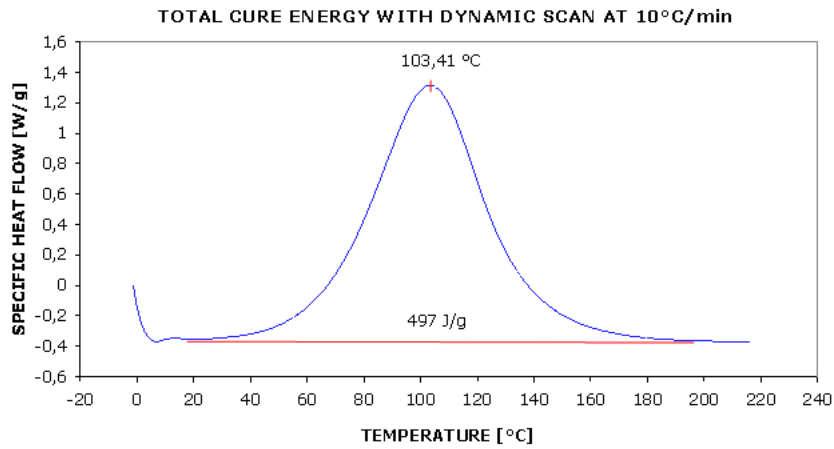


Figure 3.4: Cure enthalpy of EC 57-K 21 mixture with dynamic scan at 10°C/min.

up to 200°C on the same sample has enabled the evaluation of the glass transition temperature as shown in Figure 3.5

In this case the glass transition temperature is equal to:

$$T_g = 107,93^\circ\text{C} \quad (3.3)$$

In Table 3.1 the results of four double dynamic scans at heating rates of 5, 10, 15 and 20°C/min have been summarized.

Heating rate [°C/min]	ΔH_{TOT} [J/g]	T_p [°C]	T_g [°C]
5	485,7	91,12	106,10
10	497	103,41	107,93
15	495	112,31	107,89
20	462,2	116,18	102,92

Table 3.1: Results of DSC dynamic scans at different heating rates.

T_p is the peak temperature, that is the abscissa corresponding to the maximum

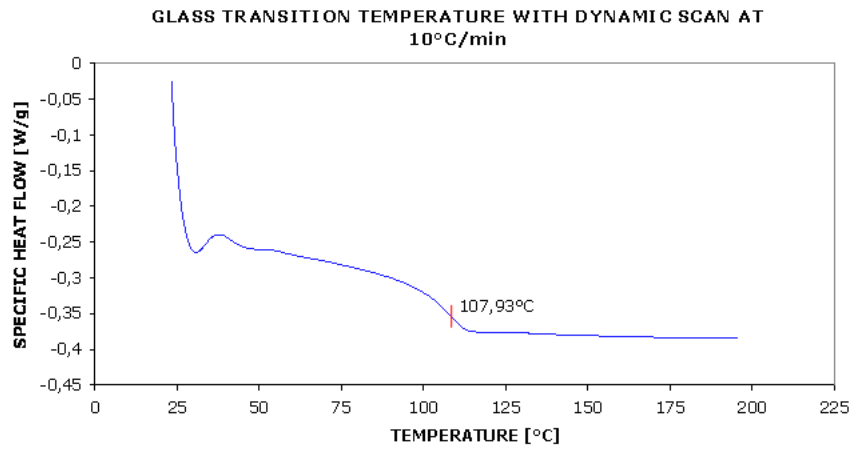


Figure 3.5: T_g of a sample cured with dynamic scan at 10°C/min.

value of specific heat flow.

The average values of the cure enthalpy and of the glass transition temperature are shown in Table 3.2.

ΔH_{TOT} [J/g]	T_g [°C]
485	106,21

Table 3.2: Average values of ΔH_{TOT} and T_g .

While the glass transition temperature of an epoxy sample microwave cured with the operative conditions listed in Table 3.3, measured through a DSC dynamic scan at heating rate of 10°C/min from 0 up to 225°C is illustrated in Figure 3.6. No residual energy is present, so these operative conditions have allowed a complete conversion of the sample. However the system has been heated for a longer time than that elapsed during the DSC dynamic cure at 10°C/min. Therefore the T_g in this case is slightly lower for two reasons:

1. During this prolonged heating time thermal degradation phenomena have been occurred;

Parameters	Value
Tray movement	ON
MW radiation time	300 s
Irradiated power	1500 W
Tray velocity	224 cm/min
IR heating	OFF
Air temperature	25°C

Table 3.3: Microwave oven parameters for the complete conversion of an epoxy sample.

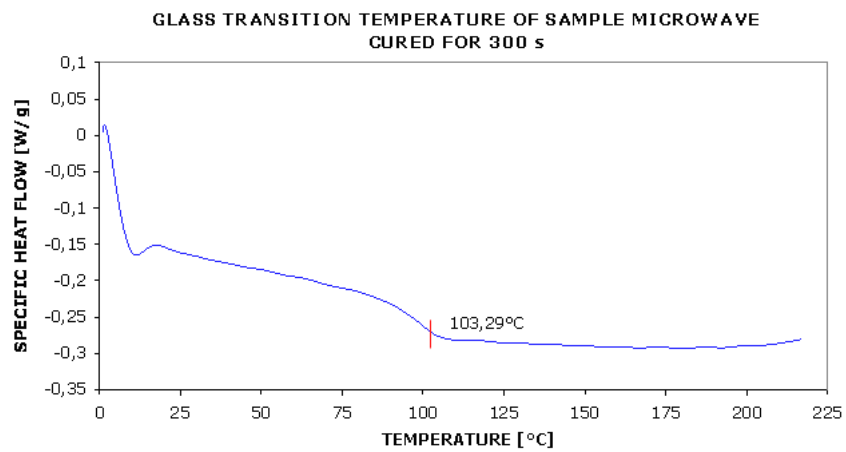


Figure 3.6: T_g of a sample microwave cured with 1500 W for 300 s.

2. The heating of the sample at elevated temperature has promoted evaporation of the reagents and therefore the onset of plasticization phenomena.

The glass transition temperature is equal to:

$$T_g = 103, 29^\circ\text{C} \quad (3.4)$$

Unfortunately the microwave radiation time can not be accurately controlled, because it must be a multiple of the time of a single sample-holder tray passage.

3.2 DSC Kinetic Analysis

The kinetic study of epoxy system has been performed using the DSC isothermal technique [16].

The first step consists of performance of isothermal DSC in a temperature range, selected on the basis of the DSC dynamic scan analysis. These temperatures should belong to the steepest portion of the dynamic thermogram, because in this case the reaction rate is the greatest. Moreover also temperatures higher than T_g should be selected for considering also curing processes, in which vitrification phenomena have been avoided. Finally also the T_g of the completely crosslinked resin has been used.

3.2.1 DSC Isothermal Scan

The temperatures chosen for this kinetic analysis are reported in Table 3.4

Isothermal Temperatures							
Isothermal DSC temperatures [$^\circ\text{C}$]	90	95	100	105	110	115	120

Table 3.4: Temperatures of isothermal DSC.

After preparation of fresh mixture, through the procedure illustrated in the section 2.1.3 on page 54, samples weighting 6 to 12 mg have been placed in an aluminum hermetic sample pans³ in nitrogen atmosphere. The cell of DSC instrument has been heated until the achievement of the desired temperature. After instrument stabilization the sample pan has been quickly inserted inside the cell and the test has been started.

As a matter of fact this experimental procedure is affected by an initial instrumental set-up, resulting in loss of data accuracy during the first 30-45 s. The test have been carried out for *40 min* for ensuring a complete conversion, confirmed by the reaching of the horizontal asymptote of the specific heat flow versus time signal.

The operative conditions, used during these test, have been summarized in Table 3.5.

Operative Conditions	
Atmosphere	Nitrogen
Sample weight	6-12 mg
Sample pan	Aluminum hermetic
Initial set-up	30-45 s
Time	40 min

Table 3.5: Operative conditions of isothermal DSC.

These test generate data in the form of time, temperature and heat flow and therefore specific heat flow from the sample weight. Therefore the curve of specific heat flow [W/g] versus time [min] can be drawn.

³The lid of the pan has been perforated for avoiding its deformation, due to the possible emission of volatiles during the DSC.

In Figure 3.7 the comparison of the seven isothermal DSC signals in the first 7 min is illustrated.

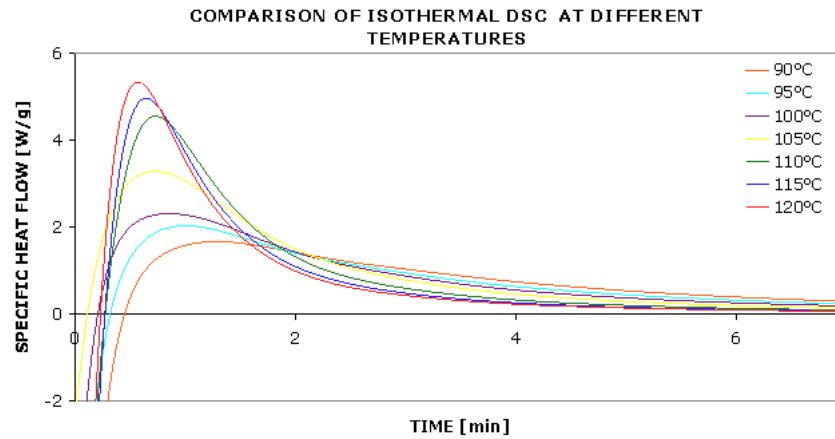


Figure 3.7: Overlay of isothermal DSC at the seven selected temperatures.

For each isothermal temperature there is a maximum of specific heat flow versus time. Increasing the temperature the position of this maximum is progressively shifted toward lower values of time. Assuming that the curing process of the epoxy mixture is the only reactive phenomenon, the rate of heat generation, during the isothermal DSC, is directly correlated to the reaction rate of the crosslinking process. Therefore the existence of a maximum of reaction rate can be deduced.

At each temperature the integration of thermogram signal is equal to isothermal enthalpy ΔH_{ISO} at this temperature. The isothermal enthalpy does not coincide with total cure energy ΔH_{TOT} , measured with dynamic scan, for the existence of the initial instrumental set-up and the resulting loss of data.

3.2.2 Data Elaboration

The data obtained with isothermal DSC have been *numerically* analyzed.

After normalization of specific heat flow [W/g] and time [min] the computation

of instantaneous enthalpy dH_i has been performed, through the trapezium rule as illustrated in the following equation:

$$dH_i = \frac{(\phi_{i+1} + \phi_i)(t_{i+1} - t_i)}{2} \cdot 60 \quad (3.5)$$

ϕ_i and ϕ_{i+1} are the specific heat flow [W/g], respectively at time t_i [min] and at the following instant t_{i+1} , measured by the DSC instrument. The isothermal enthalpy has been calculated, according to the following equation:

$$\Delta H_{\text{ISO}} = \sum_{i=1}^n dH_i \quad (3.6)$$

The sum is extended up to the last instant for $t_n = 40$ min.

The energy developed during an ideal isothermal DSC should be equal to that generated in a dynamic test. Instead the ΔH_{ISO} is always lower than the ΔH_{TOT} , because in every case there is a loss of data, due to the initial instrumental set-up. For reducing the influence of this problem, for every temperature the first value of instantaneous enthalpy dH_1 has put equal to the difference between the total cure energy ΔH_{TOT}^4 and the isothermal enthalpy ΔH_{ISO} .

The degree of cure at every instant α_i is calculated using the following equation:

$$\alpha_i = \frac{dH_i}{\Delta H_{\text{TOT}}} \quad (3.7)$$

The reaction rate α'_i has been computed as incremental ratio of degree of cure:

$$\alpha'_i = \frac{d\alpha_i}{dt} \approx \frac{\alpha_{i+1} - \alpha_i}{t_{i+1} - t_i} \quad (3.8)$$

3.2.3 Reaction Rate-Degree of Cure Plot

The curve of reaction rate versus degree of cure has been traced, using the experimental values, calculated with the equations 3.7 and 3.8.

In Figure 3.8 the plot of α' versus α for the isothermal DSC at 100°C is illustrated.

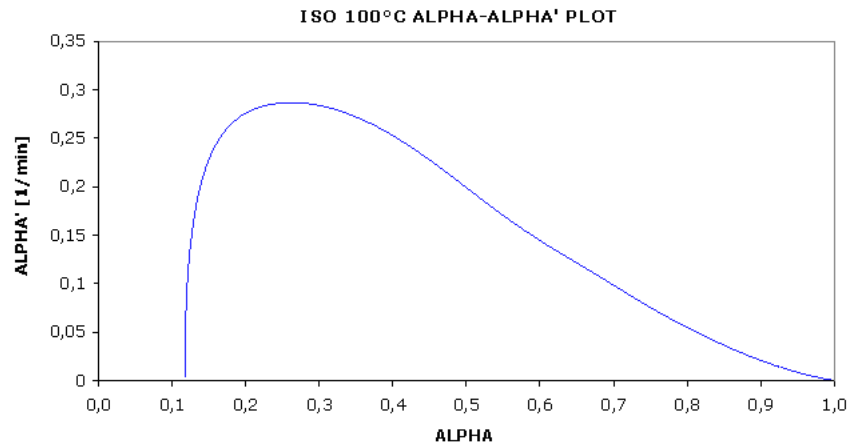


Figure 3.8: Plot of experimental reaction rate versus degree of cure for isothermal DSC at 100°C.

The curve does not start from zero as a consequence of the correction of the first value of instantaneous enthalpy dH_1 .

The maximum reaction rate corresponds to a value of α about equal to 0,25. This consideration has allowed the choice of the most appropriate kinetic model.

3.2.4 Kinetic models

The curing process of a thermosetting resin is a very complicated phenomenon in which many reaction mechanisms occur.

Generally speaking a kinetic model is a relation between the reaction rate α' , the temperature (T) and the degree of cure α :

$$\frac{d\alpha}{dt} = f(T, \alpha) \quad (3.9)$$

For studying the crosslinking reaction two types of models can be used:

⁴Evaluated as reported in Table 3.2.

1. Mechanistic models;
2. Phenomenological models.

The mechanistic models are based on the actual reaction mechanism and they are composed by the mass balances on the chemical species involved in the curing process.

While phenomenological models do not take into account the actual reaction mechanism and they are represented by a simple equation as 3.9.

The mechanistic models describe the reaction kinetic better than phenomenological models. In fact they are purely theoretical models, do not require many experiments and therefore they are faster. However they are not usable, when the exact composition of the mixture is unknown. These models are not easily derivable, because too complicated reactions are involved and in any case they require the knowledge of many parameters.

For these reasons for the kinetic analysis of a very complicated reaction system, as thermosetting resins, the phenomenological models are preferred by many authors.

The phenomenological models allow the description of the curing process with a single simple equation.

These models consist of an equation in which the reaction rate α' is expressed as product of two functions:

$$\frac{d\alpha}{dt} = k(T) \cdot f(\alpha) \quad (3.10)$$

In this equation $f(\alpha)$ depends exclusively on degree of cure α and is independent of the temperature T . While $k(T)$ is the kinetic constant. It depends on the absolute temperature T [K] as described by the Arrhenius law:

$$k(T) = k_0 \cdot e^{-\frac{E_a}{RT}} \quad (3.11)$$

In this equation the constant k_0 is the pre-exponential factor or frequency factor. It takes into account the frequency and orientation of collisions between the reacting

molecules. E_a is the activation energy, R is the ideal gas constant and T is the absolute temperature [K]. The activation energy E_a is the energy that must be overcome in order for the curing process to occur.

The kinetic models, describing the curing process of thermosetting resins, are subdivided in four main categories:

1. n-th order kinetic;
2. autocatalytic kinetic;
3. n-th order plus autocatalytic kinetic;
4. Karkanis and Partridge kinetic [17, 18, 19].

In the n-th order kinetic model the reaction rate is proportional to the reactants concentration and is expressed by the following equation:

$$\frac{d\alpha}{dt} = k \cdot (1 - \alpha)^n \quad (3.12)$$

where n is the reaction order. During an isothermal reaction, since the reactants concentration is maximum at the beginning ($t = 0$), when the degree of conversion is zero ($\alpha = 0$), also the reaction rate is maximum.

In the autocatalytic kinetic the reaction rate depends on both reactants concentration and on concentration of a product, that functions as catalyst. The model is described by the following equation:

$$\frac{d\alpha}{dt} = k \cdot \alpha^m \cdot (1 - \alpha)^n \quad (3.13)$$

In this equation m and n are the reaction orders.

The n-th order plus autocatalytic model is a combination of these two kinetic models described by the following equation:

$$\frac{d\alpha}{dt} = (k_1 + k_2 \alpha^m) \cdot (1 - \alpha)^n \quad \text{n-th order + autocatalytic model} \quad (3.14)$$

where k_1 and k_2 are two kinetic constant following the Arrhenius law 3.11.

Finally the Karkanas and Partridge model is a more complicated version of n-th order plus autocatalytic reaction, in which an attempt of taking into account the vitrification and diffusion control phenomena has been performed. It is expressed by the following equation:

$$\frac{d\alpha}{dt} = k_1 (1 - \alpha)^{n_1} + k_2 \alpha^m (1 - \alpha)^{n_2} \quad \text{Karkanas and Partridge model} \quad (3.15)$$

3.2.5 Non-linear Regression

The curves reaction rate α' versus degree of cure α have been fitted with several kinetic models.

The n-th order reaction has been immediately excluded for the particular shape of the curve, because in the n-th order kinetic model the maximum value of reaction rate α' is reached for $t = 0$ and therefore for $\alpha = 0$. While, as shown, in Figure 3.8 the maximum of α' is achieved for $\alpha \approx 0,25$.

The equations 3.13, 3.14 and 3.15 have been used for fitting the experimental DSC data and the best agreement has been achieved with autocatalytic reaction as described by equation 3.13.

The experimental DSC data for the degree of cure less than 0,15 ($\alpha < 0,15$) have been discarded, because affected by the initial instrumental set-up error. Analogously the data for $\alpha > 0,6$ have been excluded for do not taking into account the diffusion control phenomena.

The non linear regression of such data, using equation 3.13 has been performed with an appropriate software⁵, using the Levenberg-Marquardt algorithm.

In Figure 3.9 an example of the curve of reaction rate α' versus degree of cure α for isothermal DSC at 100°C is illustrated.

⁵OriginPro 7.0.

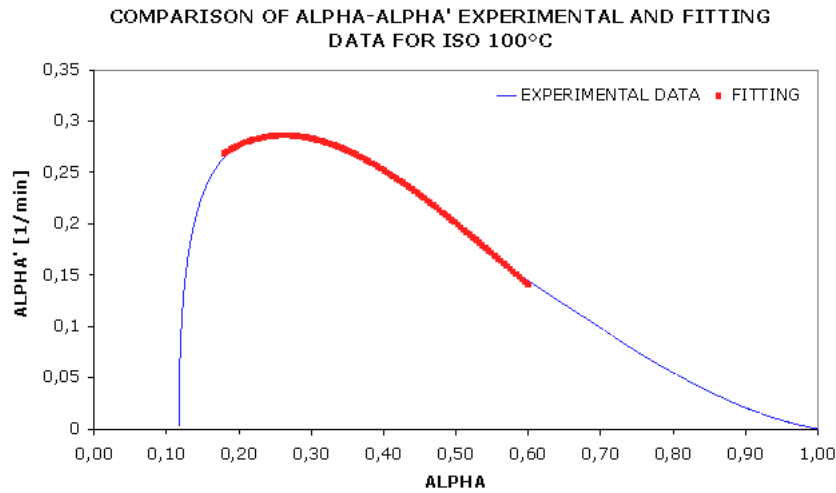


Figure 3.9: Fitting of experimental DSC data of isothermal at 100°C with autocatalytic equation.

The agreement is almost perfect.

For every isothermal DSC this non linear regression has been allowed the determination of the kinetic constant $k(T)$ and the reaction orders m and n . These values have been reported in Table 3.6.

In Table 3.7 the average values of reaction orders m and n are listed.

In this way, for every isothermal temperature, using the equation 3.13 and the values of kinetic parameters reported in Table 3.6 a theoretical reaction rate α' versus degree of cure α curve can be created.

In Figure 3.10 the comparison of experimental and theoretical α' versus α plot for isothermal DSC at 100°C is illustrated.

The agreement between experimental and theoretical data, in the range of degree of cure from 0,18 and 0,6 is almost perfect.

Theoretical values of time can be obtained, from the theoretical reaction rate,

Kinetic Constants and Reaction Orders			
Isothermal Temperature [°C]	k(T)	<i>m</i>	<i>n</i>
90	0,59	0,42	1,67
95	1,42	0,79	2,32
100	1,64	0,80	2,23
105	1,95	0,69	2,14
110	3,58	0,87	2,29
115	6,07	1,17	2,52
120	7,14	1,22	2,61

Table 3.6: Kinetic constants and reaction orders obtained at every isothermal temperature.

<i>m</i>	<i>n</i>
0,85	2,26

Table 3.7: Average reaction orders values.

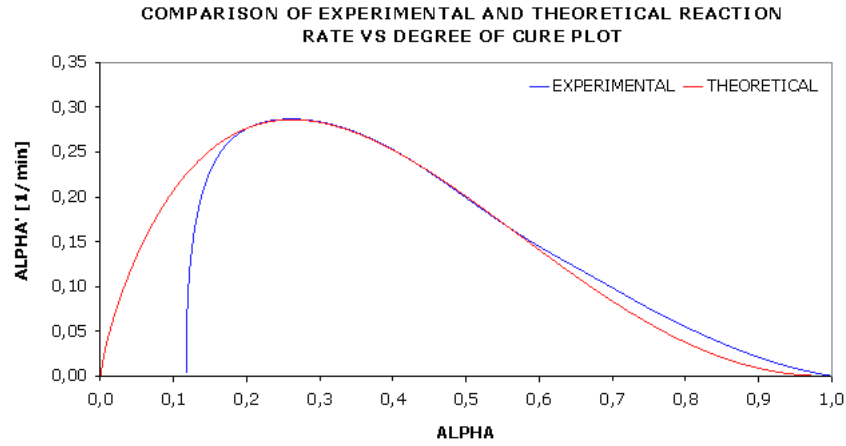


Figure 3.10: Comparison of experimental and theoretical α' versus α plot for isothermal DSC at 100°C.

using the following equation:

$$t_{i+1} = t_i + \frac{\alpha_{t_{i+1}} - \alpha_{t_i}}{\left(\frac{d\alpha}{dt}\right)_{t_{i+1}}} \quad (3.16)$$

Theoretical specific heat flow can be calculated using the equation reported here:

$$\phi = \frac{\Delta H_{TOT}}{60} \cdot \left(\frac{d\alpha}{dt}\right) \quad (3.17)$$

After normalization of theoretical values of time the curves of experimental and theoretical specific heat flow versus time can be drawn. The comparison of these curves for isothermal DSC at 100°C is illustrated in Figure 3.11.

For graphical convenience the curve of theoretical specific heat flow versus time has been shifted of a factor of -1.

Also in this case the agreement between experimental and theoretical data is reasonably good.

The analysis of Figures 3.10 and 3.11 allow to confirm the correct determination of the kinetic constant $k(T)$ and the reaction orders m and n , reported in Table 3.6.

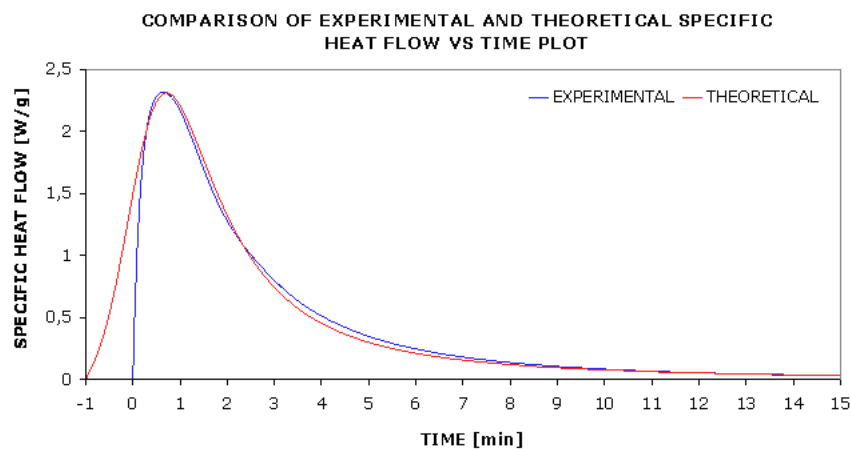


Figure 3.11: Comparison of experimental and theoretical specific heat flow for isothermal DSC at 100°C.

3.2.6 Arrhenius Plot

The evaluation of the activation energy E_a and pre-exponential factor k_0 has been performed through the analysis of the Arrhenius plot.

The hyperbolic logarithm of the kinetic constant $\ln(k)^6$ [1/min] for every isothermal DSC has been plotted against the inverse of the absolute temperature $1/T$ [1/K].

In fact the Arrhenius equation 3.11 can be written equivalently in the following form:

$$\ln(k) = \ln(k_0) - \frac{E_a}{R} \cdot \left(\frac{1}{T}\right) \quad (3.18)$$

The value of the extrapolated “y-intercept” corresponds to $\ln(k_0)$ and the slope of the line is equal to $\frac{E_a}{R}$.

For the seven isothermal DSC the corresponding Arrhenius plot is illustrated in Figure 3.12.

The seven points can be considered sufficiently well aligned.

⁶Obtained through non linear regression as illustrated in the section 3.2.5 on page 107.

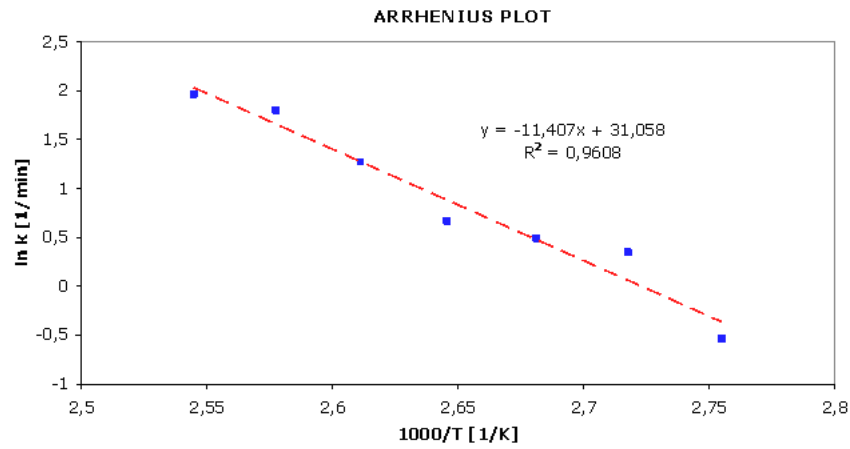


Figure 3.12: Arrhenius plot.

From the equation of the interpolating line it is possible to calculate the values of activation energy E_a and the hyperbolic logarithm of the pre-exponential factor $\ln(k_0)$ for the conventional curing process.

$$E_a = 11,41 \cdot 1000 \text{ K} \cdot R = 11,41 \cdot 1000 \text{ K} \cdot 8,314472 \frac{\text{J}}{\text{mol K}} = 94,84 \frac{\text{KJ}}{\text{mol}} \quad (3.19)$$

$$\ln(k_0) = 31,06 \frac{1}{\text{min}} \quad (3.20)$$

The kinetic parameters are reported in Table 3.8. These values are in good

Conventional Kinetic Parameters	
E_a [KJ/mol]	94,84
$\ln(k_0)$ [min^{-1}]	31,06

Table 3.8: Kinetic parameters for conventional curing reaction.

agreement with those obtained by Navabpour et al. [20].

3.3 Comparison MW versus DSC

A comparison of degree of conversion in function of reaction time during microwave and conventional DSC cure processes of the epoxy system, undergone almost the same thermal profile, has been performed for investigating the existence of the *specific microwave effect*.

3.3.1 Specific Microwave Effect

Activating effects induced by electromagnetic wave absorption, and that cannot be easily emulated through conventional heating methods, remain a very controversial topic since the beginning of the use of microwave for supplying energy for chemical reactions [21, 22].

Therefore specific microwave effect is a non thermal effect of MW field, involving an acceleration of reaction rate⁷, and a variation of chemical reaction mechanism.

Two fundamental explanations have been proposed for justifying this effect:

1. Effects depending on lifetime of transition state of reactants. In the case of short lifetime, the position hypothesis holds: the electric field would induce suitable positions of reactants that would minimize the entropy of the system. In the case of a very long lifetime, the electric field would induce an increasing probability of molecular collisions. Loupy et al. [23] have addressed the orienting effect of electric field, so microwave irradiation could induce molecular organization different from those induced by classical heating mode;
2. The occurrence of a difference between local temperature of electrical entities, i.e. dipolar moment associated with chemical bonds.

⁷Not simply attributable to differences of heating rate or thermal profile.

In the field of microwave cure of thermosetting resins there is still an ongoing debate about the existence of the specific microwave effect. It is a topic quite controversial and there have been conflicting results from different authors, a review of the state of art in this area is presented in a paper of Thostenson et al. [24].

Marand et al. [25], Wei et al. [26] and Jordan et al. [27] have studied the cure kinetics of epoxy resin systems. In all of these investigations, the reaction rates were enhanced and times to gelation and vitrification were reduced due to microwave heating. Marand et al. [25] showed that the molecular structure and curing agent affect the magnitude of the acceleration in microwave heating. Research by Wei [26] and co-workers was conducted to determine the effects of microwaves on the molecular structure, and it was shown that the molecular structure of some polymers is different when cured using microwaves as compared with conventional curing.

These results are in contrast to the work of Mijovic and co-workers [28, 29, 30], who have noticed either no change in the cure kinetics or a retardation of the cure kinetics, when cured by microwaves. In a more recent work, an in situ method was used to investigate the crosslinking of several different materials and they assert that the claims of accelerated cure kinetics are unfounded [31].

The conflicting results by different laboratories indicate the need for additional work in this area.

3.3.2 Static Operative Conditions

Experiments have been performed on epoxy samples, prepared according to the procedure, indicated in the section 2.1.3 on page 54, and using the microwave oven as a static cavity. The PP vessel containing the epoxy mixture has been cut at a height of about 4-5 cm in order to place it in the centre of the tray on a glass

pedestal at an elevation of 2 cm⁸, and allow the entrance of the vessel inside the oven cavity.

At the end of every microwave activated cure process the sample has been *quenched*, dipping it rapidly in an ice-water bath at a temperature of about 2 – 3°C, for interrupting the crosslinking reaction, avoiding further conversion at the temperature, reached at the end of the microwave heating. After the power off of the magnetron, when the automatic cycle is finished, it is necessary to wait about 10 s before quenching the sample, because the tray needs 7,5 s⁹ for going out from the cavity and other 2,5 s are necessary for quenching the sample below its glass transition temperature.

During this time τ , the system continues to polymerize, following a kinetic described by the conventional parameters, reported in Tables 3.8 and 3.7, because it has been heated at an elevated temperature, at which the reaction rate can not be neglected. The increment of the degree of cure, during the delay time τ , has been estimated, using the method described below.

The time necessary for reaching a complete conversion during the MW activated cure process, without IR radiations, with an air temperature of 25°C at the microwave radiation power of 1000, 1500 and 2000 W has been determined. They are presented in Table 3.9.

As predictable the time required for a complete conversion of the epoxy system decreases enhancing the radiation power.

The achievement of the 100% of the degree of cure has been verified, through the absence of residual energy during a DSC dynamic scan between 0 and 250°C with a heating rate of 10°C/min, performed immediatly after the quenching. For

⁸In fact this is the position of greatest electromagnetic energy density, as verified through the experiments presented in the section 2.3.2 on page 74.

⁹In fact with a tray velocity of 224 cm/min every passage under waveguide requires 15 s and the waveguide is placed in the centre of the oven cavity.

Time for the Epoxy System Complete Conversion at Different Powers	
P [W]	t [s]
1000	350
1500	175
2000	100

Table 3.9: Time required for the complete conversion of the epoxy system during MW cure processes at different radiation powers.

example the signal obtained with a fragment of the sample cured for 175 s with a power of 1500 W is illustrated in Figure 3.13.

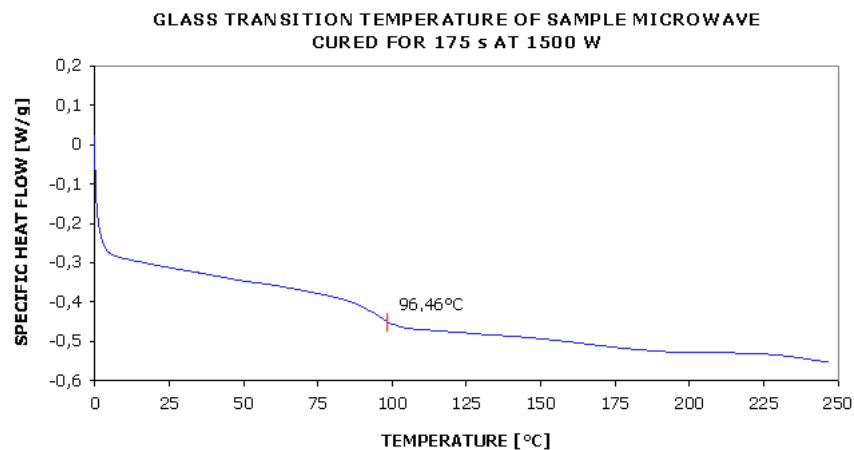


Figure 3.13: DSC dynamic scan of sample microwaved for 175 s at 1500 W.

At every power, partial microwave cure processes have been performed, for time less than that required for a complete conversion and selected in a way to obtain a representative trend of fractional degree of cure. After these time the residual enthalpy of the sample (ΔH_{RES}) has been measured with a DSC dynamic scan between 0 and 250°C with a s of 10°C/min. These data have been listed in

Tables 3.10, 3.11 and 3.12.

Residual Enthalpy versus Time for P = 1000 W	
Time [s]	ΔH_{RES} [J/g]
100	415,7
150	349,1
200	139,1
250	86,07
300	9,48
350	≈ 0

Table 3.10: Residual enthalpy against time during MW cure process at 1000 W.

In every case a sharp decrease of residual enthalpy is observed after a time depending on the heating rate and, therefore on the radiation power.

For example in Figure 3.14 the residual enthalpy after a microwave cure process at 1500 W for 125 s is shown.

During these partial crosslinking reactions the sample temperatures have been recorded every 0,5 s by datalogger¹⁰. For a clearer representation of the data, only the temperatures corresponding to the time, chosen for the residual enthalpy measurement, have been plotted. The thermal profile, followed by the system during the cure process at the power of 1000 W, illustrated in Figure 3.15, is not reproducible with a simple DSC dynamic scan and therefore, at least for the comparison between MW and DSC, has been discarded. While the thermal profiles during the cure at 1500 W and 2000 W are well comparable with DSC dynamic scan, respectively at 44 and 70°C/min, *at least for the main part of the reaction*

¹⁰Described in the section 2.5 on page 83.

Residual Enthalpy versus Time for P = 1500 W	
Time [s]	ΔH_{RES} [J/g]
50	468,7
75	363
100	331,7
125	90,13
150	43,1
175	≈ 0

Table 3.11: Residual enthalpy against time during MW cure process at 1500 W.

Residual Enthalpy versus Time for P = 2000 W	
Time [s]	ΔH_{RES} [J/g]
40	469,1
50	385,5
55	383,4
60	36,05
75	8,06
100	≈ 0

Table 3.12: Residual enthalpy against time during MW cure process at 2000 W.

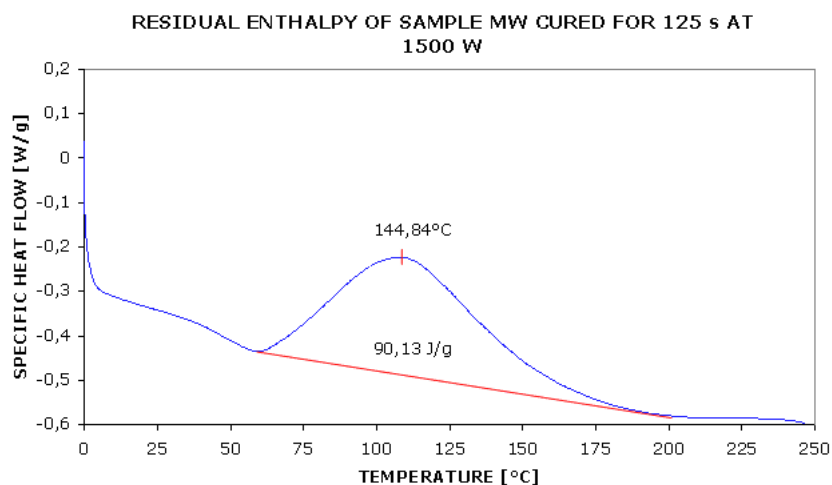


Figure 3.14: Residual energy after MW cure process at 1500 W for 125 s.

process. In Figures 3.16 and 3.17 the microwave thermal profiles, respectively at 1500 and 2000 W are plotted on the same scale with the corresponding comparable DSC temperature trend.

In order to perform a right comparison between partial MW and DSC degree of cure, the reliability of the DSC instrument at a heating rate of 44 and 70°C/min has been verified. For this reason a dynamic DSC scan at the heating rate of 70°C/min between 0 and 300°C on an *indium* sample, as illustrated in Figure 3.18, has been carried out. The indium has been chosen because it is a metallic element with a low melting point and it is used for the calibration of the DSC instruments.

The melting enthalpy, measured with this scan, equal to 28,07 J/g has been compared with the heat of fusion obtained with a standard DSC dynamic scan at the heating rate of 10°C/min between 100 and 180°C, shown in Figure 3.19.

In this case the melting enthalpy is equal to 26,79 J/g, although the signal has almost the same shape. Therefore there is a difference of about 4,77% between the

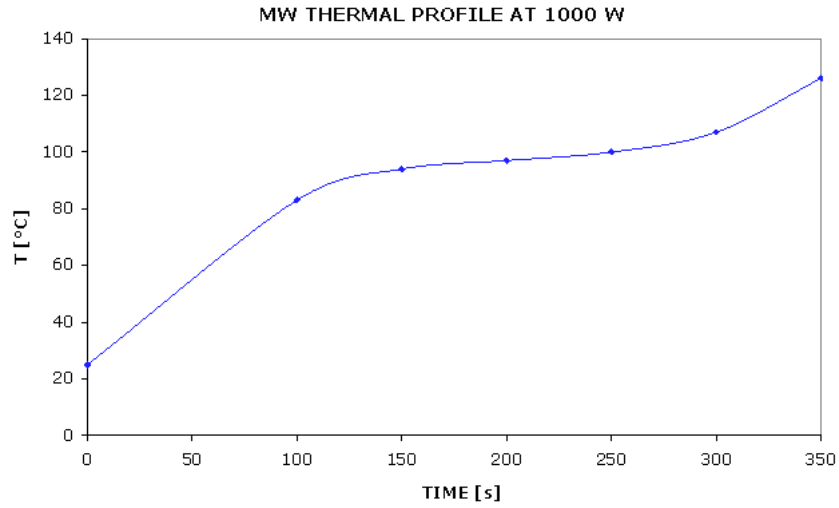


Figure 3.15: Thermal profile during MW cure process at 1000 W.

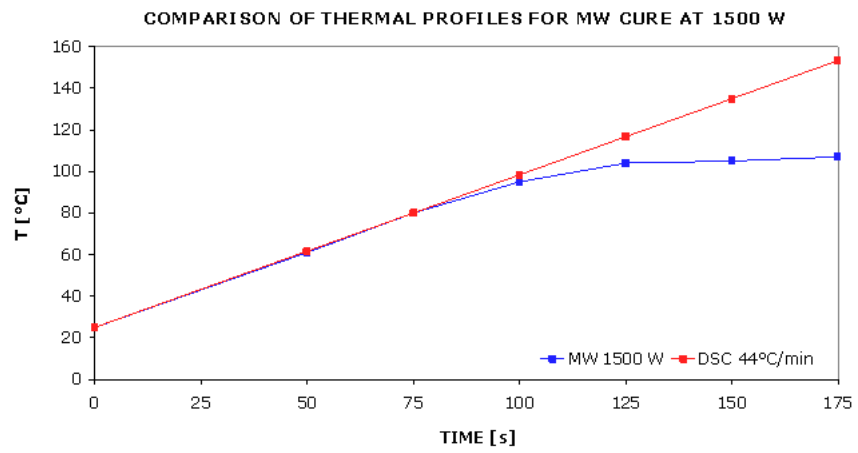


Figure 3.16: Comparison of thermal profiles between MW cure process at 1500 W and a DSC dynamic scan at 44°C/min.

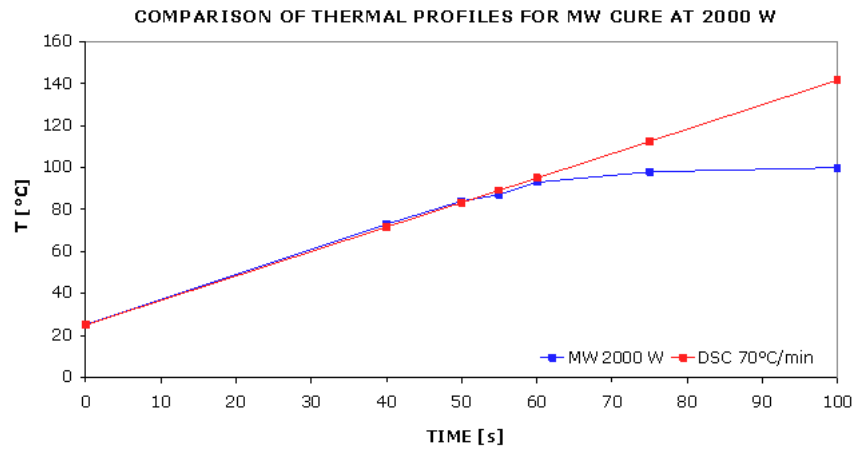


Figure 3.17: Comparison of thermal profile between MW cure process at 2000 W and a DSC dynamic scan at 70°C/min.

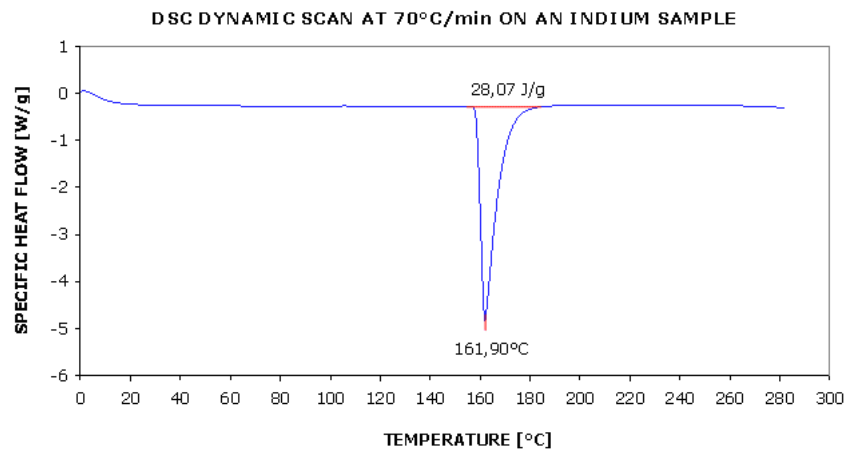


Figure 3.18: DSC dynamic scan at 70°C/min on an indium sample.

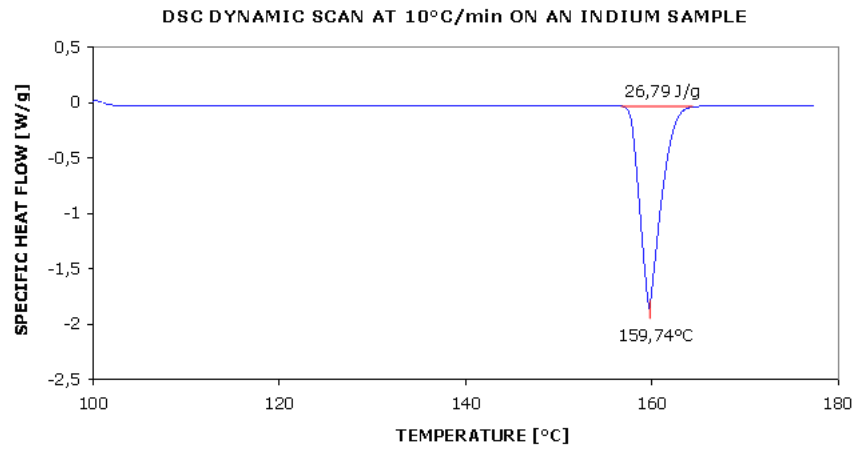


Figure 3.19: Standard DSC dynamic scan at 10°C/min on an indium sample.

values, measured with the same DSC instrument operating at these two different heating rate. For this reason the data obtained using the DSC at these elevated heating rates can be considered affected by an error at most equal to the 5%.

The fractional degree of conversion after every partial microwave cure process has been calculated using equation 3.21:

$$\alpha = 1 - \frac{\Delta H_{RES}}{\Delta H_{TOT}} \quad (3.21)$$

where ΔH_{RES} are the values reported in Tables 3.11 and 3.12, while ΔH_{TOT} is equal to 485 J/g, that is the average value of total cure energy, measured through dynamic scan at different heating rate, as reported in Table 3.2.

In Table 3.13 the degree of cure versus reaction time, obtained under microwave radiation at 1500 W has been reported.

In Figure 3.20 the same data have been plotted.

As illustrated in Figure 3.16 the thermal profile, followed by the epoxy system during microwave cure process at 1500 W is reasonably well comparable with the temperature trend during a dynamic scan at 44°C/min up to 125 s, corresponding to a degree of conversion of 81,42 %. Therefore the comparison with conventional

t_{MW} [s]	50	75	100	125	150	175
T_{MW} [°C]	61	80	95	104	–	–
α_{MW} [%]	3,36	25,15	31,61	81,42	91,10	≈ 100

Table 3.13: Time, temperature max and degree of conversion for MW cure at 1500 W.

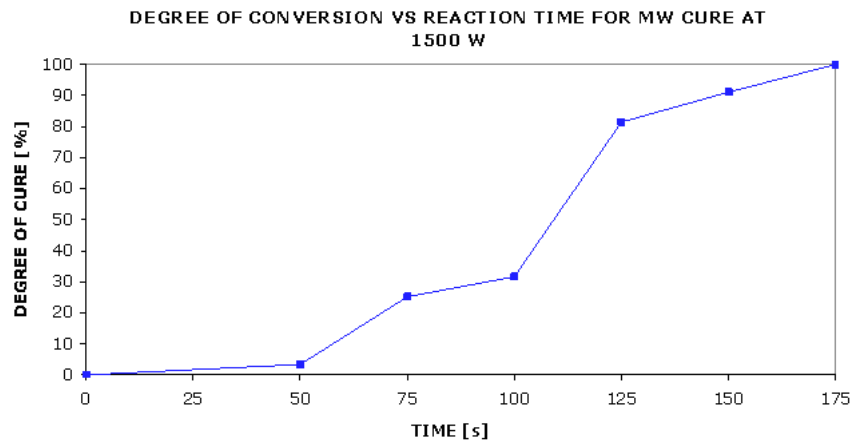


Figure 3.20: Degree of conversion against reaction time for MW cure process at 1500 W.

DSC can be carried out.

However this degree of cure is not completely attributable to the microwave process, because, as explained above, during the delay time τ ¹¹ the sample continues to react, following the conventional kinetic.

The non linear regression of degree of cure versus reaction time data¹² has been performed with the growth-sigmoidal function, described by the equation 3.22:

$$y = \frac{a}{1 + b e^{-kx}} \quad \text{SLogistic 3} \quad (3.22)$$

where, in this case, y is the simulated degree of conversion, x the reaction time, and a , b and k are numerical parameters computed by the software.

In this way a *simulated* α versus t profile has been determined, the comparison of experimental and fitting data of degree of cure against reaction time is illustrated in Figure 3.21.

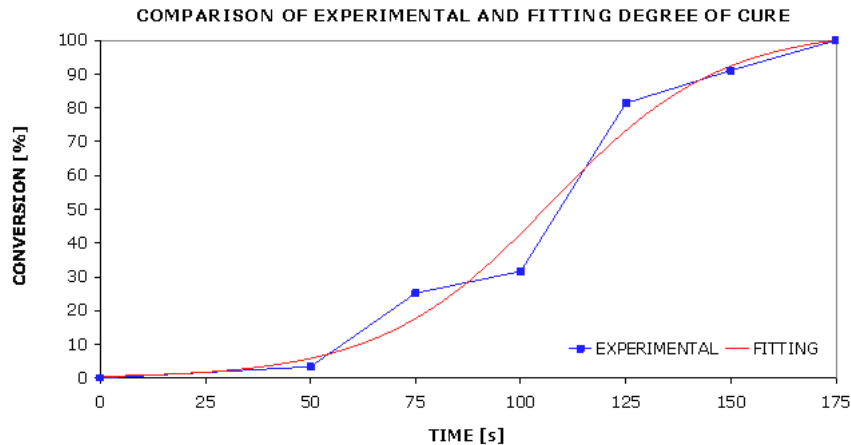


Figure 3.21: Comparison of experimental and fitting data of degree of conversion against reaction time for a MW cure process at 1500 W.

The agreement between experimental and fitting data is acceptable. Then the

¹¹Estimated equal to 10 s.

¹²Elaborated with OriginPro 7.0, using the Levenberg-Marquardt algorithm.

simulated reaction rate α'_i can be numerically calculated as incremental ratio of degree of cure:

$$\alpha'_i = \frac{d\alpha_i}{dt} \approx \frac{\alpha_{i+1} - \alpha_i}{t_{i+1} - t_i} \quad (3.23)$$

Knowing the profiles of α , α' and T in function of time, the increment of degree of cure during the delay time τ can be estimated. In fact the variation of degree of conversion $\alpha_{i+1} - \alpha_i$ is correlated to the corresponding variation of time $t_{i+1} - t_i$, through the following numerical equation:

$$t_{i+1} - t_i = \frac{\alpha_{i+1} - \alpha_i}{\alpha'_{i+1}} \Rightarrow \alpha_{i+1} = \alpha_i + \alpha'_{i+1} (t_{i+1} - t_i) \quad (3.24)$$

Therefore approximating α'_{i+1} with α'_i and considering a conversion of 50% the increase of degree of cure during the delay time τ is equal to:

$$\alpha_{0,5+\tau} = \alpha_{0,5} + \alpha'_{0,5} \cdot \tau \quad (3.25)$$

The reaction rate $\alpha'_{0,5}$ can be calculated, using the autocatalytic model and the conventional kinetic parameters, reported in Tables 3.8 and 3.7, and the temperature, recorded by the datalogger during the microwave cure at 1500 W at the time corresponding to the 50% of conversion. Table 3.14 presents the values used for the evaluation of the increment of degree of cure for the microwave cure at 1500 W.

The degree of conversion $\alpha_{0,5+\tau}$ is equal to 0,52, therefore the influence of τ on the degree of conversion is almost negligible.

The same analysis has been performed for the microwave cure process at a radiation power of 2000 W and analogous results have been achieved.

In Table 3.15 the degree of cure versus reaction time, obtained under microwave radiation at 2000 W, calculated using equation 3.21 and the residual enthalpy, reported in Table 3.12 has been presented.

The same data are also plotted in Figure 3.22.

P	1500 W
α_i	0,5
T	367,15 K
k(T)	0,99 min ⁻¹
$\alpha'_{0,5}$	0,11 min ⁻¹
$\alpha_{0,5+\tau}$	0,52

Table 3.14: Numerical values used for the evaluation of $\alpha_{0,5+\tau}$ for MW cure at 1500 W.

t_{MW} [s]	40	50	55	60	75	100
T_{MW} [°C]	73	84	87	93	–	–
α_{MW} [%]	3,28	20,51	20,95	92,57	98,34	≈ 100

Table 3.15: Time, temperature max and degree of conversion for MW cure at 2000 W.

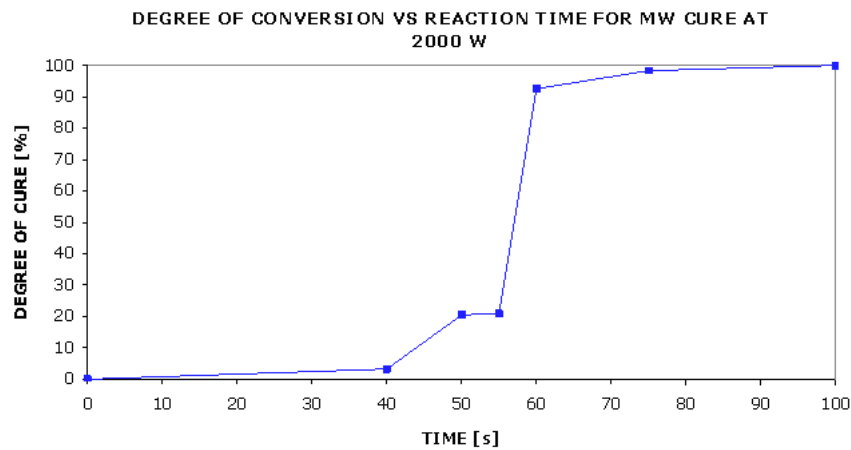


Figure 3.22: Degree of conversion against reaction time for MW cure process at 2000 W.

Figure 3.17 shows that the agreement between thermal profiles of MW cure process at a power of 2000 W and DSC at a heating rate of 70°C/min is almost perfect up to 60 s, corresponding to a degree of conversion of 92,57 %. Therefore, also in this case, the main part of the polymerization process occurs, following a thermal profile almost perfectly comparable with a DSC dynamic scan.

The degree of conversion in conventional DSC at the heating rate of 44°C/min and 70°C/min has been measured integrating the signal at different temperatures, corresponding to the maximum temperature achieved in DSC scan after the same time of MW cure respectively at 1500 and 2000 W, *increased with the delay time τ* .

Considering the comparison between the MW cure process at 1500 W and the polymerization in DSC at the heating rate of 44°C/min the degree of conversion in DSC has been calculated using the equation 3.26:

$$\alpha = \frac{\Delta H_{\text{PAR}}}{\Delta H_{\text{TOT}}} \quad (3.26)$$

where ΔH_{TOT} is the total cure energy, generated during a DSC dynamic scan between 0 and 250°C with heating rate of 44°C/min and measured as illustrated in Figure 3.23.

Therefore the value of 448,7 J/g has been used.

In Figure 3.24 an example of measurement of partial energy at a temperature of 124°C with a DSC dynamic scan at 44°C/min is illustrated.

The Table 3.16 reports degree of conversion in DSC, obtained in this way, where T_τ is the increase of temperature, during the DSC dynamic scan at heating rate of 44°C/min, due to the delay time τ and equal to 7,33°C.

As shown in the Table 3.16 after 175 s in DSC the system has reached only the 86,41% of degree of cure, while the same time in MW is sufficient to achieve the complete conversion.

The profile of degree of cure in DSC against reaction time is illustrated in Figure 3.25.

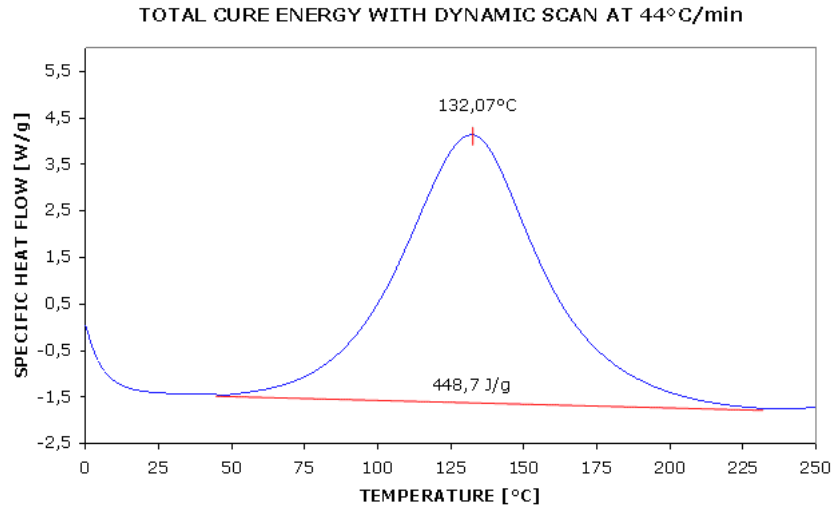


Figure 3.23: Total cure energy with DSC dynamic scan at 44°C/min.

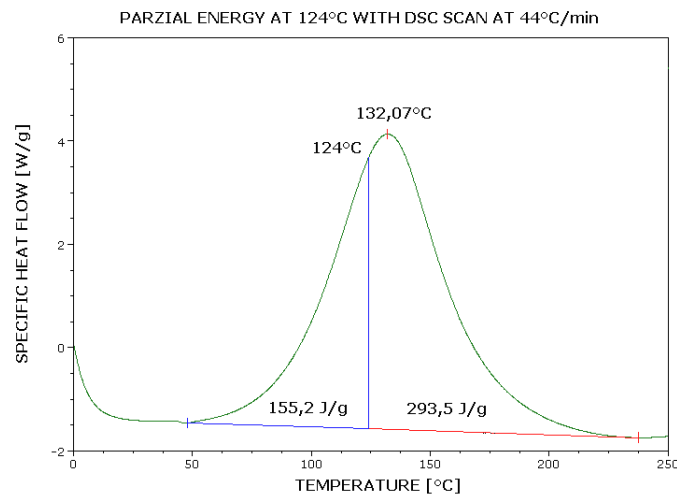


Figure 3.24: Partial energy measured at 124°C with DSC dynamic scan at 44°C/min.

t_{DSC} [s]	50	75	100	125	150	175
t_{DSC} [s] + τ	60	85	110	135	160	185
T_{DSC} [°C]	61,67	80	98,33	116,67	135	153,33
$T_{\text{DSC}} + T_{\tau}$ [°C]	69	87,33	105,67	124	142,33	160,67
α_{DSC} [%]	0,76	3,94	13,34	34,59	65,39	86,41

Table 3.16: Time, temperature max and degree of conversion for DSC cure at 44°C/min.

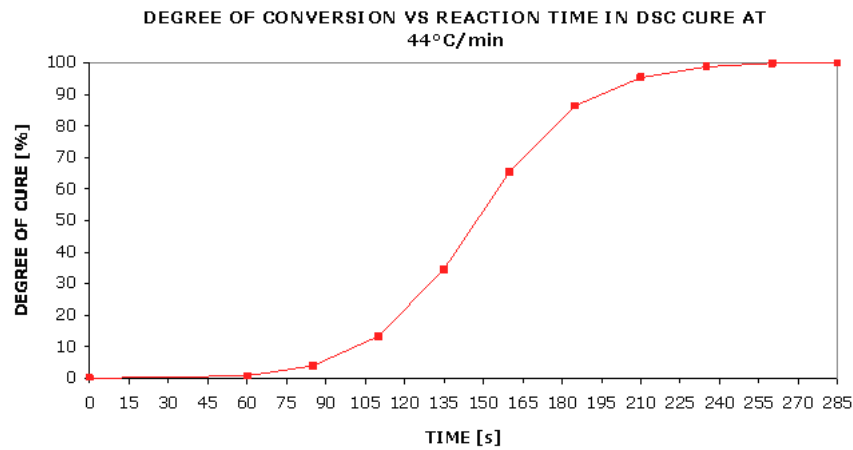


Figure 3.25: Degree of conversion versus reaction time in DSC cure process at 44°C/min.

A time of 285 s is necessary for reaching a complete conversion in DSC.

Finally a comparison of degree of conversion in function of time between MW at 1500 W and DSC at 44°C/min cure processes is presented in Figure 3.26.

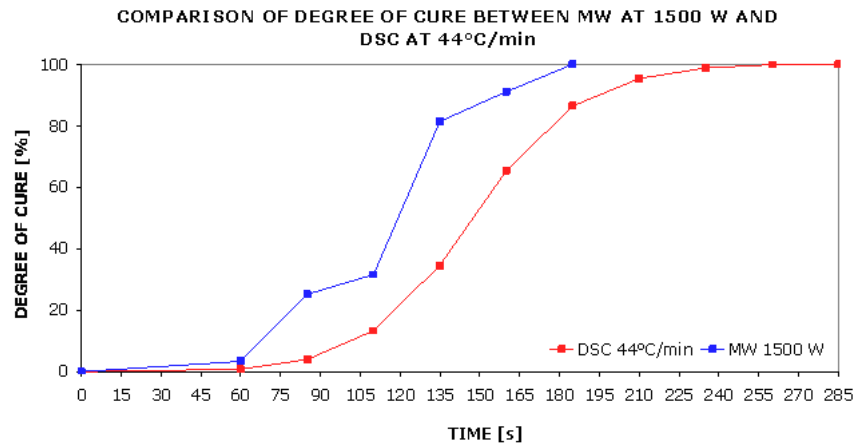


Figure 3.26: Comparison of degree of cure between MW at 1500 W and DSC at 44°C/min.

After a time of 100 s, when the two thermal profiles are almost perfectly comparable, the ratio between the degree of cure in MW and DSC is equal to $2,37$.

The same analysis procedure has been repeated for the MW cure process at 2000 W correlated to a conventional DSC at 70°C/min and the results are summarized in Figure 3.27.

Analogously after a time of 60 s the ratio between α_{MW} and α_{DSC} is equal to $13,82$.

In both the cases at every time the degree of cure achieved in MW field is always higher than that obtained with conventional DSC heating. However, at time greater than 125 s for the MW cure at 1500 W, and greater than 60 s for the cure at 2000 W, the MW thermal profile are not similar with the corresponding DSC dynamic scan and therefore the direct comparison of reaction fractional conversion slightly lacks of accuracy.

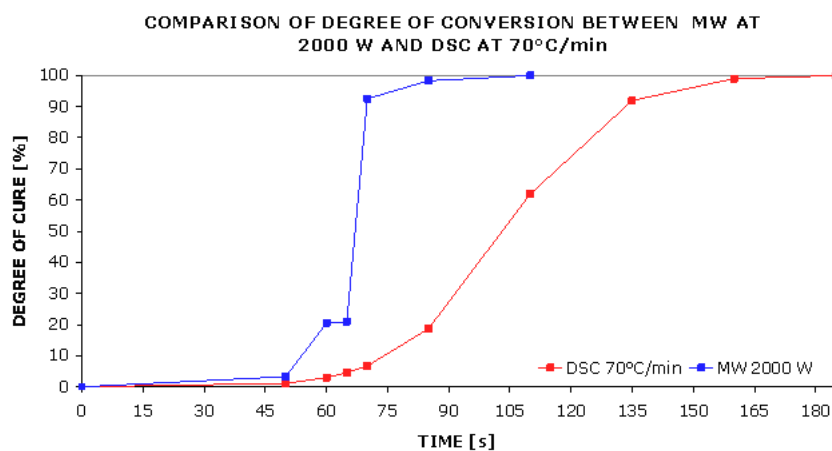


Figure 3.27: Comparison of degree of cure between MW at 2000 W and DSC at 70°C/min.

As predictable the ratio between the MW and DSC degree of cure is greater for the microwave process at 2000 W than that at 1500 W.

3.3.3 Dynamic Operative Conditions

The microwave cure process has been studied also with the oven working in *dynamic operative conditions*, i.e. with moving tray, and the same type of analysis has been extended to this case.

Further the microwave plant parameters, ensuring the complete conversion of the epoxy mixture¹³, without thermal degradation, have been determined. These parameters are reported in Table 3.17.

The attainment of the 100% of degree of cure has been verified through a DSC dynamic scan between 0 and 220°C with heating rate of 10°C/min, performed immediatly after the quenching, on a fragment of the sample cured in these conditions. The DSC signal is illustrated in Figure 3.28.

¹³Prepared as illustrated in the section 2.1.3 on page 54.

Microwave Parameters	
Tray movement	ON
MW radiation time	300 s (20 passages)
Irradiated power	1500 W
Tray velocity	224 cm/min
IR heating	OFF
Air temperature	25°C

Table 3.17: Microwave parameters for the complete conversion of epoxy system in dynamic operative conditions.

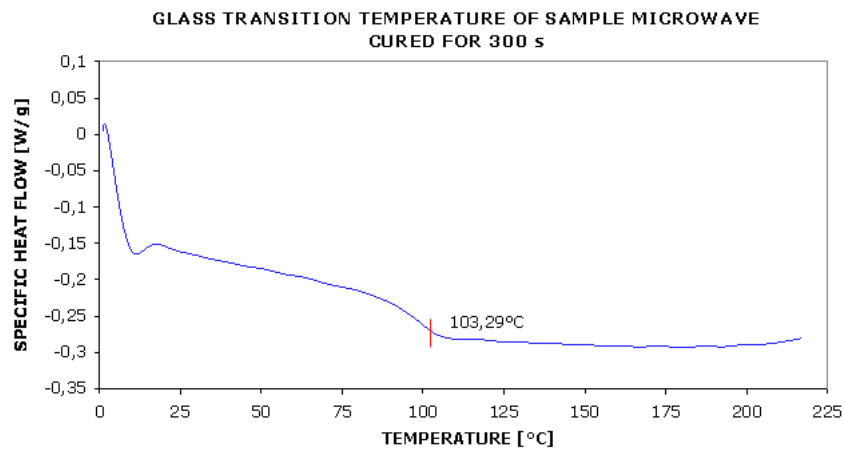


Figure 3.28: DSC dynamic scan of sample microwave cured with the operative conditions reported in Table 3.17.

Using the microwave oven in dynamic operative conditions 300 s are necessary for achieving a complete conversion with a power of 1500 W . While, when the plant operates as a static cavity at the same power, only 175 s are sufficient¹⁴. However in the first case the sample is placed in the centre of tray at a height of 2 cm , under the waveguide in a position in which it receives a greater quantity of energy, while in the second case the epoxy mixture is collocated in the position of coordinates $(0,-5,2)\text{ [cm]}$ ¹⁵ under the IR sensor, where the energy density is lower of $22,82\%$, as verified through the experiments presented in the section 2.4 on page 81. This phenomenon can be explained, because using the oven as a static cavity the sample receives the microwave radiations *continuously* and therefore the heating rate is constant, although in every time the quantity of energy transferred to the sample is lower. While when the plant works in dynamic conditions the sample gets the electromagnetic energy *intermittently*. Under the waveguide the epoxy mixture receives the maximum quantity of energy¹⁶ and the heating rate is greatest, but when the sample reaches the terminal points of the applicator cavity, it is in a *shadow zone*, in which the energy density is almost null and therefore the heating rate is slightest or even negative. For this reason the heating rate in static conditions is higher. Therefore the system reaches before the temperature corresponding to the activation of the curing process and less time is required for achieving a complete conversion, although the total quantity of electromagnetic energy received is lower. *Moreover the epoxy resin is always under the microwave radiation and therefore the polymerization is completed in less time probably not only for thermal reasons, but also for the acceleration of the reaction rate, due to the specific microwave effect.*

¹⁴The other microwave plant parameters and the composition of the epoxy mixture are the same in both the cases.

¹⁵Referred to the grid illustrated in Figure 2.11.

¹⁶Corresponding to the power selected by the user.

The power of 1500 W has been selected for two reasons:

1. The electromagnetic energy transfer with the sample is optimized, as verified in the section 2.6 on page 85;
2. The microwave thermal profile is comparable with a DSC dynamic scan.

The thermal profile of the sample, during this cure process has been monitored through the IR sensor of the microwave plant, because in dynamic operative conditions the datalogger is not usable, as explained in the section 2.5 on page 83.

A comparable thermal profile between conventional DSC and microwave cure has been chosen in a sequence of microwave cure at different time from 90 to 300 s. The best agreement between both profiles has been achieved with a microwave cure of 240 s (16 passages) and a DSC dynamic scan at heating rate of 20°C/min from room temperature up to 250°C. Figure 3.29 shows in the same scale the comparison of these two thermal profiles.

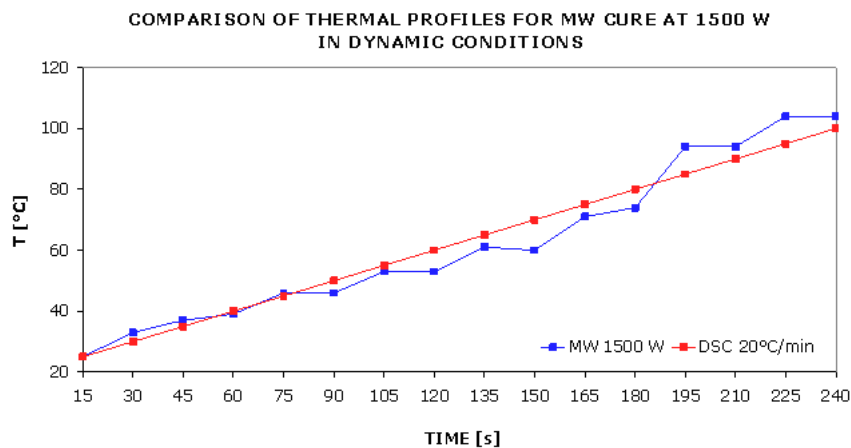


Figure 3.29: Comparison of the thermal profiles between MW cure process and DSC dynamic scan.

During the MW exposure cycle the sample is not always submitted to the same energy density, because the tray sample-holder has an alternating movement

forward and backward from the multimodal cavity applicator. Only the maximum temperature of every passage is recorded. Presumably the average temperature, experienced by sample during MW cure, is lower than the recorded values. The MW thermal profile, which have been compared with a dynamic scan at 20°C/min in DSC, is influenced by this alternating monitoring of the sample temperature.

Also in this case after every partial microwave cure process the degree of conversion of the sample has been estimated, through evaluation of residual enthalpy (ΔH_{RES}), measured with a DSC dynamic scan between 0 and 220°C with heating rate of 10°C/min according to equation 3.27.

$$\alpha = 1 - \frac{\Delta H_{RES}}{\Delta H_{TOT}} \quad (3.27)$$

For the sake of comparison with DSC curing process, the enthalpy value [16] of 462,2 J/g (ΔH_{TOT}), measured during DSC dynamic scan at 20°C/min from room temperature up to 250°C, as illustrated in Figure 3.30, has been chosen, even though results obtained at different heating rates slight differ.

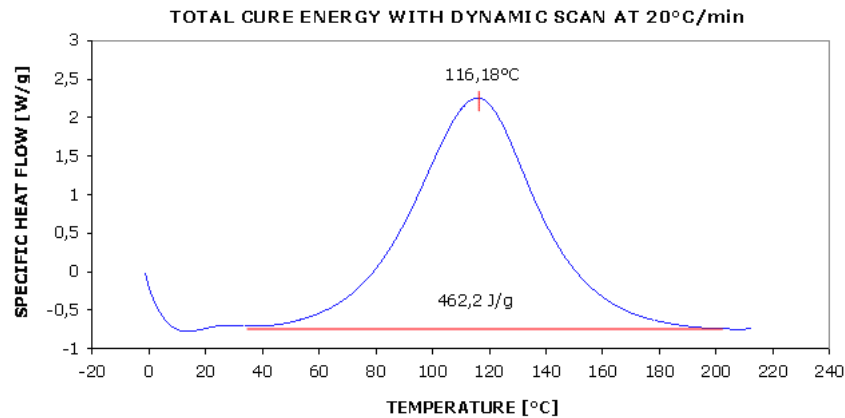


Figure 3.30: Total cure energy with DSC dynamic scan at 20°C/min.

As an example in Figure 3.31 the residual energy, after a microwave cure of 240 s, is shown.

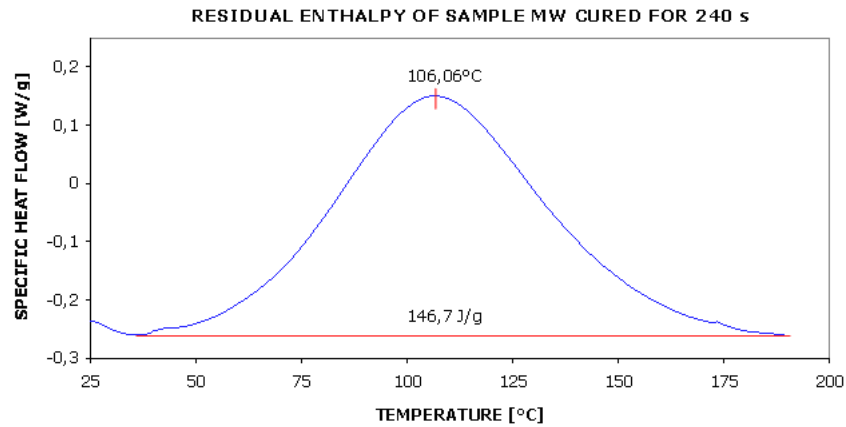


Figure 3.31: Residual energy after 240 s of MW cure.

The obtained value of 146,7 J/g corresponds to a fractional conversion of 68,26%.

However this degree of cure is not completely attributable to the microwave process, because before quenching the sample, the system has continued to react for the delay time τ^{17} following a kinetic, described by the conventional parameters, because it has been heated at a temperature greater than its T_g .

In Table 3.18 the degree of cure versus reaction time, obtained under microwave radiation has been reported.

t_{MW} [s]	90	120	150	180	210	240	270	300
T_{MAX} [°C]	46	53	60	74	94	104	–	–
α_{MW} [%]	33,08	33,45	35,66	43,47	54,44	68,26	83,86	100

Table 3.18: Time, temperature max and degree of conversion for MW cure.

The same data are also plotted in Figure 3.32.

After 300 s of microwave cure a 100% of degree of conversion has been observed. However, at time greater than 240 s, the MW thermal profile is not similar to a DSC

¹⁷Estimated equal to 10 s.

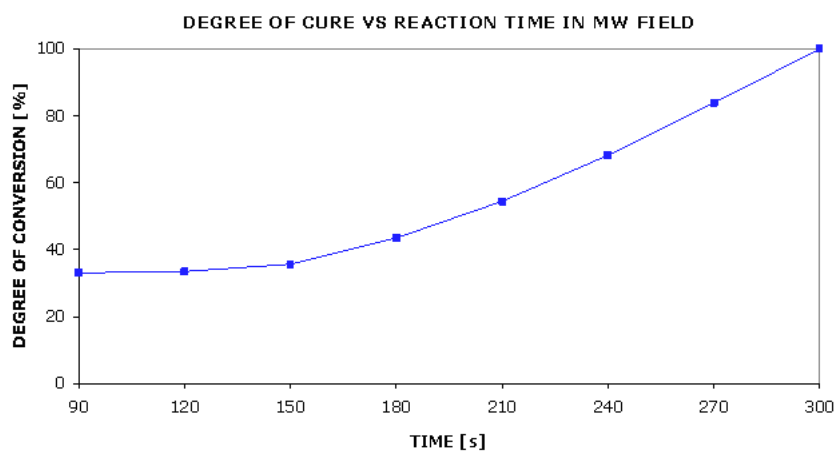


Figure 3.32: Degree of conversion versus reaction time in MW field.

dynamic scan and therefore the direct comparison of reaction fractional conversion can not be carefully proposed.

For the estimation of the degree of cure in conventional DSC process, two important considerations have been taken into account:

1. During the microwave cure process the first temperature measurement occurs after 15 s, that is the time required for the completion of the first passage under the IR sensor. Therefore, as illustrated in Figure 3.29, the temperature of 25°C, that is the first read by the IR sensor, corresponds to a time of 15 s, both along the microwave and DSC thermal profile;
2. The delay time τ .

Therefore the degree of conversion has been measured integrating the DSC signal at different temperature, corresponding to the maximum temperature achieved in DSC scan after the same time of MW cure, *increased with the delay time τ* and starting from the *time of 15 s*. Table 3.19 presents these data.

The degree of conversion has been calculated using the equation 3.28:

$$\alpha = \frac{\Delta H_{\text{PAR}}}{\Delta H_{\text{TOT}}} \quad (3.28)$$

t_{DSC} [s]	90	120	150	180	210	240	270	300
$t_{\text{DSC}} + \tau$ [s]	100	130	160	190	220	250	280	310
T_{DSC} [°C]	50	60	70	80	90	100	110	120
$T_{\text{DSC}} + T_{\tau}$ [°C]	53,33	63,33	73,33	83,33	93,33	103,33	113,33	123,33
α_{DSC} [%]	0,27	1,23	3,41	7,73	15,44	27,78	44,74	63,65

Table 3.19: Time, temperature max and degree of conversion for DSC cure.

where ΔH_{TOT} is equal to 462,2 J/g.

In Figure 3.33 an example of evaluation of partial energy at a temperature of 103,33°C with a DSC dynamic scan at heating rate of 20°C/min, is shown.

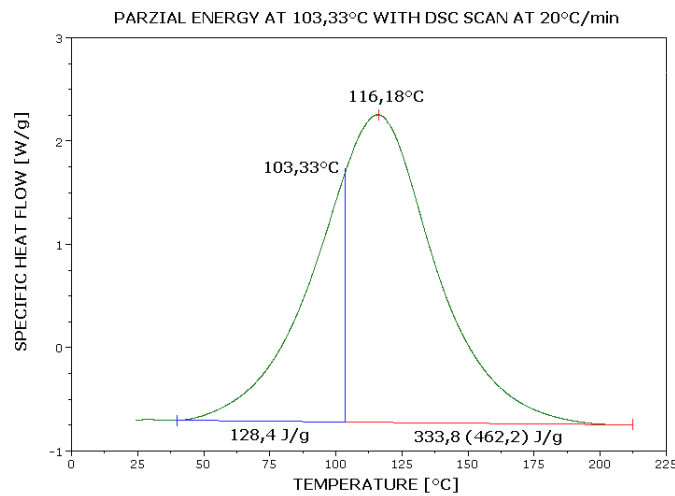


Figure 3.33: Partial energy measured at 103,33°C with DSC at 20°C/min.

The fractional conversions in conventional DSC process have been plotted in Figure 3.34.

Figure 3.35 shows in the same scale the plot of the comparison between the degree of conversion against time in MW and DSC.

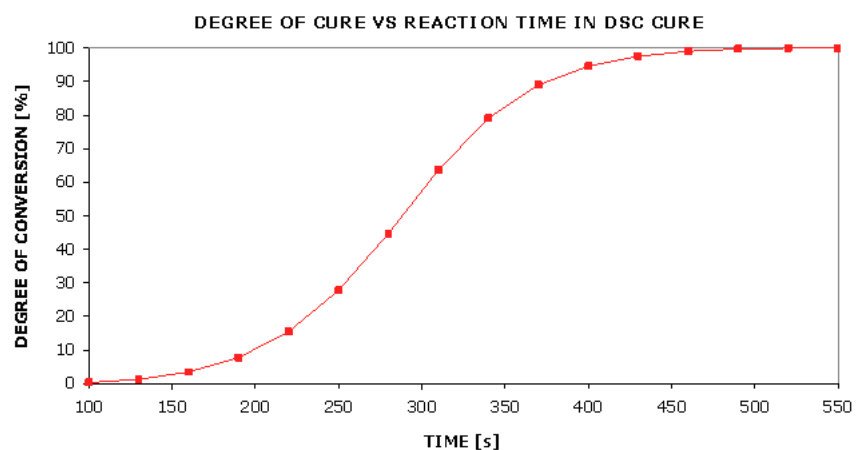


Figure 3.34: Degree of conversion versus reaction time in DSC.

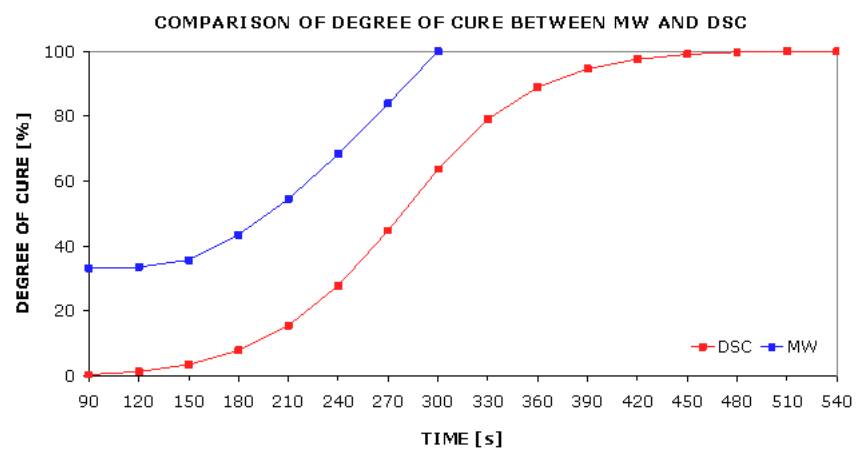


Figure 3.35: Comparison of degree of cure between MW and DSC.

As illustrated in the Figure 3.35 a complete conversion of epoxy system in conventional DSC cure is achieved after 540 s, while in MW field the same degree of cure is obtained in only 300 s. After 240 s, when the two thermal profiles are reasonably comparable, the ratio between the degree of conversion in MW and DSC field is equal to 2,46.

The ratio between α_{MW} and α_{DSC} until the two thermal profiles are comparable, in static conditions (2,37) is a little lower than that (2,46) obtained in dynamic conditions at the same power (1500 W). However only 175 s are necessary for achieve a complete conversion in static conditions, while 300 s are required in dynamic conditions. This behaviour can be explained, because the heating rate, during the main part of cure process, in static condition is much higher (44°C/min) than that measured in dynamic condition (20°C/min), and therefore the temperature increase during the *same delay time* τ , T_τ takes a role more important in the first case.

Resuming in static operative conditions at a power of 1500 and 2000 W and in dynamic conditions at a power of 1500 W suitable MW cure processes, with thermal profiles reproducible with a standard dynamic DSC, have been detected. The comparison between the both heating mechanisms has produced the results listed in Table 3.20.

Summary of comparison MW-DSC			
P [W]	1500 (static)	2000 (static)	1500 (dynamic)
α_{MW}/α_{DSC}	2,37	13,82	2,46

Table 3.20: Ratio between the conversion in MW at different powers and DSC with comparable thermal profile.

The degree of cure achieved in microwave process at every time is much higher

than the corresponding value for conventional heating, though DSC thermal profile is comparable with the temperature during MW exposure (Figures 3.16, 3.17 and 3.29). These results suggest the existence of the “specific microwave effect”.

3.4 Kinetic analysis in Microwave Field with Avrami Method

The profiles of degree of conversion in function of reaction time, obtained in static operative conditions, have been used for a *qualitative* estimation of microwave kinetic parameters¹⁸ with the Avrami method.

This method was found to account well for the autocatalytic cure behaviour of an amine-epoxy system [32, 33].

According to Avrami method the degree of cure is calculated with the following equation:

$$\alpha = 1 - e^{-kt^p} \quad (3.29)$$

The derivative form of Avrami equation is given below:

$$\frac{d\alpha}{dt} = e^{-kt^p} p k t^{(p-1)} \quad (3.30)$$

The Avrami parameters k and p are easily obtained through graphical analysis of the experimental degree of cure versus reaction time data by plotting $\log[-\ln(1 - \alpha)]$ versus $\log t$. The slope of the line is equal to p and the “y-intercept” is equal to $\log k$ according to the relationship 3.31:

$$\log[-\ln(1 - \alpha)] = \log k + p \log t \quad (3.31)$$

With the data obtained through experiments at 1500 W an example of this graphical analysis is illustrated in Figure 3.36.

¹⁸Activation energy E_a and the pre-exponential factor k_0 .

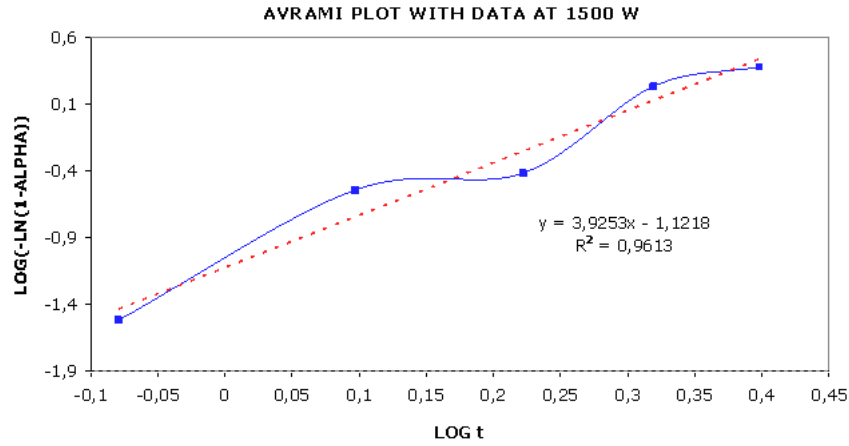


Figure 3.36: Avrami plot with the data obtained through MW experiments at 1500 W.

The derived parameters for the three different powers are compiled in Table 3.21

Power [W]	k [min ⁻¹]	p
1000	0,03	2,96
1500	0,08	3,93
2000	1,14	8,92

Table 3.21: Avrami kinetic parameters at different powers.

If it is assumed that:

- The rate factor k obeys an Arrhenius-type relationship;
- The Avrami exponents p remains constant at all temperature.

a “master” equation, describing the state of cure as a function of time at any given temperature, can be provided:

$$\alpha = 1 - \exp \left[- \exp \left(- \frac{E_a}{RT} + \ln k_0 \right) t^p \right] \quad (3.32)$$

Since every microwave cure process has been performed at a given power, but with a temperature varying at any time, as described by a thermal profile, recorded by the datalogger, as temperature T , used in the master equation 3.32, the value corresponding to the *greatest reaction rate* $\frac{d\alpha}{dt}$ has been chosen.

From the non linear regression of the master equation 3.32 carried out with a data analysis software¹⁹ the parameters E_a , k_0 and p have been calculated for every MW cure process at the three different powers. The results are listed in Table 3.22.

Power [W]	E_a [KJ/mol]	$\ln k_0$ [min^{-1}]	p
1000	4,44	0,13	2,96
1500	3,99	0,29	3,92
2000	1,90	2,01	8,40

Table 3.22: MW kinetic parameters at different powers.

The microwave cure process activation energy E_a , calculated in this way, at every power is much lower of the corresponding value, obtained from the isothermal DSC analysis and reported in Table 3.8. Moreover, as predictable, the activation energy decreases, enhancing the radiation power.

However also the natural logarithm of pre-exponential factor $\ln k_0$ is notably dropped, but in any case the kinetic constant $k(T)$, evaluated up to a temperature of 130°C is higher in microwave than in conventional field. The temperature of 130°C is meaningful, because it is the greatest temperature, reached during a microwave cure process, before the onset of thermal degradation.

Moreover a direct and rigorous comparison, between DSC and MW kinetic parameters, can not be carried out, because the microwave plant, used in this

¹⁹OriginPro 7.0.

work, do not allow the performance of isothermal cure reactions.

3.5 Dynamical-Mechanical Analysis

For a more reliable determination of the glass transition temperature and evaluation of the storage modulus at room temperature dynamical-mechanical measurements have been carried out.

DMA have been performed on samples of about 3-4 cm of length and 1 cm of width and a variable thickness ranging from 1 to 3 mm. In every case attention has been taken on a reasonably good planarity of the testing samples.

The samples have been cut from a tetrafluoroethylene mould of parallelepiped geometry, described in Table 2.9. The epoxy mixture²⁰ has been submitted to a degassing treatment under vacuum at room temperature for about 20 minutes for removing air bubbles, unavoidably formed during the stirring phase. Then the mixture has been poured inside the mould. Air bubbles still present inside the liquid mixture have been manually removed with a technical spoon.

Then the epoxy system inside the mould has been cured conventionally or in microwave field.

In the first case the polymerization protocol suggested by the supplier has been followed. Therefore the mixture has been cured in an electric oven for 24 h at room temperature, then it has been heated for 15 h at 60°C and finally a post-hardening of 3 h at 100°C has been performed. This treatment ensures a complete conversion of the epoxy resin. Lastly it seems of clear lightly yellow colour and uniformly crosslinked, without wrinkles, crannies or other surface patchiness.

While in the second case the microwave cure has been performed in the microwave plant described in the chapter 2, on page 56, operating in *dynamic con-*

²⁰Prepared as illustrated in the chapter 2, section 2.1.3 on page 54.

ditions.

The best operating conditions for the microwave curing process have been determined studying the influence above all of three parameters:

1. *power*;
2. *radiation time*;
3. *mass* of the sample.

The power and time of radiation influence the quantity and the rate of *energy transfer* between the oven and the sample. While the mass of the sample influences the *energy development* during the polymerization. In fact initially the temperature raises exclusively for dielectric heating, but as soon as the temperature overcomes a critical value, corresponding to the activation of curing process, the thermal profile is controlled, above all, by the heat generated by the exothermicity of the reaction itself. This heat is proportional to the mass of the sample and depends in a complicated way on the energy flux received from the oven, through microwave radiation, and on the energy exchange with the outer environment. Only an accurate selection of these three factors ensures a complete conversion of the sample, avoiding thermal degradation phenomena.

The values of microwave cycle parameters and reactants quantity corresponding to the achievement of this condition have been determined after several experiments and they are listed in Tables 3.23 and 3.24.

In Figure 3.37 the DSC dynamic scan between 0 up to 220°C with heating rate of 10°C/min on a fragment of epoxy resin microwave cured as reported above is illustrated.

No residual enthalpy is present, therefore a complete conversion has been reached.

Furthermore the light yellow colour of the resulted slab indicates the absence of thermal degradation phenomena. So with the parameters reported in Tables

MW Oven Parameters	
Tray movement	ON
MW radiation time	450 s (30 passages under waveguide)
Irradiated power	1500 W
Tray velocity	224 cm/min
IR heating	OFF
Air temperature	25°C

Table 3.23: Parameters of the MW cycle.

Epoxy Reactants Quantity	
EC 57	66 g
K 21	13,20 g
Weight ratio	5/1

Table 3.24: Quantity of epoxy components used during the MW cycle.

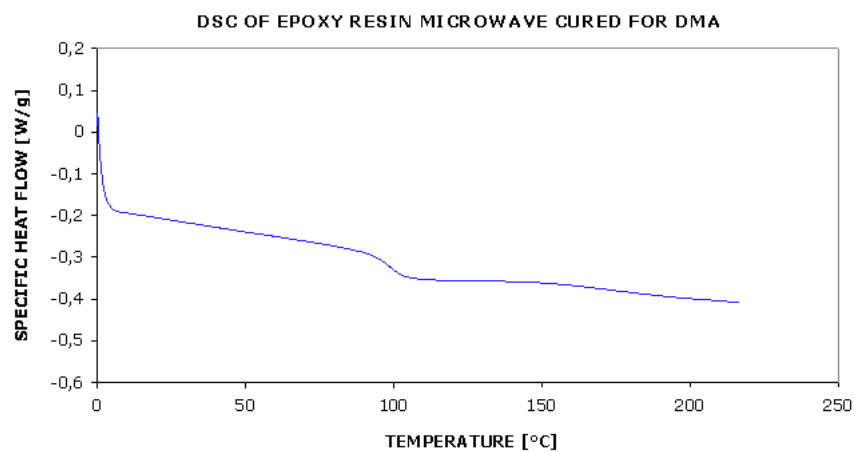


Figure 3.37: DSC Dynamic scan of epoxy resin microwave cured for DMA.

3.23 and 3.24 a right curing process has been performed.

3.5.1 Storage Modulus

A comparison of the storage modulus between samples thermally and microwave cured has been carried out.

The DMA test have been performed using the parameters listed in Table 3.25. In Figure 3.38 a comparison of storage modulus between samples conventionally

DMA Parameters	
Clamp	Single Cantilever
Frequency	1 Hz
Temperature range	from -30 to 220°C
Heating rate	$5^{\circ}\text{C}/\text{min}$

Table 3.25: DMA parameters.

and microwave cured is illustrated.

At room temperature the storage modulus of samples microwave crosslinked is much higher than that of samples thermally cured.

3.5.2 Glass Transition Temperature

Another parameter investigated during DMA test is the glass transition temperature, measured as abscissa of the signal in a plot of $\tan\delta$ against temperature. Improving T_g is a desirable feature for development of efficient and alternative mould materials.

In Figure 3.39 a comparison of T_g between samples conventionally and microwave polymerized is shown.

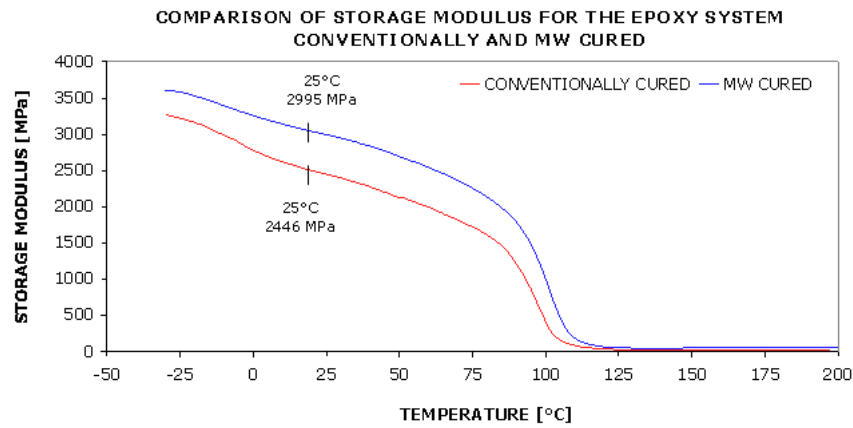


Figure 3.38: Comparison of storage modulus of epoxy samples conventionally and microwave cured.

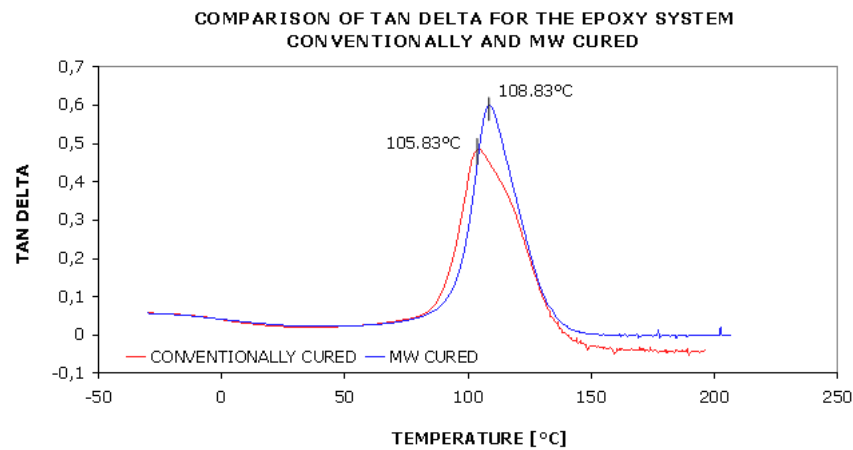


Figure 3.39: Comparison of glass transition temperature of the epoxy system thermally and microwave cured.

The T_g of samples microwave cured is significantly higher than that of specimens conventionally heated. These results are in agreement with those obtained by Yarlagadda et al. [34].

Therefore the same epoxy system when is cured in microwave field exhibits dynamical-mechanical properties better than that when it is crosslinked in conventional electric oven. This can indicate that the strength of crosslinks between the epoxy prepolymer chains is higher when the curing process has been performed with microwave radiations.

Table 3.26 recapitulates the results obtained with dynamical-mechanical tests.

Summary of Dynamical-Mechanical Properties		
	Storage Modulus at 25°C [MPa]	T_g [°C]
Conventionally Cured	2446	105,83
Microwave Cured	2995	108,83

Table 3.26: Comparison of dynamical-mechanical properties between samples conventionally and microwave cured.

3.6 Comparison of Flexural Elastic Modulus

For a more accurate characterization of the epoxy system under investigation an analysis of static mechanical properties has been carried out. Flexural strength has been chosen both for simplicity of the specimen geometry and because it is sufficiently meaningful for a right characterization.

Three point bending static tests²¹ have been performed on samples thermally

²¹According to D 790 standard.

and microwave cured for the evaluation of flexural elastic modulus and the stress-strain curves. In these test a beam of the specimen is supported at two points and loaded in the midpoint.

For this purpose specimens of rectangular shape of size reported in Table 3.27 have been used.

Flexural Test Specimen Size	
Length	≈ 12 cm
Width	≈ 1 cm
Thickness	≈ 2 mm

Table 3.27: Size of specimens used for flexural tests.

The load has been applied on the specimen with a rate of crosshead motion calculated with the following relation:

$$R = \frac{ZL^2}{6d} \quad (3.33)$$

where R [mm] is the rate of crosshead motion, L [mm] is the support span, d [mm] is the depth of the beam and Z [mm/mm/min] the rate of straining of the outer fiber. Z shall be equal to 0,01.

The loading nose and the supports have been aligned so that the axes of the cylindrical surfaces are parallel and the loading nose is midway between the supports.

The test has been interrupted when the 5% of deformation of the specimens has been reached.

During the test simultaneous load-deflection data have been measured.

3.6.1 Stress-Strain Plot

The investigation of flexural properties of the epoxy system has been performed through analysis of stress-strain curves during three point bending test on specimens cured in both the way.

The *flexural stress* may be calculated for any point on the load-deflection curve by means of the following equation:

$$\sigma_f = \frac{3 P L}{2 b d^2} \quad (3.34)$$

where σ_f [MPa] is the stress in the outer fibers at midpoint, P [N] is the load at a given point on the load-deflection curve, L [mm] is the support span, b [mm] the width of the beam tested and d the depth.

The *flexural strain* is the nominal fractional change in the length of an element of the outer surface of the test specimen at midpoint, where the maximum strain occurs. It may be calculated for any deflection using the following equation:

$$\epsilon_f = \frac{6 D d}{L^2} \quad (3.35)$$

where ϵ_f [mm/mm] is the strain in the outer surface, D [mm] is the maximum deflection of the center of the beam, L [mm] is the support span and d [mm] the depth.

In Figure 3.40 a comparison of stress-strain curves of the best specimens conventionally and microwave cured is shown.

The stress necessary for achieve a given strain is much higher for specimens microwave cured than that thermally crosslinked. Moreover for samples conventionally polymerized the elongation at break is greater. Plasticization phenomena can be occurred.

The *tangent modulus of elasticity*, often called *modulus of elasticity*, is the ratio, within the elastic limit, of stress to corresponding strain. It is calculated by

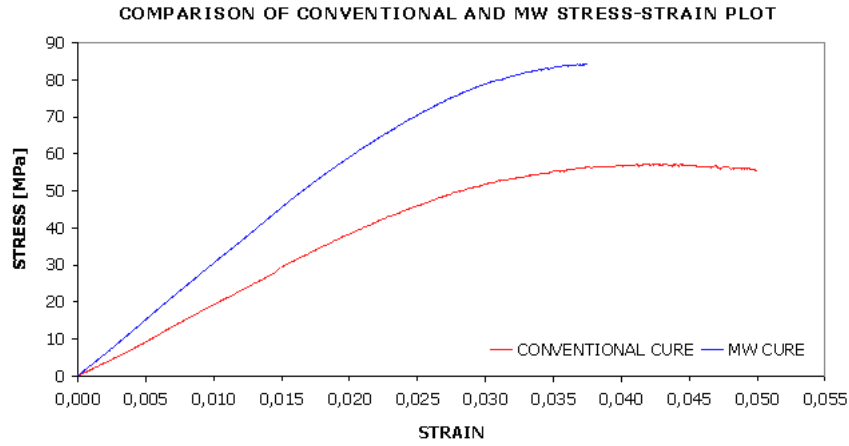


Figure 3.40: Comparison of stress-strain curves of samples conventionally and microwave cured.

drawing a tangent to the steepest initial straight-line portion of the load-deflection curve using the following equation:

$$E_B = \frac{L^3 m}{4 b d^3} \quad (3.36)$$

where E_B [MPa] is the modulus of elasticity in bending, L [mm] the support span, b [mm] and d [mm] respectively the width and depth of the beam tested and m [N/mm] the slope of the tangent to the initial straight-line portion of the load-deflection curve.

In Table 3.28 the average flexural modulus of elasticity for samples thermally and microwave cured are reported.

The modulus of elasticity is higher for specimens microwave cured. This is in agreement with the results, obtained by Singer et al. [35] in a comparison of the mechanical properties of epoxy resin microwave and thermal cured. The more elevated modulus could be due to molecular arrangement in the electric field, because alignment may produce higher molecular packing with lower free volume resulting in an enhanced modulus. Also Yarlagadda et al. [34] have noticed an

Flexural Modulus		
	Conventional	Microwave
Modulus [MPa]	1475,78	2515,87

Table 3.28: Flexural elastic modulus for specimens conventionally and microwave cured.

improvement of the flexural strength of the samples microwave cured compared to that thermally polymerized.

3.7 Spectroscopic Characterization

A spectroscopic analysis in infrared and near infrared region has been performed for measuring the residual concentration of the functional groups after polymerization process. In particular the possible presence of epoxy group and primary amino group has been studied.

The tests have been carried out using the Fourier transform technique. For EC 57 epoxy prepolymer and K 21 hardener agent, that are liquid at room temperature, small droplets have been spread on a potassium bromide (KBr) pastille. While epoxy samples microwave and thermally cured, that are solid at room temperature, have been crushed in a agate mortar with a pestle and then a small amount of powder has been mixed with a potassium bromide pastille.

3.7.1 FT-IR Spectra

In Figure 3.41 the spectrum of EC 57 epoxy prepolymer is shown and the peak at $916\text{-}918\text{ cm}^{-1}$, corresponding to epoxy group has been highlighted.

While in Figure 3.42 the region of infrared spectrum between 750 and 1000

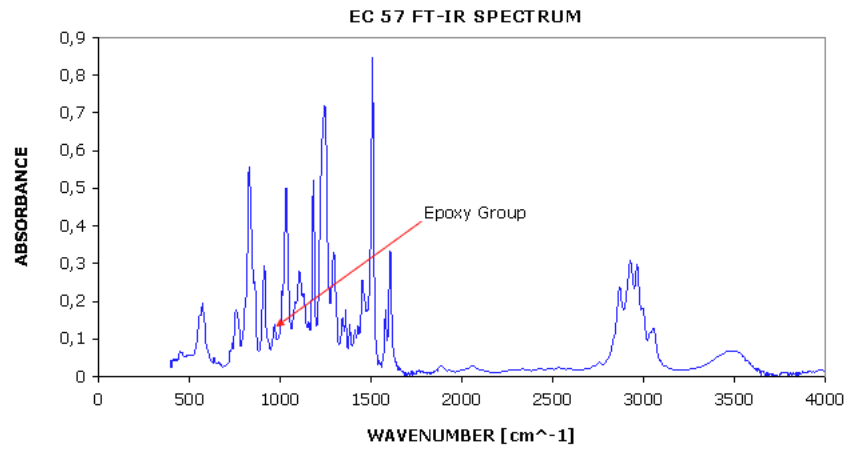


Figure 3.41: EC 57 FT-IR spectrum.

cm⁻¹ of the epoxy system microwave cured is illustrated.

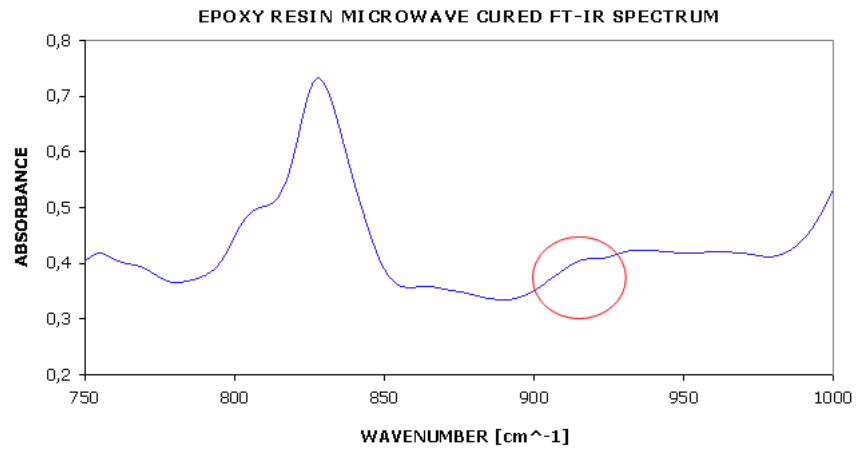


Figure 3.42: Zoom of FT-IR spectrum of an epoxy sample microwave cured.

No peaks corresponding to epoxy group can be observed in the wavenumber region of 916 cm⁻¹.

3.7.2 FT-NIR Spectra

The spectroscopic analysis has been extended also to near infrared region²² for verifying the disappearance of the peak corresponding to primary amino group at about 4930 cm^{-1} .

In Figure 3.43 the FT-NIR spectrum of the hardener agent K 21 is illustrated.

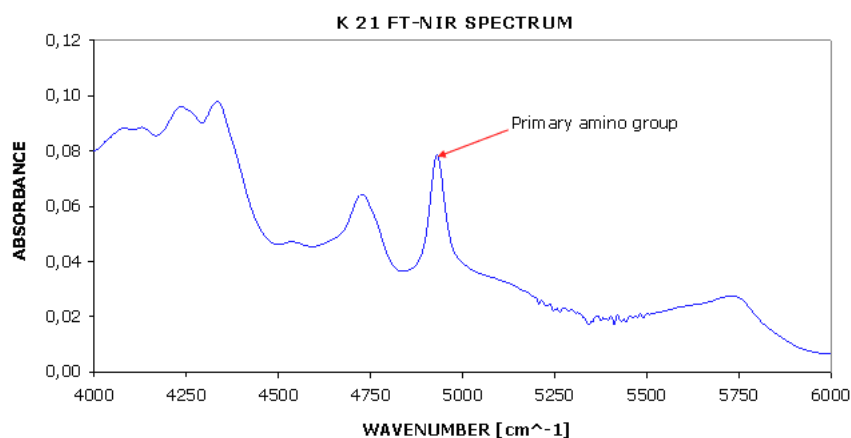


Figure 3.43: K 21 FT-NIR spectrum between 4000 and 6000 cm^{-1} .

Finally in Figure 3.44 a comparison of the FT-NIR spectra of the epoxy system microwave and conventionally cured is shown.

The two FT-NIR signals are very similar, and no peaks are present in the region around 4930 cm^{-1} . Therefore it is not possible to relate the observed behaviour to differences in fractional conversion or reaction path possibly induced by the use of microwave radiations.

No residual reagents, epoxies or amines, can be found in samples cured in both the way. Therefore a complete conversion has been reached, and the absence of homopolymerization reactions has been also verified.

²²Wavenumber between 4000 and 1000 cm^{-1} .

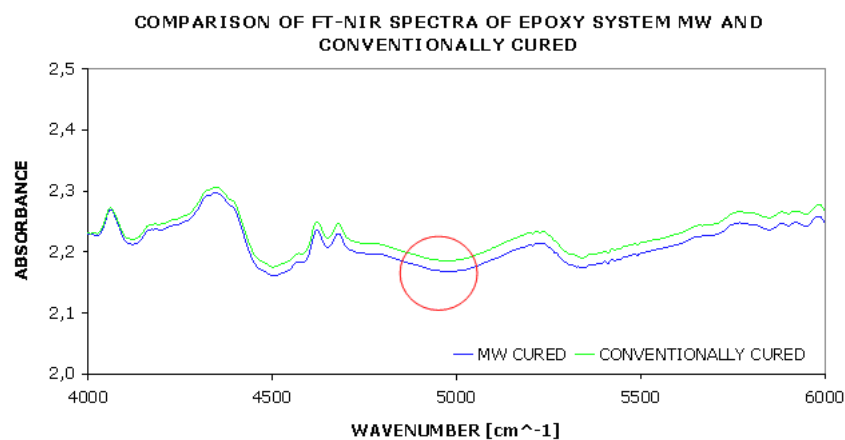


Figure 3.44: Comparison of FT-NIR spectra in the region between 4000 and 6000 cm^{-1} .

3.8 Sensitizers

A preliminary investigation about the influence of suitable microwave sensitizers on the heating rate and thermal profile of the epoxy system has been carried out.

3.8.1 Organic oligomers

A low molecular weight organic compound sensitive to electromagnetic field and completely miscible with the epoxy mixture²³ has been identified, after an introductory chemistry research.

The amount to add to the epoxy system must be carefully selected. In fact an excessive amount interferes with the curing process, avoiding the formation of the 3-D epoxy network. While a too small amount is not sufficient to activate the sensitizing effect.

After a preliminary optimization, the quantity of about 2 p.h.r. has been

²³The exact denomination has been omitted for enabling a possible patent.

identified as the best weight percentage.

The epoxy mixture containing about 2 p.h.r. of this organic sensitizer has been prepared according to the procedure illustrated in the section 2.1.3 on page 54. The components quantity used in these experiments are listed in Table 3.29. The system has been submitted to a microwave curing process in the oven, working as a static cavity, and selecting the oven parameters reported in Table 3.30. These parameters allow the complete conversion of the epoxy mixture free from additives, as verified through the experiments presented in the section 3.9 on page 116.

Components Amount of Epoxy Mixture Containing the Organic Sensitizer	
EC 57	≈ 3
K 21	$\approx 0,6$
Organic Sensitizer	$\approx 0,07$

Table 3.29: Quantity of the components of the epoxy mixture used for experiments with the organic sensitizer.

Parameters	Value
Tray movement	OFF
MW radiation time	175 s
Irradiated power	1500 W
Tray velocity	224 cm/min
IR heating	OFF
Air temperature	25°C

Table 3.30: Microwave oven parameters used for the experiments with the sensitizers.

A remarkable increase of the thermal profile in term of heating rate and absolute temperature values has been noticed, as illustrated in Figure 3.45.

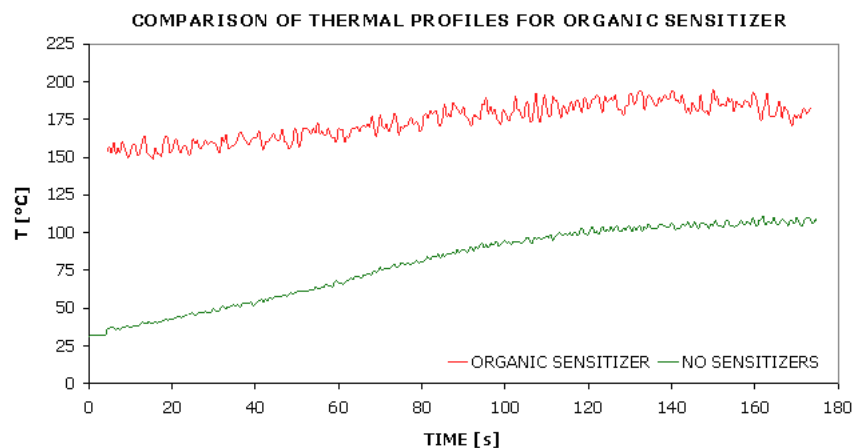


Figure 3.45: Comparison of the thermal profiles between the epoxy system incorporating 2 p.h.r. of an organic sensitizer with the same resin free from additives.

However this investigation is still in progress and there is again a range of uncertainty of about 10°C. In fact the sensitizing effect of this organic compound is so strong, that also a little variation of its percentage can determine a not negligible difference of the thermal profile of the epoxy mixture.

In any case the effect of this substance as microwave sensitizer has been observed also by other authors [36, 37], but they have reported only a modicum temperature enhancement.

The electromagnetic energy absorbed by the mixture containing this sensitizer is very great. In fact under microwave radiation not only the epoxy group, but also the specific polar group of this organic sensitizer rotate around their electric centre, following the oscillation of the EM field. In this way the kinetic rotational energy is converted to heat and therefore the temperature of the whole mixture strongly increases.

This effect operates both during the initial dielectric heating of the epoxy mixture and after the following activation of the curing reaction.

Probably using 2 p.h.r. of this organic sensitizer the complete conversion of the epoxy system can be achieved in a shorter time or alternatively with a lower radiations power, in both the cases with a considerable energy saving.

3.8.2 Metallic Nanopowders

The influence of another type of sensitizer has been studied.

Nickel nanopowders have been chosen, because they can improve the microwave absorption. In fact they sensitive to the oscillating EM field, due to their ferromagnetic properties [38]. However these metallic nanopowders increase also the thermal conductivity of the epoxy mixture and therefore improve the energy dissipation, during both the initial dielectric heating and the following exothermic curing reaction. For this reason the sensitizing effect is partially downsized.

Instead of the organic sensitizer, the nickel nanopowders do not interfere with the curing reaction. In fact they do not possess functional groups able to interact with the reagents of the epoxy mixture.

A 20 p.h.r. quantity has been identified as the most suitable amount for the temperature raising. The formulation of the epoxy mixture, used in these experiments is reported in Table 3.31.

The mixture containing 20 p.h.r. of nickel nanopowder has been prepared as illustrated in the section 2.1.3 on page 54. It has been microwave cured using the operative conditions listed in Table 3.30 and the temperature of sample has been recorded by datalogger.

Figure 3.46 shows a comparison of thermal profiles followed by the epoxy mixture free from additives and by the same system incorporating the nickel nanopowders.

Components Amount of Epoxy Mixture Incorporating Nickel Nanopowders	
EC 57	≈ 3
K 21	$\approx 0,6$
Nickel Nanopowders	$\approx 0,72$

Table 3.31: Quantity of the components of the epoxy mixture used for experiments with nickel nanopowders.

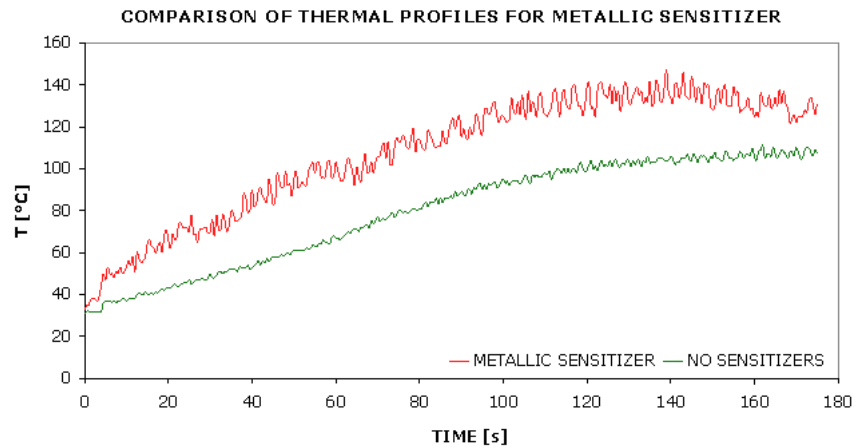


Figure 3.46: Comparison of the thermal profiles between the epoxy system containing 20 p.h.r. of nickel nanopowders with the same resin free from additives.

Also in this case an increase of the heating rate and temperature values has been observed. However the heat generated in this case is not so high as with the organic sensitizer, presented in the previous section. Probably the energy conversion due to magnetic field is less efficient than the corresponding heat generation for dielectric loss.

Chapter 4

Conclusions and Outlook

Epoxies are the most promising thermosetting resins. These polymers have many industrial applications because after curing they possess excellent mechanical, electrical and chemical properties. However the conventional polymerization process involves time of several hours and elevated temperature, resulting in remarkable production costs.

The work reported here illustrates the appealing advantages of the alternative microwave heating technology¹ in term of higher efficiency, shortening processing time, energy saving, more uniform cure and improving physical-mechanical properties.

The kinetic parameters in microwave field have been qualitatively estimated, using the Avrami method, and compared with those, calculated through analysis of isothermal DSC. A remarkable *decrease of the activation energy* has been observed. Moreover the existence of the “specific microwave effect” has been verified, comparing the partial degree of conversion, after the same reaction time in MW and DSC cure processes, *undergoing similar thermal profiles*. In all the cases the

¹This heating mechanism is suitable for epoxy resins, because they contain polar functional groups.

degree of cure in MW field is always much higher than the corresponding conversion achieved in DSC, and the time required for a complete polymerization of the epoxy resin is considerably lower when the system is heated with microwave radiations. Therefore, the claim of an *acceleration of the reaction rate*, due to the effect of the electromagnetic field², can be supported.

Moreover, samples microwave cured show better thermo-mechanical properties. In particular, the glass transition temperature, dynamic storage modulus and flexural elastic modulus of samples crosslinked, using both the heating mechanisms, have been measured and compared among them. An increase of the strength of the 3-D epoxy network for samples microwave cured has been noticed. As verified, through FT-IR and FT-NIR analysis, spectra of samples conventionally and microwave cured are very similar and no residual reagents, epoxies or amines, have been found in the resin cured in both the way.

Finally the possible microwave heatability of non polar polymers³, through incorporation of suitable organic and metallic sensitizers, has been preliminarily investigated.

According to these results and considerations the microwave curing process of epoxy systems can be considered a valid alternative for the polymerization of this thermosetting resin.

4.1 Outlook

Further information on the cure kinetic of the epoxy resin heated in both the way can be obtained through a spectroscopic analysis. Besides the development of a microwave calorimeter can allow the performance of isothermal microwave cure and the measurement of the specific heat flow during the process. In this way

²Not simply explainable with differences of the thermal profile.

³ Electromagnetically insensitive.

a direct comparison between DSC and MW curing reactions can be carried out. Moreover a more complete investigation of the final properties of the epoxy system cured in both the way can be accomplished through the dielectric characterization.

Appendix A

A Brief History of Microwave Oven

Like many great inventions in history, the microwave oven was also a product of past technology.

It was during a radar-related research project around 1946 that Dr. Percy Spencer, a self-taught engineer with the *Raytheon Corporation*, noticed something very unusual. He was testing a new vacuum tube called magnetron, when he discovered that the chocolate bar in his pocket had melted. This interested Dr. Spencer, so he tried another experiment. This time he placed some popcorn kernels near the tube and watched as popcorn sputtered, cracked and popped all over his laboratory.

Another experiment, that he conducted, involved an egg, which he placed near the magnetron tube. That time, he asked his colleague to accompany him so that they can both see the phenomena.

Because of the elevated pressure, the egg began to tremor. The temperature inside the egg got so high, that the egg exploded. Hot yolk splattered all over his

colleagues face. Because of these results, they realized that they can cook other foods using the low-density microwave energy.

Dr. Spencer created a metal box with an opening into which he fed microwave power. The energy entering the box was unable to escape, thereby creating a higher density electromagnetic field. When food was placed in the box and microwave energy fed in, the temperature of the food rose very rapidly. Dr. Spencer had invented what was to revolutionize cooking, and form the basis of a multimillion dollar industry, the microwave oven.

Engineers went to work on Spencer's new idea, developing and refining it for practical use. By late 1946, the *Raytheon Company* had filed a patent proposing that microwaves be used to cook food. An oven that heated food using microwave energy was then placed in a Boston restaurant for testing. At last, in 1947, the first commercial microwave oven, called "Radaranges" hit the market. These primitive units were gigantic and enormously expensive, standing 5,5 feet tall, weighing over 750 pounds, and costing about 5000 \$ each. The magnetron tube had to be water-cooled, so plumbing installations were also required.

Not surprisingly, many were highly reluctant about these first units, and so they found only limited acceptance. Further improvements and refinements soon produced a more reliable and lightweight oven that was not only less expensive, but, with the development of a new air-cooled magnetron, there was no longer any need for a plumber. Figure A.1 shows a picture of one of the first domestic microwave oven produced.

Technological advances and further developments led to a microwave oven that was polished and priced for the consumer kitchen. However, there were many myths and fears surrounding these mysterious new electronic "radar ranges" By the seventies, more and more people were finding the benefits of microwave cooking to outweigh the possible risks, and none of them were dying of radiation poisoning.



Figure A.1: One of the first domestic microwave oven.

As fears faded, a swelling wave of acceptance began filtering into the kitchens of America and other countries. Myths were melting away, and doubt was turning into demand.

By 1975, sales of microwave ovens would, for the first time, exceed that of gas ranges. The following year, a reported 17% of all homes in Japan were doing their cooking by microwaves, compared with 4% of the homes in the United States the same year. Before long, though, microwave ovens were adorning the kitchens in over nine million homes, or about 14%, of all the homes in the United States. In 1976, the microwave oven became a more commonly owned kitchen appliance than the dishwasher, reaching nearly 60%, or about 52 million U.S. households. America's cooking habits were being drastically changed by the time and energy-saving convenience of the microwave oven. Once considered a luxury, the microwave oven had developed into a practical necessity for a fast-paced world.

An expanding market has produced a style to suit every taste; a size, shape, and color to fit any kitchen, and a price to please almost every pocketbook. Options and features, such as the addition of convection heat, probe and sensor cooking, meet the needs of virtually every cooking, heating or drying application.

The microwave oven had reached a new level of acceptance, particularly with regard to certain industrial applications. By having a microwave oven available, restaurants and vending companies could now keep products refrigerator-fresh up to the point of service, then heat to order.

As the food industry began to recognize the potential and versatility of the microwave oven, its usefulness was put to new tests. Industries began using microwaves to dry potato chips and roast coffee beans and peanuts. Meats could be defrosted, precooked and tempered. Even the shucking of oysters was made easier by microwaves. Other industries found the diverse applications of microwave heating quite advantageous. In time, microwaves were being used to dry cork, ceramics, paper, leather, tobacco, textiles, pencils, flowers, wet books, plastics and match heads. The microwave oven had become a necessity in the commercial market and the possibilities seemed endless.

Bibliography

- [1] W. Callister, “Materials Science and Engineering: An Introduction”, *Fifth Ed.-New York, s.e.*, (1999).
- [2] H. Lee, K. Neville, “Epoxy Resins”, *McGraw-Hill Book Company, Inc.*, (1957).
- [3] J. March, “Advanced organic chemistry: reactions, mechanisms, and structure”, 4^o *Ed.-New York: John Wiley & Sons*, (1992).
- [4] E. B. Moullin, “The Principles of Electromagnetism”, *Oxford: Clarendon press*, (1955).
- [5] <http://en.wikipedia.org/wiki/Electromagnetism>.
- [6] R. Meredith, “Engineers’ Handbook of Industrial Microwave Heating”, *IEE Power Series 25*, (1997).
- [7] J. Mijovic, J. Wijaya, “Review of cure of polymers and composites by microwave energy”, *Polymer Composites*, Vol. 11, No. 3, pp. 184-190, (1990).
- [8] M. Chen, E. J. Siochi, T. C. Ward, J. E. McGrath, “Basic ideas of microwave processing of polymers”, *Polymer Engineering and Science*, Vol. 33, No. 7, pp. 1092-1109, (1993).
- [9] V. V. Daniel, “Dielectric relaxation”, *New York: Academic Press*, (1967).

- [10] G. Roussy, J. A. Pierce, "Foundations and industrial applications of microwave and radio frequency fields", *New York: Wiley*, (1995).
- [11] J. D. Ferry, "Viscoelastic properties of polymers", *New York: Wiley*, (1980).
- [12] R. E. Collin, "Foundation for microwave engineering", *New York: McGraw-Hill*, (1966).
- [13] W. H. Sutton, "Microwave processing of ceramics – an overview", In: R. L. Beatty, M. F. Iskander, W. H. Sutton, editors. "Microwave processing of materials III", *Materials Research Society Proceedings, San Francisco, 269, Pittsburgh: Materials Research Society*, pp. 3, (1992).
- [14] R. E. Thomas, A. J. Sosa, "The Analysis and Design of Linear Circuits", *Englewood Cliffs, NJ: Prentice-Hall*, (1994).
- [15] B. Fu, Hawley, "Comparative study of continuous-power and pulsed-power of microwave curing of epoxy resins", *Polymer Engineering and Science*, Vol. 40, pp. 1333-1338, (2000).
- [16] J. M. Barton, "The Application of Differential Scanning Calorimetry (DSC) to the Study of Epoxy Resin Curing Reactions", *Advances in Polymer Science, Vol. 72, Springer-Verlag, Berlin*, (1985).
- [17] P. I. Karkanias, I. K. Partridge, D. Attwood, "Modelling the Cure of a Commercial Epoxy Resin for Applications in Resin Transfer Moulding", *Polymer International*, Vol. 41, pp. 183-191, (1996).
- [18] P. I. Karkanias, I. K. Partridge, "Cure Modeling and Monitoring of Epoxy/Amine Resin Systems. I. Cure Kinetics Modeling", *Journal of Applied Polymer Science*, Vol. 77, pp. 1419-1431, (2000).

- [19] P. I. Karkanas, I. K. Partridge, "Cure Modeling and Monitoring of Epoxy/Amine Resin Systems. II. Network Formation and Chemoviscosity Modeling", *Journal of Applied Polymer Science*, Vol. 77, pp. 2178-2188, (2000).
- [20] P. Navabpour, A. Nesbitt, B. Degamber, G. Fernando, T. Mann, R. Day, "Comparison of the Curing Kinetics of the RTM6 Epoxy Resin System Using Differential Scanning Calorimetry and a Microwave-Heated Calorimeter", *Journal of Applied Polymer Science*, Vol. 99, pp. 3658-3668, (2006).
- [21] D. Stuerger, P. Gaillard, "Microwave Athermal Effects in Chemistry: A Mith's Autopsy, Part I: Historical background and fundamentals of wave-matter interaction", *Microwave Power Electromagnetic Energy*, Vol. 31, pp. 87-100, (1996).
- [22] D. Stuerger, P. Gaillard, "Microwave Athermal Effects in Chemistry: A Mith's Autopsy, Part II: Orienting effects and thermodynamic consequences of electric field", *Microwave Power Electromagnetic Energy*, Vol. 31, pp. 101-113, (1996).
- [23] A. Loupy, M. Ramdani, P. Pigeon, H. Julien, M. Delmotte, "Microwave induced organic synthesis: anionic activation in "dry media" conditions", *High Frequency and Microwave (International Conference Nine) Proc.*, pp. 261-264, (1991).
- [24] E. T. Thostenson, T. W. Chou, "Microwave processing: fundamentals and applications", *Composites: Part A*, Vol. 30, pp. 1055-1071, (1999).
- [25] E. Marand, K. B. Baker, J. D. Graybeal, "Comparison of Reaction Mechanisms of Epoxy Resins Undergoing Thermal and Microwave Cure from in Situ

- Measurements of Microwave Dielectric Properties and Infrared Spectroscopy”, *Macromolecules*, Vol. 25, pp. 2243-2252, (1992).
- [26] J. Wei, M. C. Hawley, J. D. Delong, M. Demeuse, “Comparison of Microwave and Thermal Cure of Epoxy Resins”, *Polymer Engineering and Science*, Vol. 33, No. 17, pp. 1132-1140, (1993).
- [27] C. Jordan, J. Galy, J. P. Pascault, “Comparison of Microwave and Thermal Cure of an Epoxy/Amine Matrix”, *Polymer Engineering and Science*, Vol. 35, No. 3, pp. 233-239, (1995).
- [28] J. Mijovic, J. Wijaya, “Comparative Calorimetric Study of Epoxy Cure by Microwave vs Thermal Energy”, *Macromolecules*, Vol. 23, pp. 3671-3674, (1990).
- [29] J. Mijovic, A. Fisbain, J. Wijaya, “Mechanistic Modeling of Epoxy-Amine Kinetics. 1. Model Compound Study”, *Macromolecules*, Vol. 25, pp. 979-985, (1992).
- [30] J. Mijovic, A. Fisbain, J. Wijaya, “Mechanistic Modeling of Epoxy-Amine Kinetics. 2. Comparison of Kinetics in Thermal and Microwave Fields”, *Macromolecules*, Vol. 25, pp. 986-989, (1992).
- [31] J. Mijovic, W. V. Corso, L. Nicolais, G. d’Ambrosio, “In Situ Real-time Study of Crosslinking Kinetics in Thermal and Microwave Fields”, *Polymers for Advanced Technologies*, Vol. 9, pp. 231-243, (1998).
- [32] J. M. Hurley, T. Berfield, S. Ye, R. W. Johnson, R. Zhao, G. Tian, “Kinetic Modeling of No-Flow Underfill Cure and Its Relationship to Solder Wetting and Voiding”, *Electronic Components and Technology Conference*, (2002).
- [33] S. W. Kim, M. G. Lu, M. J. Shim, *Polymer Journal*, Vol. 30, pp. 90-94, (1998).

- [34] K. D. V. Prasad Yarlagadda, Shu-Hau Hsu, "Experimental studies on comparison of microwave curing and thermal curing of epoxy resins used for alternative mould materials", *Journal of Materials Processing Technology*, Vol. 155-156, pp. 1532-1538, (2004).
- [35] S. M. Singer, J. Jow, J. D. Delong, M. C. Hawley, "Effects of processing on tensile properties of an epoxy/amine matrix: continuous electromagnetic and/or thermal curing", *SAMPE Quarterly*, Vol. 20, No. 2, pp. 14-18, (1989).
- [36] <http://www.wipo.int/pctdb/en/wo.jsp?IA=US1986001164&DISPLAY=DESC>
- [37] <http://www.wipo.int/pctdb/en/wo.jsp?IA=US2001049199&DISPLAY=DESC>
- [38] X. Feng, G. Liao, J. Du, L. Dong, K. Jin, X. Jian, "Electrical conductivity and microwave absorbing properties of nickel-coated multiwalled carbon nanotubes/poly(phthalazinone ether sulfone ketone)s composites", *Polymer Engineering and Science*, Vol. 48, No. 5, pp. 1007-1014, (2008).